

AD-A135 675

ACROSS ELEVEN (ACTIVE CONTROL OF SPACE STRUCTURES)
VOLUME 1(U) CHARLES STARK DRAPER LAB INC CAMBRIDGE MA
E FOGEL ET AL JUL 83 CSDL-R-1598-VOL-1

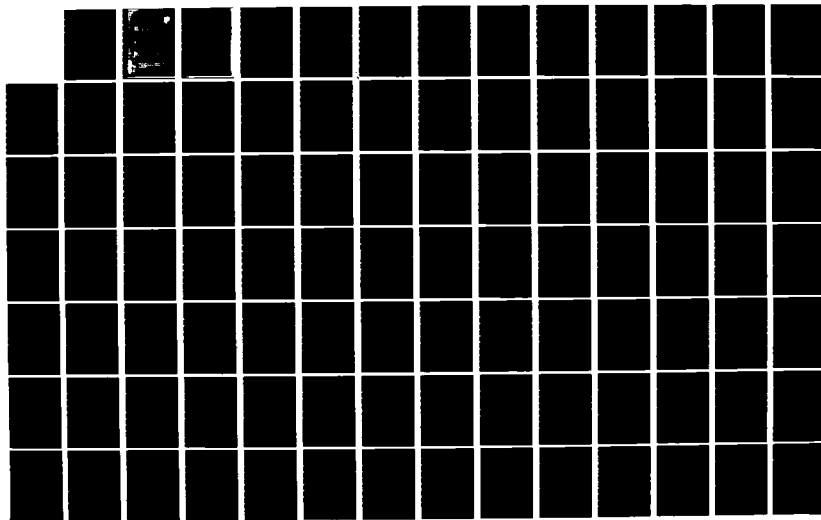
1/2

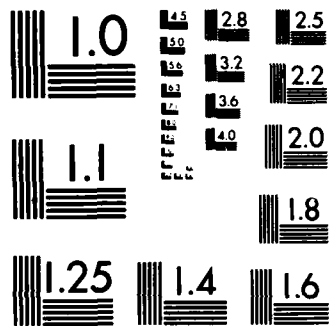
UNCLASSIFIED

RADC-TR-83-158-VOL-1 F38602-81-C-0180

F/G 22/1

NL





MICROCOPY RESOLUTION TEST CHART
NATIONAL BUREAU OF STANDARDS-1963-A

12

RADC-TR-83-158, Vol I (of two)
Interim Report
July 1983



ACROSS ELEVEN (ACTIVE CONTROL OF SPACE STRUCTURES)

Charles Stark Draper Laboratory, Inc.

Sponsored by
Defense Advanced Research Projects Agency (DOD)
DRA Order No. 3655

APPROVED FOR PUBLIC RELEASE; DISTRIBUTION UNLIMITED

The views and conclusions contained in this document are those of the author and should not be interpreted as necessarily representing the official policies, either expressed or implied, of the Defense Advanced Research Projects Agency or the U.S. Government.

AIR DEVELOPMENT CENTER
Air Force Systems Command
Wright Air Force Base, NY 13441

DTIC
ELECTE
DEC 13 1983
A

88 12 12 072

This report has been reviewed by the RADC Public Affairs Office (PA) and is releasable to the National Technical Information Service (NTIS). At NTIS it will be releasable to the general public, including foreign nations.

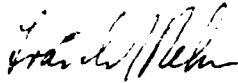
RADC-TR-83-158, Volume I (of two) has been reviewed and is approved for publication.

APPROVED:



RICHARD W. CARMAN
Project Engineer

APPROVED:



FRANK J. REHM
Technical Director
Surveillance Division

FOR THE COMMANDER:



JOHN P. HUSS
Acting Chief, Plans Office

If your address has changed or if you wish to be removed from the RADC mailing list, or if the addressee is no longer employed by your organization, please notify RADC (OCSE) Griffiss AFB NY 13441. This will assist us in maintaining a current mailing list.

Do not return copies of this report unless contractual obligations or notices on a specific document requires that it be returned.

UNCLASSIFIED

SECURITY CLASSIFICATION OF THIS PAGE (When Data Entered)

REPORT DOCUMENTATION PAGE		READ INSTRUCTIONS BEFORE COMPLETING FORM
1. REPORT NUMBER RADC-TR-83-158, Vol I (of two)	2. GOVT ACCESSION NO. A135675	3. RECIPIENT'S CATALOG NUMBER
4. TITLE (and Subtitle) ACOSS ELEVEN (ACTIVE CONTROL OF SPACE STRUCTURES)		5. TYPE OF REPORT & PERIOD COVERED Interim Report Apr 82 - Nov 82
		6. PERFORMING ORG. REPORT NUMBER CSDL-R-1598 ✓
7. AUTHOR(s) Eli Fogel N. Harris McClamroch Daniel R. Hegg Jiguan G. Lin		8. CONTRACT OR GRANT NUMBER(s) F30602-81-C-0180
9. PERFORMING ORGANIZATION NAME AND ADDRESS The Charles Stark Draper Laboratory, Inc. 555 Technology Square Cambridge MA 02139		10. PROGRAM ELEMENT, PROJECT, TASK AREA & WORK UNIT NUMBERS 62301E C6550104
11. CONTROLLING OFFICE NAME AND ADDRESS Defense Advanced Research Projects Agency 1400 Wilson Blvd Arlington VA 22209		12. REPORT DATE July 1983
		13. NUMBER OF PAGES 126
14. MONITORING AGENCY NAME & ADDRESS (if different from Controlling Office) Rome Air Development Center (OCSE) Griffiss AFB NY 13441		15. SECURITY CLASS. (of this report) UNCLASSIFIED
		15a. DECLASSIFICATION/DOWNGRADING SCHEDULE N/A
16. DISTRIBUTION STATEMENT (of this Report) Approved for public release; distribution unlimited.		
17. DISTRIBUTION STATEMENT (of the abstract entered in Block 20, if different from Report) Same		
18. SUPPLEMENTARY NOTES RADC Project Engineer: Richard Carman (OCSE)		
19. KEY WORDS (Continue on reverse side if necessary and identify by block number) LSS Identification Actuator Dynamics Modal Spring Spectral Resolution Electromechanical Actuators Systematic ACOSS Sampling Rates Control Design Design Zoom-in Procedures Modal Dashpot		
20. ABSTRACT (Continue on reverse side if necessary and identify by block number) This volume documents the progress made in four principal areas during this reporting period: (1) The difficulties encountered in the Large Space Structure (LSS) system identification were studied. Focusing on the high-resolution identification problem, a procedure for identifying lightly damped, closely spaced modes is derived; (2) Two approaches to the incorporation of actuator dynamics and the role of actuator transducers in LSS vibration control were explored; (3) A modal dashpot/modal		

UNCLASSIFIED

SECURITY CLASSIFICATION OF THIS PAGE(When Data Entered)

CAZ → spring control design is presented, and (4) A controlled experiment for the ACOSS design is proposed in which each principal element in the overall synthesis process is systematically examined. ↗

UNCLASSIFIED

SECURITY CLASSIFICATION OF THIS PAGE(When Data Entered)

ACOSS ELEVEN (ACTIVE CONTROL OF SPACE STRUCTURES)

Eli Fogel
Daniel R. Hegg
N. Harris McClamroch
Jiguan G. Lin

Contractor: The Charles Stark Draper Laboratory, Inc.
Contract Number: F30602-81-C-0180
Effective Date of Contract: 27 April 1981
Contract Expiration Date: 27 April 1984
Short Title of Work: ACOSS Eleven (Active Control of
Space Structures)
Program Code Number: 1E20
Period of Work Covered: Apr 82 - Nov 82
Principal Investigator: Dr. Keto Soosaar
(617) 258-2575
Project Engineer: Richard Carman
(315) 330-3148

Approved for public release; distribution unlimited

This research was supported by the Defense Advanced
Research Projects Agency of the Department of
Defense and was monitored by Richard Carman (OCSE),
Griffiss AFB NY 13441 under Contract F30602-81-C-0180

ACKNOWLEDGMENT

The report was prepared by the Charles Stark Draper Laboratory, Inc., under Contract F30602-81-C-0183. This research was supported by the Advanced Research Projects Agency of the Department of Defense and monitored by the Rome Air Development Center.

The program manager is Dr. Keto Soosaar and the project leader for Active Control of Space Structures (ACOSS) is Mr. Robert R. Strunce. The authors of this report are: Dr. Eli Fogel (Sections 1, 2), Dr. Harris N. McClamroch (Section 3), Dr. Jiguan G. Lin (Section 4), and Dr. Daniel R. Hegg (Section 5). Assistance from Mr. Michael Villalba (Section 2) is gratefully acknowledged.

Publication of this report does not constitute approval by the Defense Advanced Research Projects Agency or the United States Government of the findings or conclusions contained herein. It is published for the exchange and stimulation of ideas.



TABLE OF CONTENTS

<u>Section</u>		<u>Page</u>
1	INTRODUCTION.....	1
	1.1 Scope.....	1
	1.2 LSS Identification.....	1
	1.3 Actuator Dynamics.....	1
	1.4 Modal Spring and Modal Dashpot Design.....	2
	1.5 A Controlled Experiment for ACOSS Design.....	2
	LIST OF REFERENCES.....	3
2	STRUCTURE IDENTIFICATION--THE RESOLUTION PROBLEM AND ITS SOLUTIONS.....	4
	2.1 Introduction.....	4
	2.2 Spectral Estimation and Sampling.....	7
	2.3 Nonparametric Spectral Estimation.....	10
	2.4 Sampled Data Spectral Analysis.....	12
	2.5 The Role of Sampling Rate.....	17
	2.6 Zooming In.....	34
	2.7 Simulation Results.....	42
	2.8 General Comments.....	52
	2.9 Concluding Remarks.....	52
	LIST OF REFERENCES.....	55
3	CONTROL OF LARGE SPACE STRUCTURES USING ELECTROMECHANICAL ACTUATORS.....	57
	3.1 Introduction.....	57
	3.2 Modelling.....	58
	3.3 Centralized Control Design Viewpoint.....	67
	3.4 Decentralized Control Design Viewpoint.....	77
	3.5 Examples.....	90
	3.6 Conclusions.....	106
	LIST OF REFERENCES.....	108
4	MODAL-SPRING PLUS MODAL-DASHPOT DESIGN OF OUTPUT FEEDBACK VIBRATION CONTROLLERS.....	110
	LIST OF REFERENCES.....	117
5	A CONTROLLED EXPERIMENT FOR ACOSS DESIGN.....	118
	5.1 Motivation.....	118
	5.2 Preliminary Observations.....	118
	5.3 Definition of a "Controlled Experiment".....	119
	5.4 Expected Outcome.....	123
	LIST OF REFERENCES.....	126

SECTION 1

INTRODUCTION

1.1 Scope

The present report gives an account of the progress made during the reporting period in four principal subject areas:

- (1) Large Space Structure (LSS) system identification.
- (2) The effect of actuator dynamics on LSS control.
- (3) Modal dashpot/modal spring control design.
- (4) A controlled experiment for ACOSS design.

1.2 LSS Identification

In Section 2, the basic approaches to LSS identification and the major difficulties encountered in the identification are discussed. Subsequently, attention is focused on the high-resolution identification problem typifying LSS. A novel procedure for identifying lightly damped, closely spaced modes is derived. The approach is rooted in the notion of numerical rank of matrices which has bearing upon the spectral estimation problem. Optimizing the sampling rate and relaxing the Nyquist rate to construct a "zoom-in" procedure are utilized in deriving efficient and numerically stable high-resolution spectral analysis algorithms.

Although the procedures reported here are obtained in the context of LSS identification, they can also be applied to arbitrary high-resolution spectral analysis problems such as radar signal processing.

1.3 Actuator Dynamics

The common assumption in work on LSS control is the availability of ideal sensors and actuators. Namely, the bandwidth and the power of the devices are assumed unlimited and structure/actuator interaction is ignored. Section 3 reports our observations on the effects of incorporating the actuator dynamics in the model. The proper way to model conventional actuators is presented first. Subsequently, two approaches to the incorporation of the actuator dynamics are explored.

- (1) The structural model is augmented by the actuator model, and the controller is designed for the augmented plant. It is seen that the augmented plant has the same dynamic representation as structures with optimal actuators. Thus, the conventional LSS control design approaches are applicable to the augmented system.

- (2) A controller is designed assuming ideal actuators, and a compensator is designed around the actuator. The design issues for actuator compensators are addressed and some solutions are proposed.

1.4 Modal Spring and Modal Dashpot Design

Section 4 is complementary to the second ACOSS 11 semiannual report [1-1], where various designs to accommodate a broadband disturbance are considered. In the present section, a procedure for a combined velocity and position feedback (dashpot and spring, respectively) are to be designed to augment damping and move frequencies of the closed-loop plant. A root locus procedure for assessing the impact on the full order closed-loop eigenvalue behaviour is also described.

1.5 A Controlled Experiment for ACOSS Design

Our previous efforts to design a control system to accommodate a broadband disturbance and achieve stringent line-of-sight (LOS) error requirements ([1-1] and Section 3 of this report) have achieved only partial success. Either the control design has met the LOS error requirement for the design model, but proved unstable when applied to the full-order LSS (adverse spillover effect); or spillover effect has been accommodated, only to fail to meet LOS error requirements. We attribute lack of success to certain mutual incompatibilities in the distinct processes of reduced-order model selection, sensor/actuator placement, and reduced-order controller design.

In Section 5, an account is given of a procedure we have devised to combine the various selection and design steps to simultaneously achieve spillover accommodation and meet LOS error requirements. We have not reported here on the progress made on the design itself. This will be discussed when the iterative procedure has converged into an acceptable design.

1.6 Perspective

An attempt is made to document major achievements and observations, even if they are merely stepping stones towards the design and implementation of identification and active control of LSS. Such stepping stones might be discarded in the study if they are found to have little merit.

Some work in progress has not been discussed in this report since it has not matured enough for documentation. In the context of identification for example, the procedures for recovering the mode amplitudes at the sensors, how amplitude information would be used to construct mode shapes, and our work in input-output characterization from measurement and the subject of input design have not been reported.

The discussion on actuator-structure dynamic interaction is the first, to our knowledge, in the ACOSS literature. It is the first step towards the rigorous analytic incorporation of actuators into models. More work is being done to evaluate its impact on ACOSS design.

SECTION 1
LIST OF REFERENCES

- 1-1 ACOSS Eleven Second Semiannual Technical Report, CSDL-R-1583, August 1982.

SECTION 2

STRUCTURE IDENTIFICATION--THE RESOLUTION PROBLEM AND ITS SOLUTION

2.1 Introduction

The organization of Section 2 is as follows. Section 2.1 discusses the background and difficulties encountered in structure identification problems and their solutions. Section 2.2 gives the background of the role of the sampling rate in system identification and spectral estimation. In Section 2.3, we discuss the effect of sampling rate on the fast Fourier transform (FFT). This is a rather straightforward discussion. Section 2.4 establishes the foundation for parametric spectral analysis for a sampled data stochastic process. The role of the sampling rate within the classical Nyquist constraints is discussed in Section 2.5. A zoom-in procedure is described in Section 2.6. Generic examples are brought in Section 2.7. The foregoing sections were devoted to narrowband signals. Section 2.8 describes a decimation technique to enable the analysis of broadband signals.

In applying identification to Draper model simulated data, we so far demonstrated limited success in the sense that we have successfully identified reduced-order models, where the reduction in order corresponds to a failure to resolve closely spaced modes. The decimation procedure and the zoom-in algorithm are presently being tested against Draper model structural data. Thus, the report of the experiment results is deferred for future documentation.

2.1.1 Background

One of the first tasks to be undertaken in the quest for large space structure (LSS) deployment and application is the establishment of procedures for modelling such structures. Analytical modelling, although an essential step, does not provide sufficient information for practical utilization of LSS for a few reasons.

- (1) Some phenomena, like the damping mechanism, high-frequency behavior, and joint dynamics, are not well understood, and thus cannot be reliably incorporated into analytical models.
- (2) LSSs are properly modelled by distributed parameter systems (partial differential equations). However, such models are often too difficult to construct, and are usually not amenable to control design. Furthermore, the state-of-the-art of identifying distributed parameter systems has not matured enough for routine applications. Hence, the usual models for LSS are of the lumped-parameter, finite-dimensional type. Such models can be derived using an approximation of the distributed parameter model, e.g., using finite-element techniques, or can be obtained directly from the physical structure, say, by representing it as a mesh of rigid

bodies subject to massless elastic constraints. The final model is often represented via the vibration equation

$$M\ddot{x} + D\dot{x} + Kx = f \quad (2-1)$$

The evaluation of such an approximation and the estimation of the unknown entities in Eq. (2-1) (e.g., the D matrix) will require the implementation of a parameter estimation technique, henceforth referred to as identification.

The problem of identification can be philosophically addressed from two points of view.

- (1) Model Validation--Construct an experiment and employ a procedure to estimate the parameters of a model constructed from physical considerations. For example, estimate the mass and stiffness matrices in Eq. (2-1). On a more fundamental level, estimate the elastic properties of the structure, such as Young's moduli.
- (2) Engineering Modelling--Estimate input/output characteristics of the "plant", i.e., the LSS response to actuator or disturbance forces as observed via a given set of sensors. Both actuators, sensors, and their dynamic characteristics and placement on the structure, might be determined based on control considerations using an analytical approximation of the plant.

Obviously, the two approaches are not disjoint. Information extracted from either approach might be utilized beneficially to construct the complementary model.

This section concentrates on the extraction of frequency/damping information from LSS measured data. Such information is the basis for constructing engineering models as discussed in Option 2 above.

2.1.2 Difficulties

There are a few features of LSS which hamper the extraction of frequency/damping information from experimental data.

- (1) The "Curse of Dimensionality"--As already discussed, LSSs are essentially infinite dimensional. Even if attention is restricted to the bandwidth of the sensors and actuators, the number of modes to be identified is still large. For example, Figure 2-1 gives the frequency response of Draper Model #2 to a 15-Hz disturbance. (See Reference 2-28 for more information.) The identification of a high-dimensional system has so far not been successfully demonstrated in the literature.
- (2) Closely Spaced Modes--The signal-processing literature has devoted a considerable amount of attention to constructing algorithms which are capable of estimating sinusoids with small frequency separations (closely spaced modes). As is obvious from Figure 2-1, this is a fundamental problem for LSS identification.

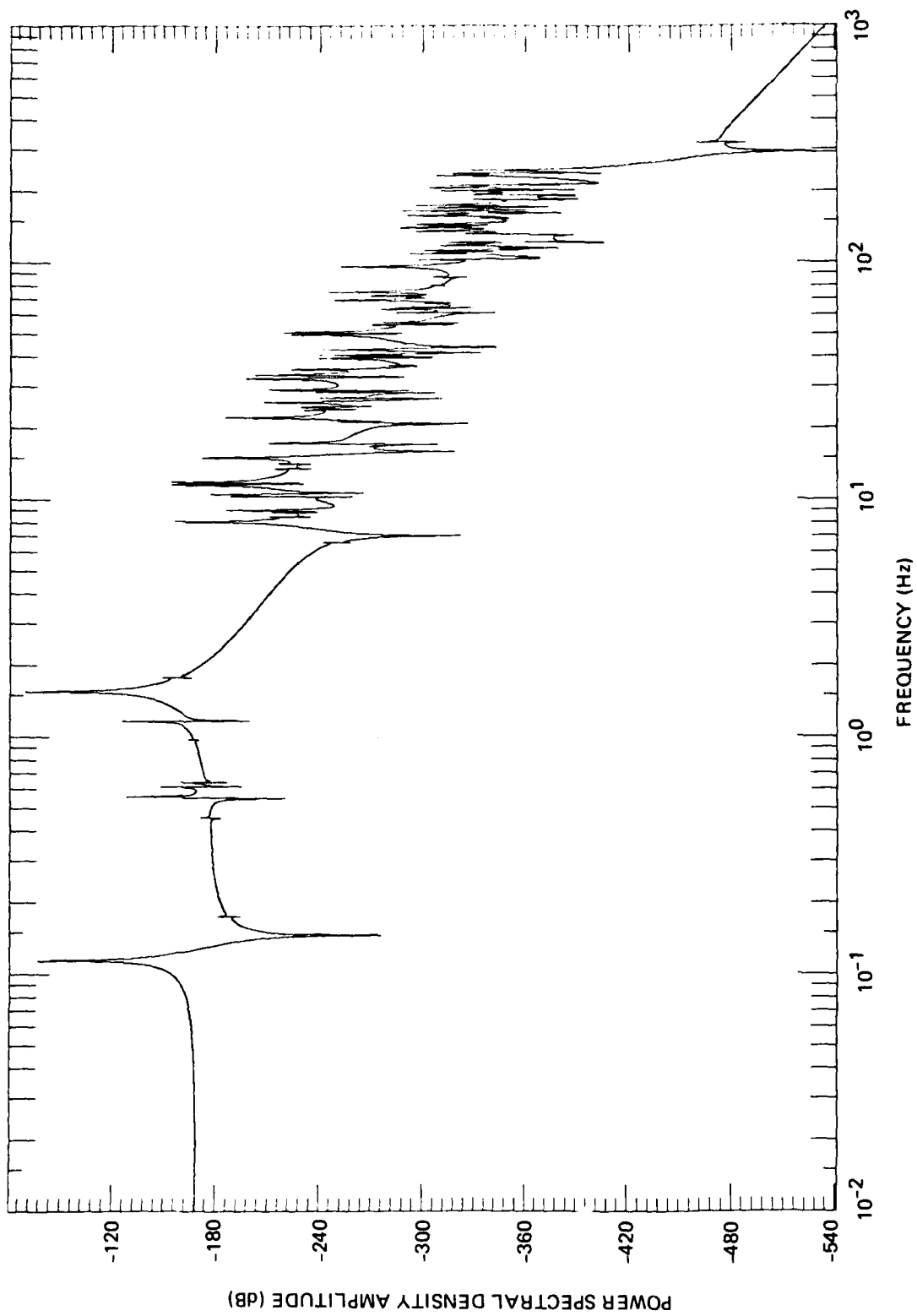


Figure 2-1. Draper model frequency response to 15-Hz disturbance.

- (3) Small Damping--The identification of poles close the the $j\omega$ axis has also been a challenge to the signal processor. The difficulty in estimating small damping is nicely explained in Reference 2-29 using statistical arguments. The damping ratios commonly assumed in the context of LSS are of the order of 0.1 to 1 percent.
- (4) High Process and Measurement Noise--The present state-of-the-art in sensor technology in the very low frequency range for LSS application suggests that the quality of measurements to be used in the identification process might require an estimation technique tailored for a high-noise environment.

One or more of the above-mentioned problems appear in a variety of identification applications. It is the culmination of all four difficulties which makes the identification of LSS especially challenging.

Difficulties (2) and (3) can be classified as spectral resolution problems. In this section, we report a novel approach to the high resolution spectral analysis problem developed at CSDL. The algorithm developed is especially suited for handling difficulties (2) and (3). However, it is also shown to be noise resilient. The modification of the algorithm to handle high dimensional models is also discussed.

Although we have developed our high resolution spectral analysis technique in the context of LSS identification, it should be noted that the procedure is valuable in any signal-processing application, where high resolution is desirable, as in radar signal processing or geophysical data analysis.

2.2 Spectral Estimation and Sampling

High resolution spectral estimation has been the subject matter of numerous recent publications in the signal-processing literature. The wide range of applications and the theoretical interest in the subject are reflected in the special issue on spectral estimation of the IEEE Proceedings [2-1].

In surveying the literature devoted to spectral estimation, we have found that the premise of most of the work is the availability of a sequence of uniformly sampled data points of a continuous (stochastic) process. The analysis and the subsequently constructed algorithms treat the discrete time process while ignoring the sampling rate issue.

It is the purpose of this section to demonstrate the crucial dependence of spectral resolution on the sampling rate. It is shown that by examining the sampling rate issue we obtain, using a computationally simple algorithm, spectral resolution as good as with other more complex procedures.

To be more specific in the discussion following, let

$$[y(t): 0 < t < t_f] ; t_f \text{ finite or } \infty$$

be the (stochastic) process to be analyzed. Digital spectral analysis is performed on the data

$$[y(kT): k = 0, 1, \dots, N] ; N \text{ finite or } \infty$$

Intuitively, the information contained in the data is inversely proportional to T . Furthermore, if the process is band-limited ($t_f = \infty$ in this case) by the Shanon interpolation formula, the data to represent the process if $T < T_{\text{Nyq}} = \pi/BW$, where Nyq abbreviates Nyquist, and $BW =$ bandwidth (in rad/s). Since t_f is usually finite, aliasing can be reduced only by choosing T to be as small as possible. We believe that these mathematically sound and intuitively appealing statements have hindered the use of T as a parameter in improving spectral resolution. Specifically, most of the work on spectral estimation is based on the availability of the sequence $[y(k)]$, i.e., T --the sampling interval is usually suppressed and subsequently ignored (e.g., Reference 2-1).

The sampling rate plays a role in nonparametric spectral estimation, though not as dramatic a role as in the parametric analysis. In Section 2.3, the role of T when spectral analysis is performed using the conventional discrete Fourier transform (DFT) will be discussed. The discussion is rather straightforward and probably would not surprise practitioners in the field. We bring up this result only for the sake of completeness.

The dramatic role of the choice of T is in the domain of parametric spectral estimation. Assuming t_f large enough to enable resolution, say, of two sinusoids in white noise, then the problem of resolution is fundamentally a numerical one. Namely, regardless of the sophistication and statistical soundness of an algorithm employed, if the frequency separation is small enough, the algorithm will fail. To demonstrate this point consider the following:

Example 1: We have applied covariance least squares* to 128 samples of

$$y(t) = \sin(\omega_1 t) + \sin(\omega_2 t) + v(t)$$

with 1-percent frequency separation, i.e., $\epsilon = (\omega_1 - \omega_2)/\omega_1 = 0.01$. For $v(t) \equiv 0$, the frequencies ω_1 and ω_2 were successfully identified. However, with $v(t)$ white Gaussian noise with $\text{Var}[v(t)] = 10^{-7}$, the algorithm failed.

The reason for this failure is explained in Section 2.5. In Section 2.4, the problem of parametric spectral estimation for sampled data is formulated and some modelling questions are discussed. Section 2.5 is devoted to

*This algorithm has been proposed by Beex and Scharf [2-2] and by Cadzow [2-3]. It will be further discussed in the following.

the question of spectral resolution as a function of the sampling rate for $T < T_{Nyq}$. In Section 2.6, a zoom-in procedure is described. The procedure allows for a choice, $T > T_{Nyq}$, for the purpose of resolving closely spaced frequencies. Our observations and algorithms are demonstrated via simulations in Sections 2.7 and 2.8. Section 2.9 contains concluding remarks.

2.2.1 Historical Perspective

Although we have failed to find articles addressing the impact of sampling rate on spectral resolution, the general problem of sampling rate in parameter estimation (system identification) has received attention in the literature.

We have found the most extensive treatment of the problem in the econometric literature. A compendium of results on the subject can be found in Bergstrom's book [2-4]. The main concern in the econometric work is the approximation, or the exact representation of continuous stochastic differential equations by difference equations. Consequently, an effort is made to assess the quality of the identification of the continuous equation as inferred from the estimation of the discrete approximation. This evaluation is performed via bias and variance evaluation for $T \rightarrow 0$. However, this work does not provide us with useful tools in the context of high resolution spectral analysis.

Some work on the sampling rate issue has been done and some practical experience gained by researchers in the system identification field. Notable is the work by Åström [2-5] Goodwin, Pain, and Zarrop [2-7]. Åström has analyzed a first-order stochastic process, the parameters of which are identified using maximum likelihood (ML) estimation employing the sampled data. He has shown that the error variance is minimized for the choice $T * \alpha = 0.797$ where α is the time constant of the process. Goodwin, et al., have addressed the problem of the experiment design, including sampling rate determination, data filtering, and optimal input design using measures of the information matrix. They have shown that with an anti-aliasing filter and a finite number of data points, the Fisher information matrix is inversely proportional to T , and thus, is maximized by the choice $T = (1 - \epsilon)T_{Nyq}$, ϵ being an arbitrarily small value. This result coincides with our observations in Section 2.3. However, it does not agree with our observations on parametric spectral estimation (Section 2.5 and 2.6) nor with practical considerations for spectral resolution.

We should note that practitioners of spectral estimation have often used good "rules of thumb" for obtaining high resolution, although we could not find the justification for this practice. For example, Bendat and Pearsol suggest ([2-8], page 288) $T = 0.5 T_{Nyq}$ if "the correlation function has frequencies near $1/(2T_{Nyq})$," and $T = 0.8 T_{Nyq}$ "if power spectra measurements are of prime consideration" (compare these to Sections 2.5 and 2.3, respectively). In the context of identification, Iserman [2-9] recommends $T = (5...15)*T_{95}$ where T_{95} is the 95-percent settling time of the transient function. This we found to be impractical for very low damping ratios.

Finally, an important result, noteworthy and relevant to our problem, was reported recently by Kay [2-10]: In estimating the autocorrelation function, the sampling rate should be at least twice the Nyquist rate ($T < 0.5 T_{Nyq}$), but statistically, there is insignificant gain in sampling faster than that rate. This result coincides with the Bendat-Pearsol recommendation cited previously and nicely complements our observation in Section 2.5.

2.3 Nonparametric Spectral Estimation

The most widely used tool in spectral analysis is the discrete Fourier transform implemented via the FFT algorithm on N samples of a continuous signal. Typical commercial spectrum analyzers [2-11 to 2-13] are based on $N = 2^{10} = 1024$ point FFT. In analyzing the effect of the sampling interval T on spectral resolution when using the FFT, the following facts should be noted.

- (1) The Fourier transform is represented by $N/2 + 1$ points spaced at frequency intervals $\Delta\omega = 2\pi/NT$. Thus, the relative resolution around a frequency ω_0 is

$$\Delta\omega/\omega_0 = 1/n$$

where n is the number of cycles of a sinusoid with frequency ω_0 .

- (2) The width of the main lobe associated with N points sampled with interval T is

$$\delta\omega = 4\pi/NT$$

Consider the signal of Example (1). The two frequencies are resolvable in light of the above facts if

$$T > T_{Nyq} \cdot 4 \cdot \frac{\omega_1}{N \cdot (\omega_1 - \omega_2)}$$

Thus for $N = 1024$ and $(\omega_1 - \omega_2)/\omega_1 = 0.01$, frequency resolution is attainable for $T > 0.391 T_{Nyq}$. Note, however, that aliasing the main lobe with itself is prevented if $T < T_{Nyq} \cdot \frac{N-2}{N}$ which is 0.2 percent faster than the Nyquist rate.

In the above discussion, we have completely ignored the effects of leakage which will require even tighter bounds than presented. From the above discussion, $0.688T_{Nyq}$ is the sampling rate required to resolve ω_2 from ω_1 if $\omega_2/\omega_1 = 9/11$ and $N = 32$. The FFTs for $T/T_{Nyq} = 0.3, 0.35, 0.45,$ and 0.975 are given in Figure 2-2.

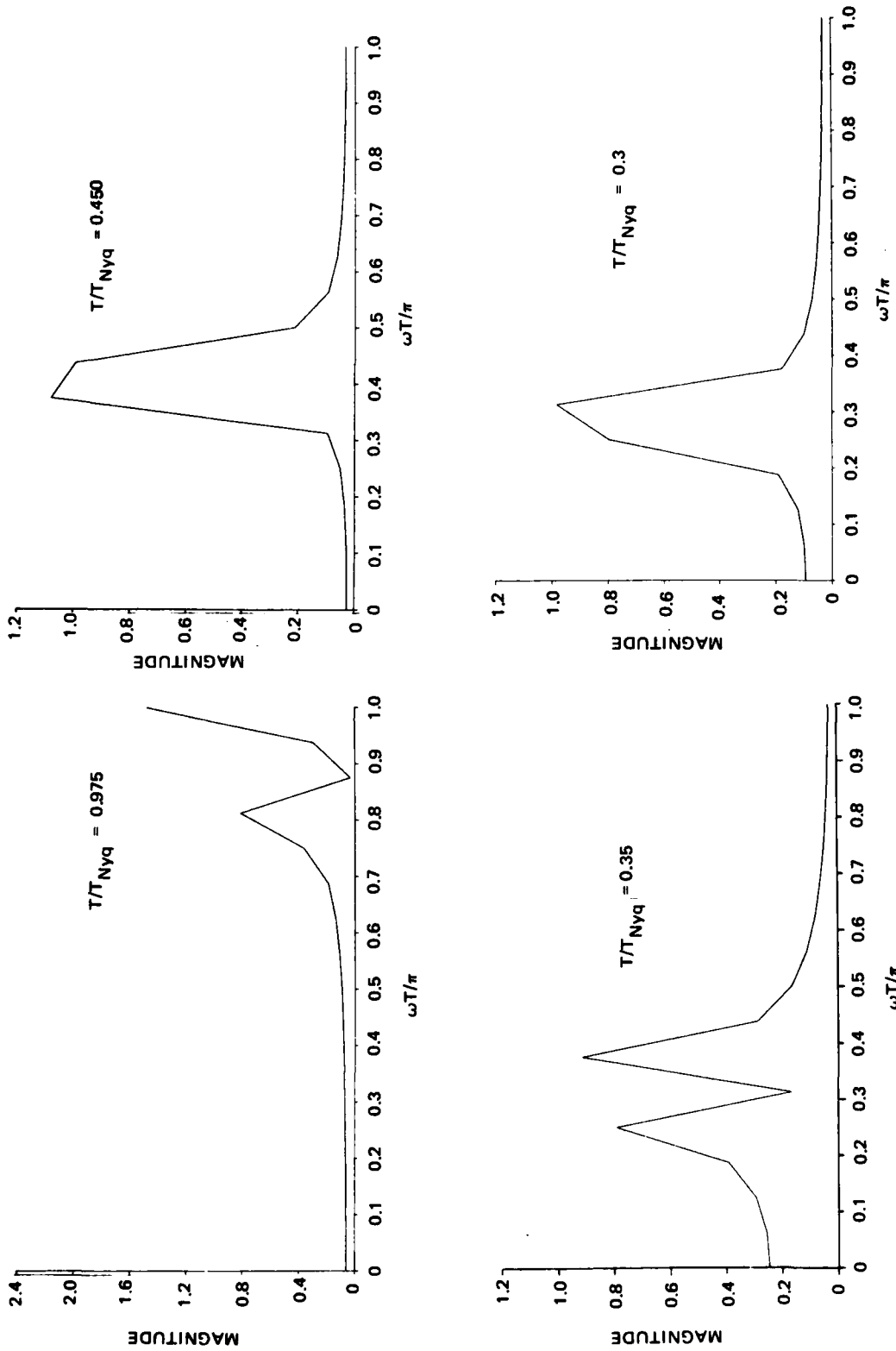


Figure 2-2. 32-point FFTs of 2 sinusoids with $\omega_1/\omega_2 = 9/11$.

The preceding discussion is admittedly rather elementary. We have presented it to illustrate the often overlooked upper bound on the sampling rate. Furthermore, it demonstrates in the frequency domain our main results to be derived below in the context of parametric spectral estimation.

It should be noted that the preceding results stem from the practical constraint on finite N . If N is not limited, T can be chosen arbitrarily small. However, even for $N \rightarrow \infty$ in the context of parametric spectral estimation, T should be carefully chosen.

2.4 Sampled Data Spectral Analysis

In this section, we shall establish the relationship between a continuous time stochastic process and the discrete time representation of its samples, which is appropriate for spectral estimation. Subsequently, the parametric spectral estimation problem is stated. This section is the basis for assessing the impact of the sampling rate on spectral analysis as presented in Sections 2.5 and 2.6.

2.4.1 Continuous and Discrete Models

System identification in general, and spectral estimation in particular, are usually based on the second-order statistics of the data. Thus, in determining a suitable discrete time representation of a continuous time process, a modelling criterion that Perl and Scharf call "covariance invariance" [2-14] plays a fundamental role. Covariance invariant models are discussed first.

It is assumed throughout this section that the discussed processes are wide sense stationary (WSS).

We shall use the subscripts "c" and "d" to denote continuous and discrete time entities respectively. Continuous time is denoted by τ , $\tau \in \mathbb{R}^+$ (the positive reals), and the discrete time by k , $k \in \mathbb{I}^+$ (the positive integers). k actually represents the time instant kT where T is the sampling interval being suppressed if it is not discussed explicitly.

A stochastic (continuous or discrete time) process with a rational spectrum can be formally represented in the state space via the state equation

$$D^* x(t) = A x(t) + \omega(t) ; \quad x \in \mathbb{R}^n, \omega \in \mathbb{R}^n \quad (2-2)$$

the output equation

$$y(t) = C x(t) ; \quad y \in \mathbb{R}^l \quad (2-3)$$

and the measurement equation

$$z(t) = y(t) + v(t) \quad (2-4)$$

Or, in terms of the impulse response convolved with the input $\omega(t)$

$$y(t) = h(t) * \omega(t) ; \quad z(t) = y(t) + v(t) \quad (2-5)$$

which corresponds to the transfer function representation

$$Y(q) = H(q) W(q) ; Z(q) = Y(q) + V(q) \quad (2-6)$$

$$H(q) = C(qI - A)^{-1}$$

The various entries in Eq. (2-2) to (2-6) are interpreted as follows:

<u>Term</u>	<u>Continuous Time</u>	<u>Discrete Time</u>
time t	$t \in \mathbb{R}^+$	$k \in \mathbb{I}^+$
D	differentiation $\frac{d}{dt}$	forward shift Z
ω, v	Wiener processes*	uncorrelated white noise
$h(t)$	$t \geq 0$ $h_c(\tau) = Ce^{A\tau} = \sum \alpha(i)e^{\lambda(i)\tau}$ $t < 0$ $h_c(\tau) = 0$	$h_d(k) = CA^k = \sum \alpha(i)\lambda(i)^k$ $h_d(k) = 0$
q	s = the Laplace transfer variable	z = the z transform variable

The input noise ω and the measurement noise v are assumed to be white and mutually uncorrelated with covariance matrices

$$E[\omega(t_1)\omega(t_2)'] = W\delta(t_1 - t_2)$$

$$E[v(t_1)v(t_2)'] = V\delta(t_1 - t_2)$$

where $\delta(t)$ is the Dirac delta function in the continuous time case, and a Kronecke delta in the discrete time case.

Of special interest is the output covariance function associated with Eq. (2-2) and (2-3), i.e., $R_{yy}(\tau) = E[y(t_1)y(t_1 + \tau)']$

$$R_c(\tau) = \begin{cases} Ce^{-A\tau}V_cC' & \tau < 0 \\ CV_c e^{A'\tau}C' & \tau > 0 \end{cases} \quad R_d(k) = \begin{cases} CA^{-k}V_dC' & k < 0 \\ CV_d(A')^kC' & k > 0 \end{cases} \quad (2-7)$$

(Note that in (2-7) we have replaced the subscript yy by d or c to indicate discrete or continuous time.)

* We are using here formally and somewhat loosely constructed, the representation of the continuous stochastic process. More precise treatment can be found in Reference 2-7.

$V = E[x(t)x(t)']$ is the state covariance matrix, satisfying the Liapunov equation

$$A_c V_c + V_c A_c' + R_{\omega\omega} = 0 \quad V_d = A_d V_d A_d' + R_{\omega\omega} \quad (2-8)$$

or equivalently

$$V_c = \int_0^{\infty} e^{A_c \tau} R_{\omega\omega} e^{A_c' \tau} d\tau \quad V_d = \sum_{k=0}^{\infty} A_d^k R_{\omega\omega} (A_d')^k \quad (2-9)$$

In terms of the impulse response and the transfer function we have

$$R_c(\tau) = \int_{t=0}^{\infty} h_c(t) R_{\omega\omega} h_c(t + \tau)' dt \quad R_d(k) = \sum_{\ell=0}^{\infty} h_d(\ell) R_{\omega\omega} h_d(\ell + k)' \quad (2-10)$$

$$= \sum_{i=1}^n \beta_c(i) e^{\lambda_c(i)\tau} \quad = \sum_{i=1}^n \beta_d(i) \lambda_d(i)^k \quad (2-11)$$

$$= \frac{1}{2\pi j} \int H_c(-s) R_{\omega\omega} H_c(s)' e^{s\tau} ds \quad = \frac{1}{2\pi j} \int H(z^{-1}) R_{\omega\omega} H(z)' z^{k-1} dz \quad (2-12)$$

where the coefficients $\beta(i)$ satisfy

$$\beta_c(i) = - \sum_{j=1}^n \alpha_c(i) R_{\omega\omega} \alpha_c(j)' / [\lambda_c(i) + \lambda_c(j)] \quad (2-13)$$

$$\beta_d(i) = \sum_{j=1}^n \alpha_d(i) R_{\omega\omega} \alpha_d(j)' / [1 - \lambda_d(i)\lambda_d(j)]$$

Definition: (Rephrasing [2-14]). A WSS discrete time stochastic process is T-covariance invariant (TCI) with its continuous counterpart if

$$R_c(kT) = R_d(k) \quad \forall k \quad (2-14)$$

In this section we shall not delve into the theory of covariance invariance, but rather state a few facts (without proof) which can be derived from Eq. (2-3) to (2-14).

Let $\Sigma_d = (A_d, C_d, B_d)$ and $\Sigma_c = (A_c, C_c, B_c)$ be the triplets characterizing a discrete time and a continuous time stochastic process as defined above. Here, B_d and B_c represent the square root of R_{ww} - the input covariance matrix for the discrete time and continuous time cases, respectively. We ignore R_{vv} since its inclusion is straightforward.

Fact A Σ_d is T covariance invariant with Σ_c if the following are satisfied

$$A_d \stackrel{\cdot}{=} e^{A_c T} \quad (\text{necessary condition}) \quad (2-15)$$

$$C_d \stackrel{\cdot}{=} C_c \quad (2-16)$$

$$C_d V_d \stackrel{\cdot}{=} C_c V_c \quad (2-17)$$

where $\stackrel{\cdot}{=}$ means equality up to a similarity transformation. Equations (2-16) and (2-17) give sufficient conditions. It is not clear that Eq. (2-16) and (2-17) are necessary.

Fact B Let Eq. (2-15) through (2-17) be satisfied. A necessary condition for the existence of Σ_d , which is covariance invariant with Σ_c , is

$$\rho(B_d) = \rho(C_c) \quad (2-18)$$

where $\rho(A)$ denotes the rank of A.

Fact B follows from stochastic realization theory and from the spectral factorization theorem [2-7]. This statement imposes a condition on the minimum number of uncorrelated inputs which are required to realize a discrete time covariance invariant representation of a continuous WSS stochastic process. Note, in particular, that replacing Eq. (2-17) by $V_c = V_d$ [2-14] implies $\rho(B_d) = n$. Fact B has ramifications beyond the scope of this section and will be discussed in a separate publication.

Fact C Let $\rho(C_c) = \rho(B_d) = 1$ (Single Output and thus Single Input by Fact B). The relative degree of $H_d(z^{-1})$, which is T covariance invariant with $H_c(s)$, is almost always one.

Fact C is a crucial observation which is too often overlooked in the system identification/spectral estimation literature. It implies simply that autoregressive (AR) models, and hence, the Yule-Walker equation and the maximum entropy method as in [2-15], are not appropriate techniques for spectral estimation of sampled data. Any failure of these methods in spectral estimation of "two sinusoids in white noise" should first of all be attributed to the wrong formulation of the estimation problem rather than to a deficiency in

these algorithms. Note, however, that an autoregressive moving average ARMA (n,m) can be approximated by an AR(N) process with $N \gg n$, and thus, a methodology for spectral estimation developed for AR models can be applied to ARMA models by considering high order models.

2.4.2 Problem Formulation

With the above background, we are ready to state the parametric spectral estimation problem.

Main Problem: Assume the sequence $[z(kT): k = 0, 1, \dots, N]$ represents or can be closely approximated by Eq. (2-2) to (2-3). (See Reference 2-2.) Estimate Σ_c .

The above problem can be broken into two

Subproblem 1: Suppress T. Estimate Σ_d . Denote the estimate by $\hat{\Sigma}_c$.

Subproblem 2: Given $(\hat{\Sigma}_d(T))$, evaluate a TCI $\hat{\Sigma}_c$.

Our main concern is usually in estimating the following

(1) The system eigenvalues

$$\lambda_c(i) = -\zeta(i)\omega(i) + j(-1)^i \omega(i) ; \omega(2i) = \omega(2i - 1) : i = 1 \dots 2\ell_1$$

$$\lambda_c(i) = -\sigma(i) : i = 2\ell_1 + 1 \dots \ell_2 ; 2\ell_1 + \ell_2 = n$$

n being the assumed or estimated order.

(2) The system input output matrices B_c, C_c where $B_c B_c' = R_c$.

Note that by a proper transformation to canonical form, C_c can be assumed known. Furthermore, recall that there exists B_c such that $\rho(B_c) = \rho(C_c)$, which solves the problem at hand.

In the following sections, we shall concentrate on Subproblem 1 and the role of T in its solution, and on Subproblem 2(1). The problem of estimating the structure of Σ_c is beyond the scope of this section. We shall only consider here the problem of spectral estimation under the assumption of a single input/single output (SISO) system driven by white noise. In this context, the estimation of closely spaced modes and the dependence of the estimation on T is our main concern. This yields the formulation of the problem via Eq. (2-11), i.e., we assume (like Beexe and Scharf [2-2]) that the covariance function of the WSS process measured can be represented, or can be closely approximated, by a finite linear combination of stable exponential functions.

2.5 The Role of Sampling Rate

Assuming the covariance sequence to be as defined in Eq. (2-11) for the SISO case, i.e.

$$R_d(k) = \sum_{i=1}^n \beta_d(i) \lambda_d(i)^{|k|} \quad k = 0; \pm 1; \pm 2 \quad (2-19)$$

we have the recursive relation

$$R_d(\ell) = \sum_{i=1}^n a(i) R_d(\ell - i) \quad \ell \geq n \quad (2-20)$$

Rewriting Eq. (2-20) L times, i.e., $\ell = n, n+1, \dots, n+L-1$, where $L \geq n$, we obtain in matrix form

$$\underline{R}(0, n, L) \cdot \underline{a}(n) = \underline{R}(n, L) \quad (2-21)$$

where $\underline{R}(j, n, L)$ is the $n \times L$ Toeplitz matrix defined as

$$\underline{R}(j, n, L) \triangleq \begin{bmatrix} R(j+n-1) & R(j+n-2) & \dots & R(j) \\ R(j+n) & R(j+n-1) & & \cdot \\ \cdot & & & \cdot \\ \cdot & & & \cdot \\ R(j+n+L-2) & \cdot & \cdot & R(j+L-1) \end{bmatrix} \quad (2-22)$$

and the vectors $\underline{a}(n)$ and $\underline{R}(n, L)$ are

$$\underline{a}(n) = [a(1) \dots a(n)]' \quad (2-23)$$

$$\underline{R}(n, L) = [R(n) \dots R(n+L-1)]' \quad (2-24)$$

Equations (2-20) to (2-24) are the basis for many parametric spectral estimation techniques [2-2, 2-3, 2-16 through 2-18]. Since Eq. (2-19) is often an approximate relation, and since the covariance sequence is often obtained from the measurements of a sample pass of the WSS ergodic stochastic process, a reasonable approach to the spectral estimation problem is that of solving Eq. (2-20) to (2-24) using a large L . By solving the equations, we mean solving in the least-squares sense, where one allows for weighting on the equations using the weighting matrix W , i.e.

$$\hat{\underline{a}} = \underline{R}(0, n, L)_W^\dagger \cdot \underline{R}(n, L) \quad (2-25)$$

where

$$\mathbf{R}_w^{\dagger} = (\mathbf{R}^T \mathbf{W} \mathbf{R})^{-1} \mathbf{R}^T \mathbf{W} \quad (2-26)$$

The following observations can be made.

- (1) If the process is an AR process (an unlikely event in the case of sampled data), Eq. (2-20) to (2-24) are valid for all ℓ . Writing the equations for $\ell = 1 \dots n$, and taking advantage of the symmetry $R(i) = R(-i)$, yield the celebrated Yule-Walker equations and estimation procedures which are recursive in order.
- (2) Assuming an ARMA (n,m) model, i.e.

$$y(k) = \sum_{i=1}^n a(i)y(k-i) + \sum_{i=0}^m b(i)\omega(k-i) \quad (2-27)$$

we have Eq. (2-20) to (2-24) satisfied for $\ell > m$. Using the instrumental variable (IV) approach to system identification [2-19] with $\{y(k-\ell)\}; \ell = m+1 \dots m+n\}$ as the "instrument", and assuming the approximation

$$R(k) = \frac{1}{N} \sum_{i=1}^N y(i) y(i+k) ; y(j) = 0 \forall j \leq 0 \quad (2-28)$$

we have another way of justifying Eq. (2-20) through (2-26). In particular, for the AR case ($m = 0$) the least-squares procedure is equivalent to the IV procedure, which is equivalent (with Eq. (2-28)) to the Yule-Walker equations.

- (3) To accommodate the inaccuracies in the values of $R(\cdot)$ used in Eq. (2-20) through (2-24), one has to solve a structured total least-squares problem. This subject is addressed in Reference 2-20.
- (4) If $\{z(\cdot)\}$, rather than $\{y(\cdot)\}$, is used in estimating $\{R(\cdot)\}$, $R(1, n, L)$ and $R(n+1, L)$ should be used in Eq. (2-25) and (2-26).

Since our main concern is using the sampling rate to improve resolution, we consider here the case

$$\lambda_d(i) = e^{\lambda_c(i)T} ; i = 1 \dots n \quad (2-29)$$

where

$$\lambda_c(2i-1) = \bar{\lambda}_c(2i) = -\zeta_i \omega_i + j\omega_i ; i = 1 \dots n/2$$

$\bar{\lambda}$ denotes the complex conjugate of λ , ζ_i being the i^{th} damping ratio and ω_i the i^{th} frequency.*

Assuming

$$T < T_{\text{Nyq}}, \quad (T \cdot \omega_i < \pi \forall i) \quad (2-30)$$

we proposed the following criterion for choosing T

Definition: The optimal sampling period T^* ($T^* < T_{\text{Nyq}}$) satisfies

$$\kappa[R(0, n, L)(T^*)] \leq \kappa[R(0, n, L)(T)] \quad \forall T < T_{\text{Nyq}} \quad (2-31)$$

where $\kappa[A]$ is the condition number (CN) of the matrix A . (See References 2-21 through 2-24 for definition and properties of κ .)

Note the explicit dependence of R on T induced by the substitution of Eq. (2-29) into (2-19), and subsequently into R as defined in Eq. (2-22).

Rationale: Although the choice of the optimal sampling rate, T^* , as defined above, and the modification to be discussed in Section 2.6 are based on a concept from numerical analysis--the condition number--it should be stressed that the reason for defining T^* that way lies in the domain of estimation theory. If the covariance sequence were known exactly, if Eq. (2-20) through (2-24) were satisfied exactly, and if the computer used to solve the set of equations, say via Eq. (2-25), was of infinite precision; the solution, i.e., the vector \underline{a} and the corresponding set of eigenvalues $[\lambda_d(i)]$, could be determined (estimated) with no error. Unfortunately, none of the above suppositions are valid, the computer accuracy being the lesser evil.

The inaccuracy in the representation (Eq. (2-20) through (2-24)) is handled rather routinely by applying the least-squares concept to a large number of equations, i.e., taking L large in Eq. (2-20) through (2-24). The most severe obstacle to the spectral estimation is induced by the inaccuracy of the entries to the matrix $R(0, n, L)$ in Eq. (2-22). This inaccuracy stems from using the estimated covariance sequence. In solving a set of linear equations like Eq. (2-22), perturbation of the coefficient matrix ($R(0, n, L)$) has a severe consequence on the solution, if and only if this perturbation is of the order of the inverse condition number (ICN) of the matrix [2-23]. Closely spaced modes are shown in the following to cause the matrix to be numerically rank degenerate [2-23] (i.e., to have a small ICN). Hence, our objective as stated above is to minimize this negative effect.

* In the engineering context, the convention is to consider the second-order equation, $\lambda^2 + 2\zeta\omega\lambda + \omega^2 = 0$, which gives $\lambda = -\zeta\omega \pm j\omega\sqrt{1 - \zeta^2}$, as opposed to the present convention. For $\zeta \ll 1$, the above is a close approximation.

The actual procedure for solving Eq. (2-22), say, via Eq. (2-25), (2-26), or by using a numerical procedure based on the singular value decomposition (SVD), or the QR factorization [2-22], is of secondary importance.

To demonstrate the preceding discussion and to establish rules for choosing T^* , we analyze the two sinusoid cases, i.e., let

$$R(\tau) = \beta_1 \cos \omega_1 \tau + \beta_2 \cos \omega_2 \tau ; \beta_1 + \beta_2 = 1, \beta_1 > 0$$

with the corresponding sampled covariance sequence

$$R(k) = \beta_1 \cos (\omega_1 T k) + \beta_2 \cos (\omega_2 T k) ; \omega_2 > \omega_1$$

We thus obtain ($n = 4$)

$$\mathbf{R}(0,4,4) = \mathbf{A}_d^3 \mathbf{R}(-3,4,4)$$

where, taking advantage of the symmetry $R(-j) = R(j)$

$$\mathbf{R}(-3,4,4) = \begin{bmatrix} R(0) & R(1) & R(2) & R(3) \\ R(1) & R(0) & R(1) & R(2) \\ R(2) & R(1) & R(0) & R(1) \\ R(3) & R(2) & R(1) & R(0) \end{bmatrix}$$

and \mathbf{A}_d is the state transition matrix of the process in companion form

$$\mathbf{A}_d = \begin{bmatrix} 0 & & & \\ \cdot & & & \\ \cdot & & \mathbf{I} & \\ \cdot & & & \\ 0 & & & \\ \hline a(4) \dots a(1) \end{bmatrix}$$

it follows from the definition of the condition number that

$$1 \leq \max \left[\frac{\kappa(A)}{\kappa(B)} ; \frac{\kappa(B)}{\kappa(A)} \right] \leq \kappa(AB) \leq \kappa(A) \cdot \kappa(B)$$

Hence, if A is a well-conditioned matrix ($\kappa(A)$ is "small"), AB is ill-conditioned if and only if B is ill-conditioned. Since \mathbf{A}_d is a well-conditioned matrix, it suffices to consider $\kappa[\mathbf{R}(-3,4,4)]$. We prefer to discuss $\mathbf{R}(-3,4,4)$, since we can derive analytical expressions for its condition number.

Some algebra, taking advantage of the symmetric Toeplitz structure of $\mathbf{R}(-3,4,4)$, yields the ICN

$$1/\kappa[R (-3,4,4) = \min (\lambda_1, \lambda_2)$$

$$\lambda_1 = 1 + \frac{R(1) + R(3)}{2} - \frac{1}{2} \{ [R(1) - R(3)]^2 + 4[R(1) + R(2)]^2 \}^{1/2}$$

$$\lambda_2 = 1 - \frac{R(1) + R(3)}{2} - \frac{1}{2} \{ [R(1) - R(3)]^2 + 4[R(1) - R(2)]^2 \}^{1/2}$$

Assuming $T < T_{\text{Nyq}}$, and closely spaced modes $(\omega_2 - \omega_1)/\omega_2 \ll 1$, the ICN can be shown (using standard approximation techniques) to be of the order of $[(\omega_2 - \omega_1)T]^2$. Furthermore, if $R (-3,4,4)$ is rank degeneration [2-23] for $T \approx T^*$, it is seen that the numerical rank of R is two, i.e., only one sinusoid describes the data. As $T \rightarrow 0$, the numerical rank approaches 1. Note that for $T \approx 0$, the perfect predictor is $\hat{y}[(k+1)T] = y(kT)$ which corresponds to rank one covariance matrix. Plots of the ICN for few values of ω_1 , ω_2 , β_1 , and β_2 are given in Figures 2-3 through 2-11. Figure 2-12 gives the value of T^* (normalized by T_{Nyq}) as function of the frequency ratio. We note that as ω_1/ω_2 approaches one, the dependence of T^* on β_1 and β_2 diminishes. Furthermore, it is seen that $\frac{\omega_1 + \omega_2}{2} T^* \approx \frac{\pi}{2}$ for high ω_1/ω_2 . We propose the following "rule of thumb" for selecting the sampling rate

$$\bar{T} = \pi/(\omega_1 + \omega_2) \quad (2-32)$$

instead of T^* . It follows that \bar{T} satisfies the following properties (see Tables 2-1 through 2-4)

- (1) \bar{T} is a good approximation of T^* , except for $\omega_1/\omega_2 < 1/3$.
- (2) $\kappa[R (\bar{T})] \approx \kappa[R (T^*)]$, except for small frequency ratio and large β_1 (i.e., large frequency separation and the signal energy concentrated at the lower frequency).
- (3) For $\omega_1/\omega_2 < 1/3$, \bar{T} poorly approximates T^* , but $\kappa^{-1}[R (\bar{T})]$ is sufficiently large to enable good estimation of ω_1 , ω_2 via Eq. (2-25) and (2-26).

To summarize, we note that the choice \bar{T} as in Eq. (2-32) provides good resolution when Eq. (2-25) and (2-26) are used as the means for spectral estimation. In particular, for $\frac{\omega_2 - \omega_1}{\omega_2} \ll 1$ we have

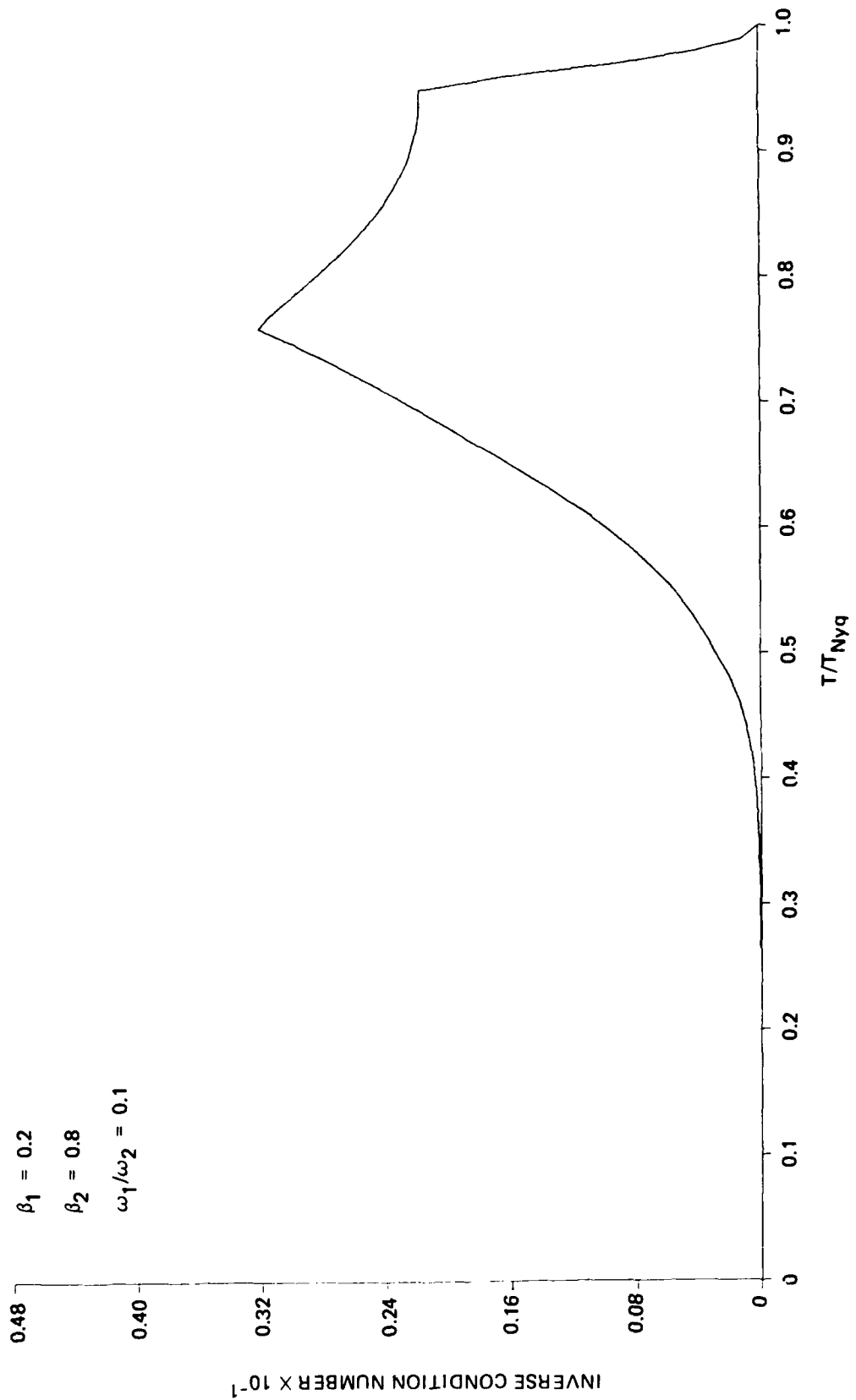


Figure 2-3. ICN vs. T/T_{Nyq} .

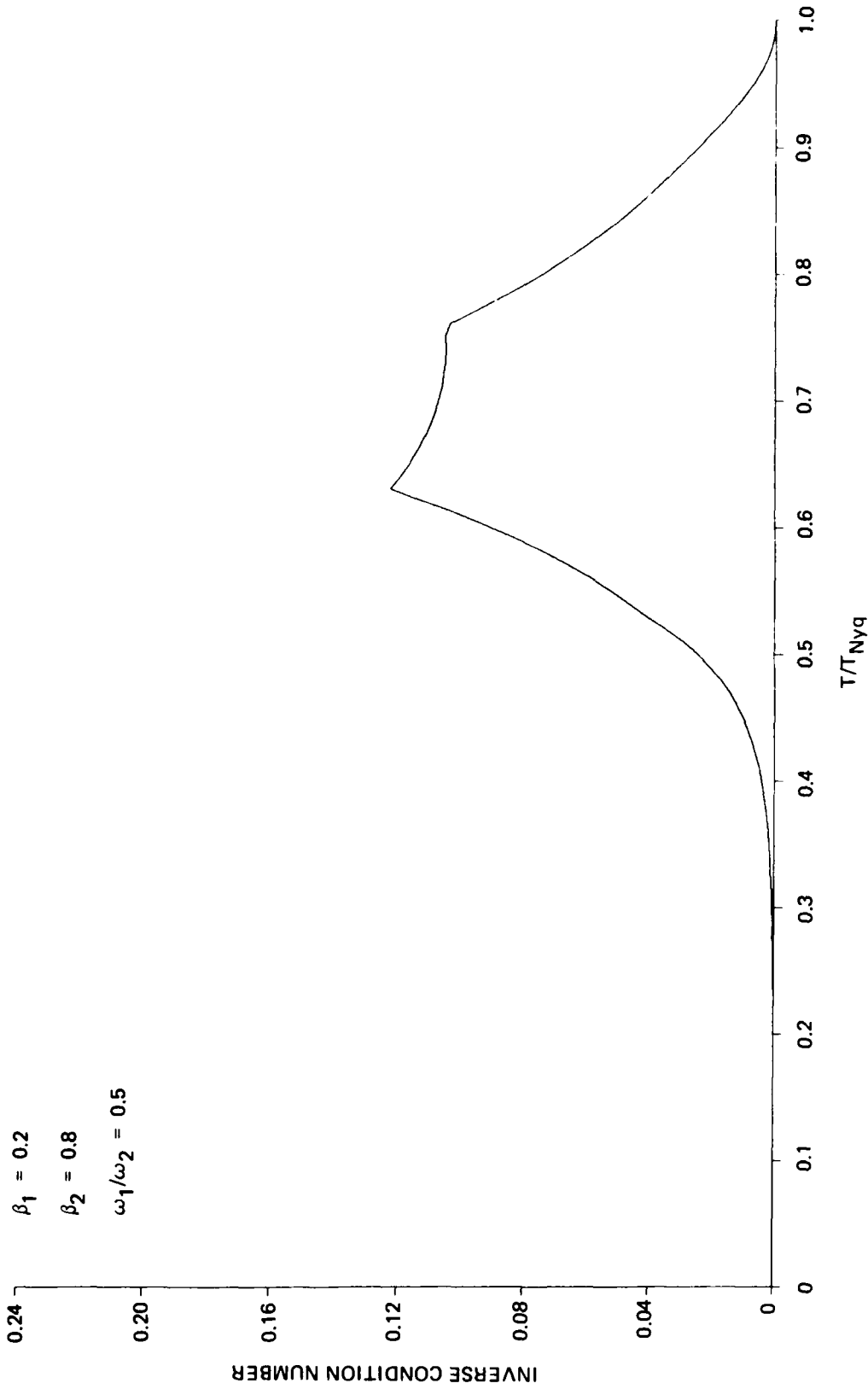


Figure 2-4. ICN vs. T/T_{Nyq} .

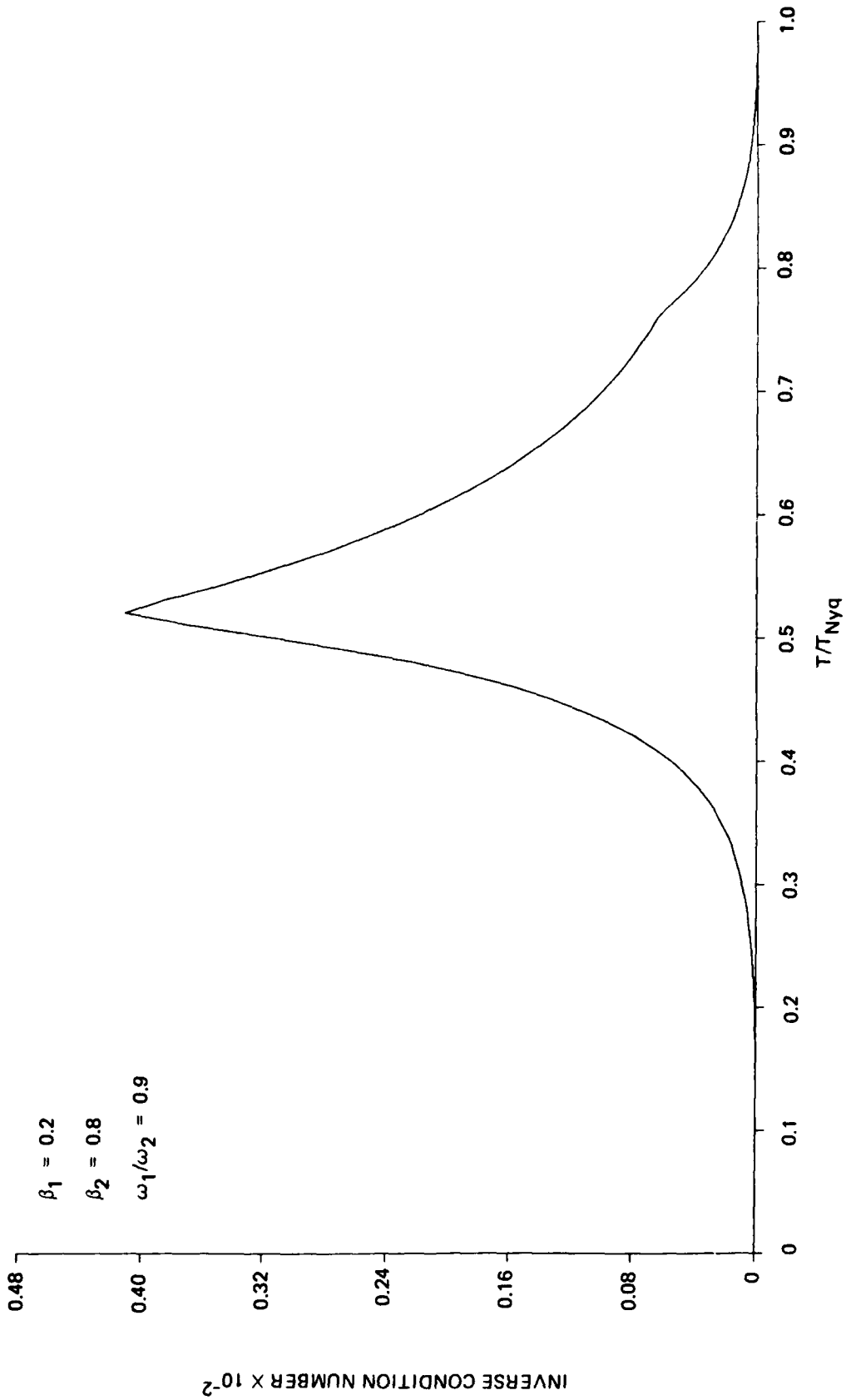


Figure 2-5. ICN vs. T/T_{Nyq} .

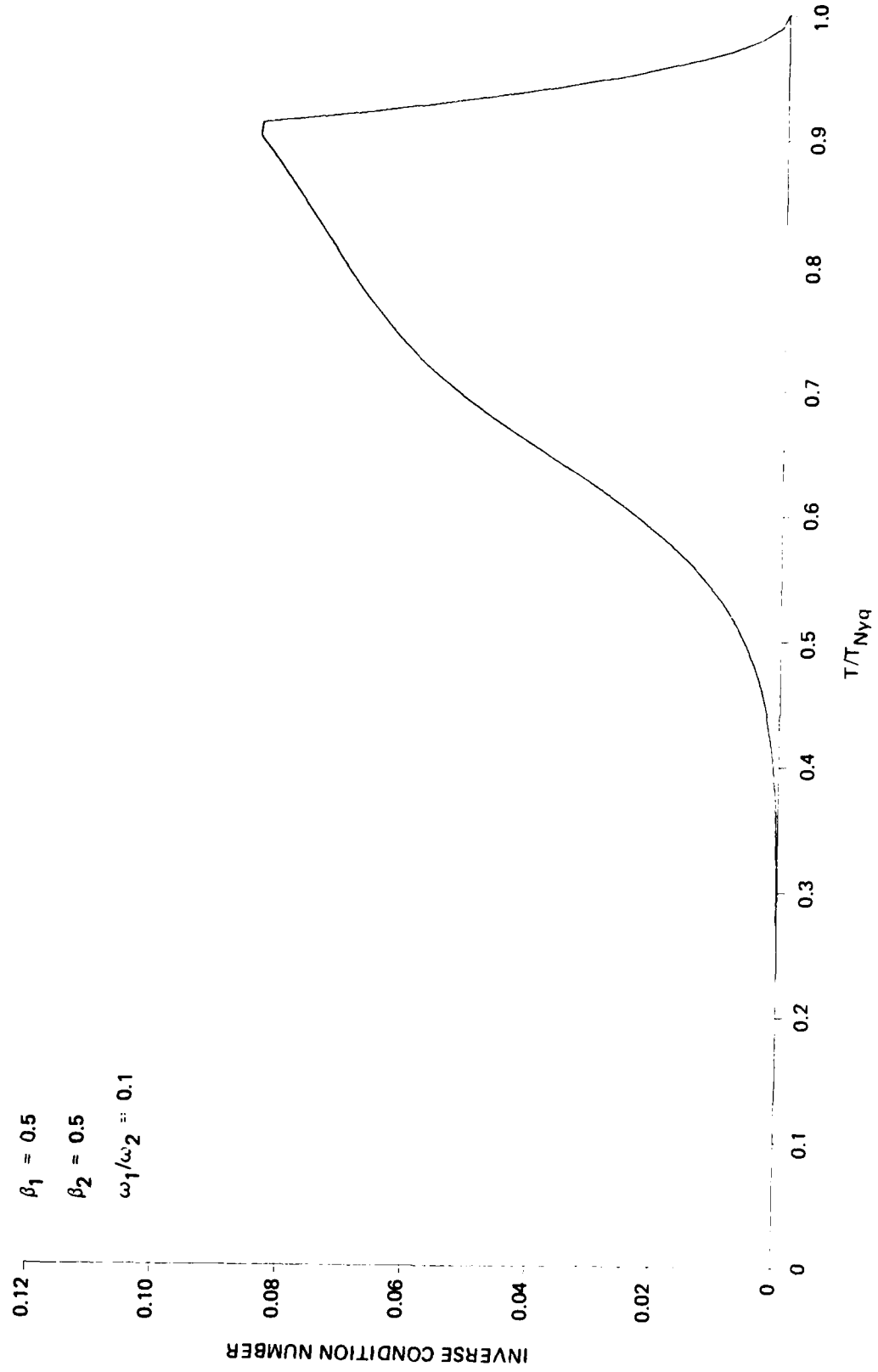


Figure 2-6. ICN vs. T/T_{Nyq} .

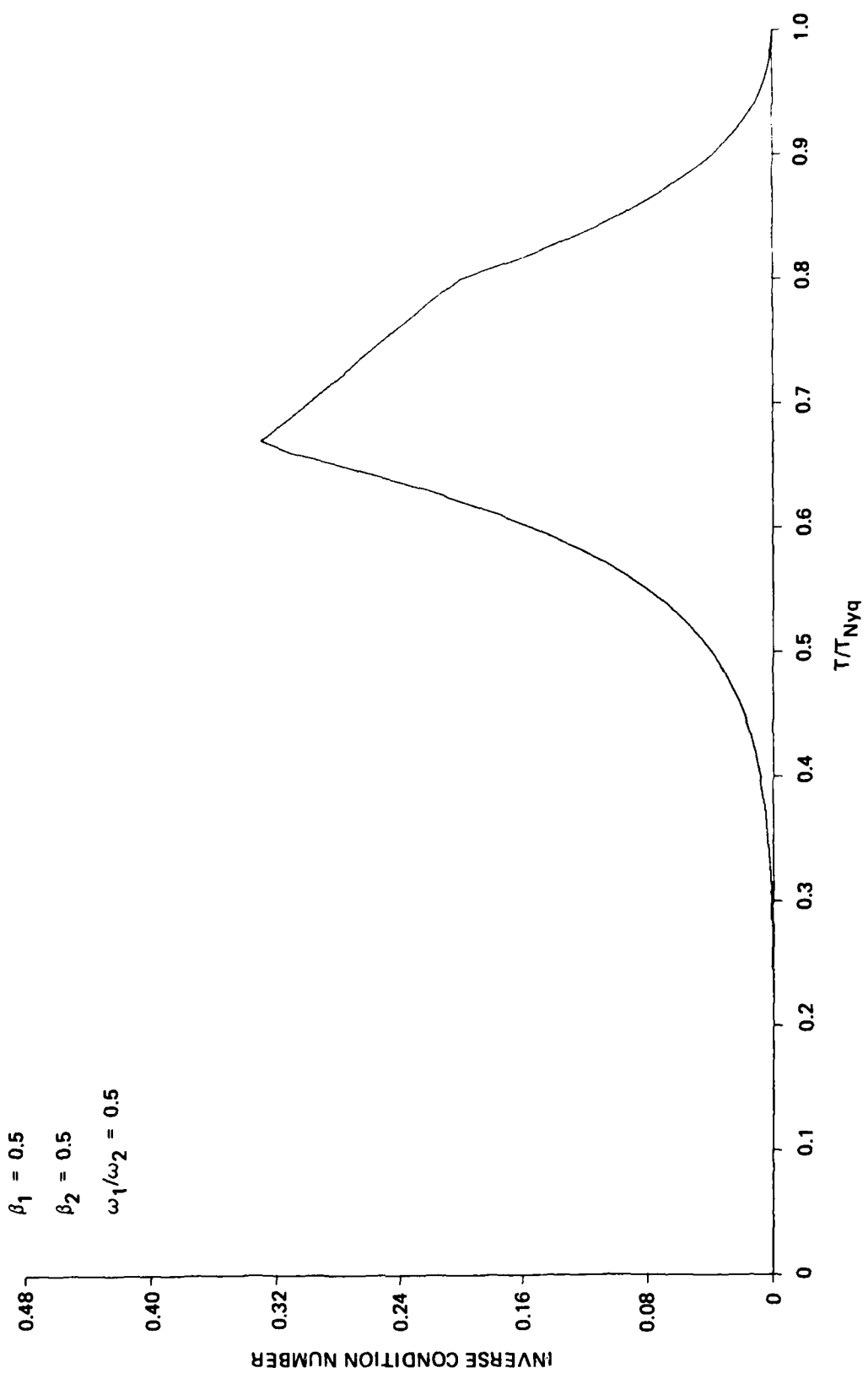


Figure 2-7. ICN vs. T/T_{Nyq} .

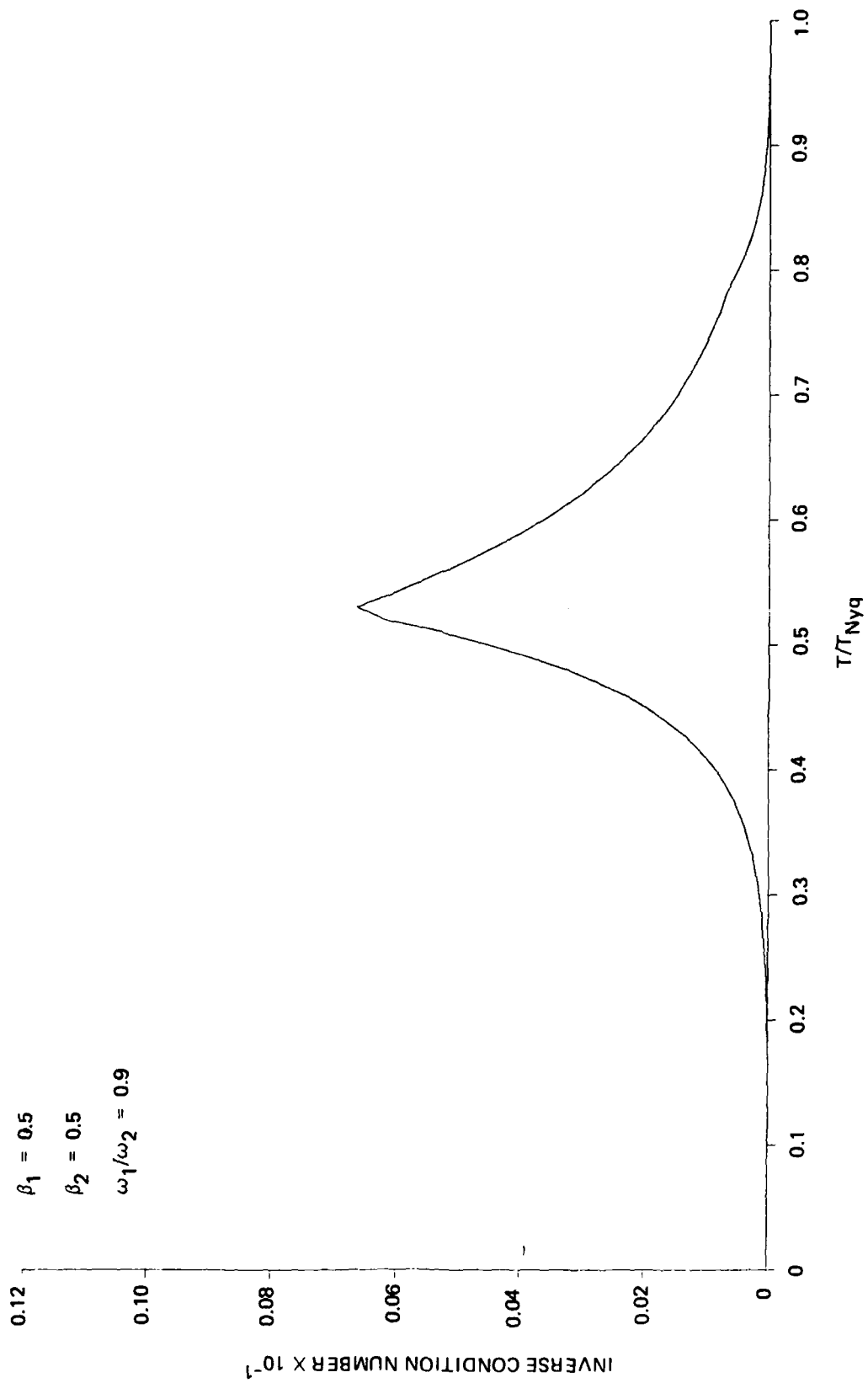


Figure 2-8. ICN vs. T/T_{Nyq} .

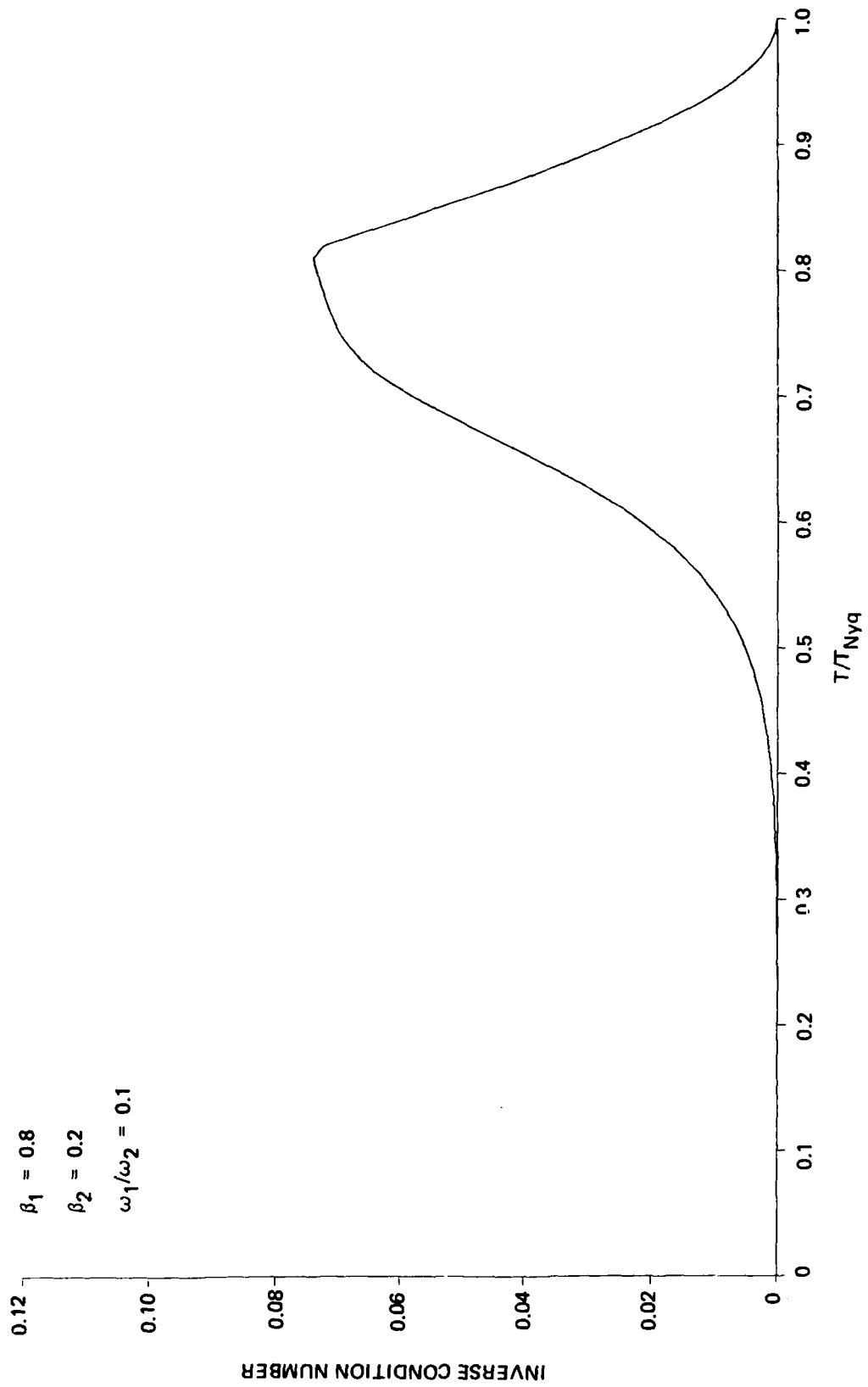


Figure 2-9. ICN vs. T/T_{Nyq} .

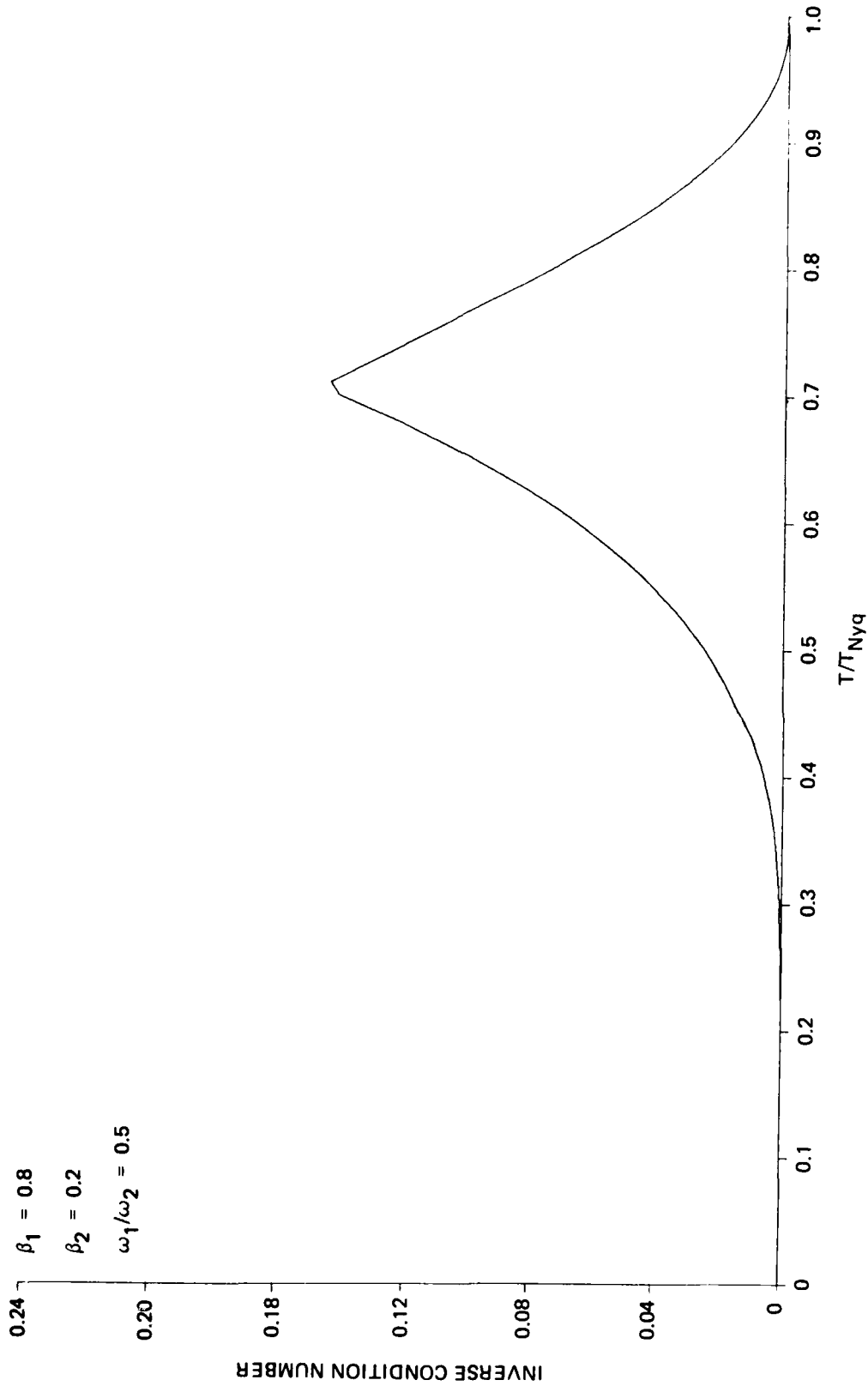


Figure 2-10. ICN vs. T/T_{Nyq} .

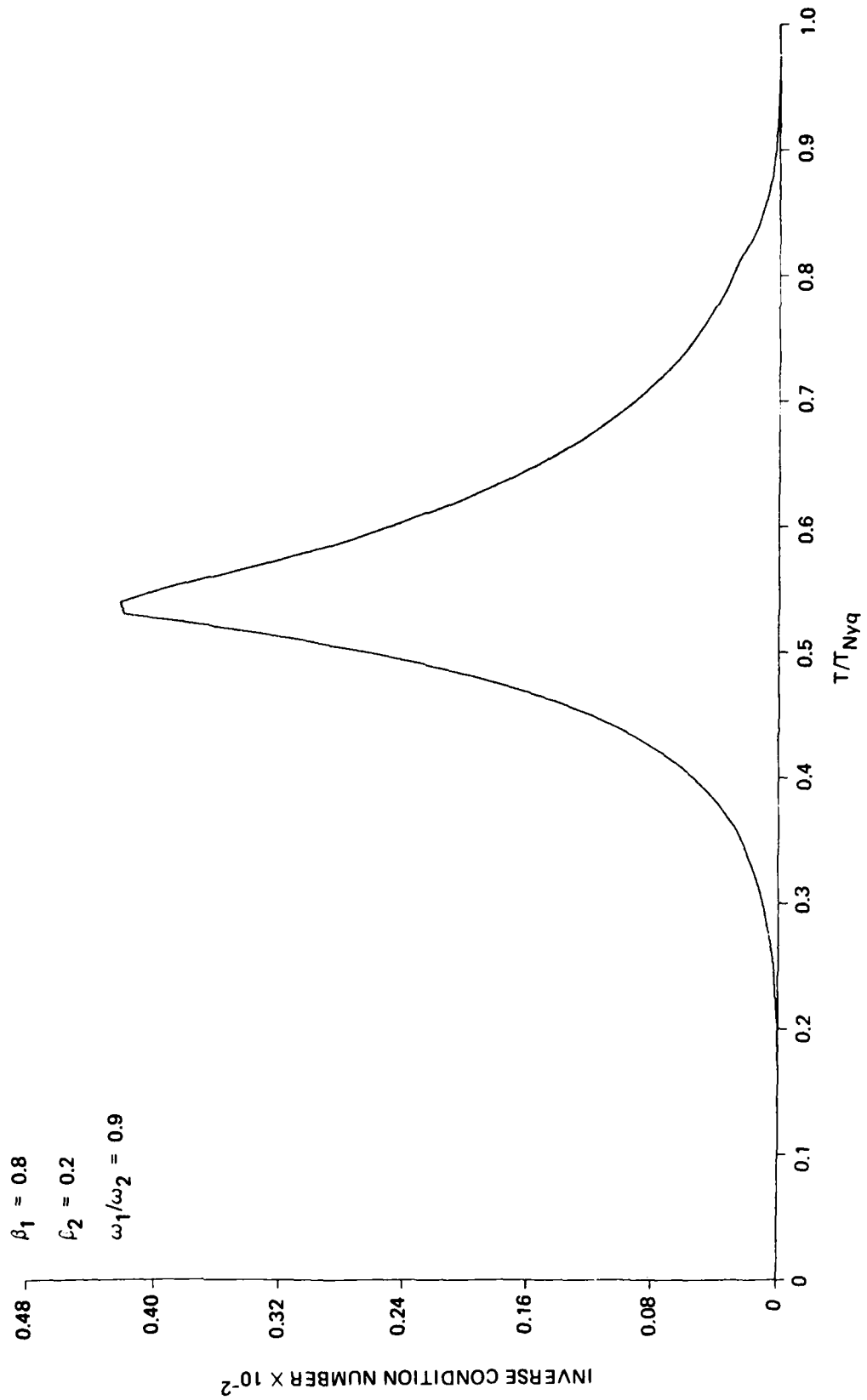


Figure 2-11. ICN vs. T/T_{Nyq} .

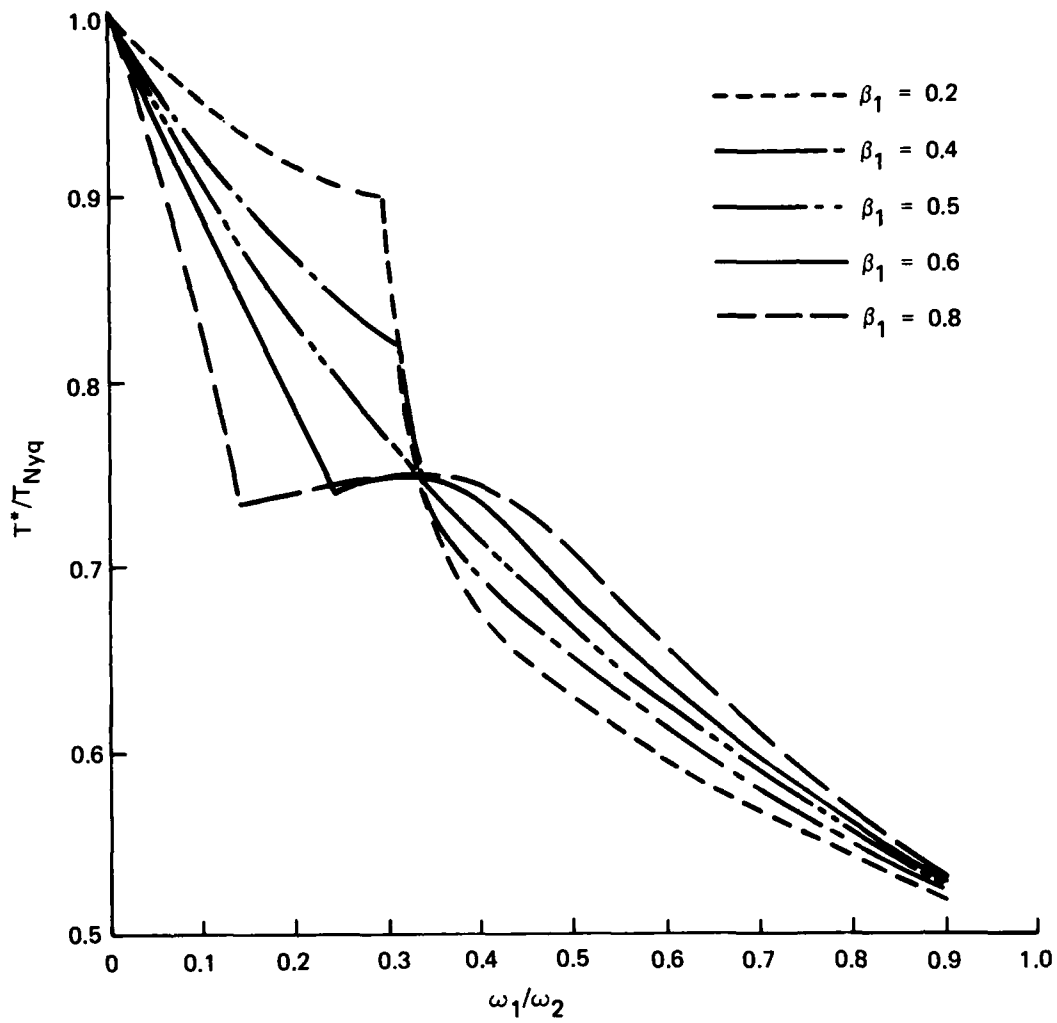


Figure 2-12. T^*/T_{Nyq} ($T^*/T_{Nyq} < 1$) as a function of ω_1/ω_2 .

Table 2-1. $1/\kappa [R(-3,4,4)(T^*)]$.

$\omega_1/\omega_2 \backslash \beta_1^2$	0.2	0.4	0.5	0.6	0.8
0.1	0.068	0.132	0.159	0.185	0.221
0.2	0.224	0.414	0.502	0.575	0.383
0.4	0.358	0.678	0.778	0.731	0.387
0.6	0.162	0.270	0.293	0.288	0.191
0.8	0.037	0.057	0.060	0.059	0.040
0.9	0.009	0.013	0.014	0.013	0.009

Table 2-2. Optimal sampling rate, T^* .

$\omega_1/\omega_2 \backslash \beta_1^2$	0.2	0.4	0.5	0.6	0.8
0.1	0.954	0.925	0.909	0.889	0.817
0.2	0.918	0.866	0.833	0.789	0.740
0.4	0.675	0.694	0.714	0.734	0.743
0.6	0.596	0.614	0.625	0.636	0.656
0.8	0.544	0.551	0.556	0.560	0.568
0.9	0.521	0.524	0.526	0.528	0.532

Table 2-3. $\kappa[R (-3,4,4)(T^*)] / \kappa[R (-3,4,4)(\bar{T})]$.

$\omega_1/\omega_2 \backslash \beta_1^2$	0.2	0.4	0.5	0.6	0.8
0.1	0.947	0.968	01.00	0.693	0.292
0.2	0.927	0.985	01.00	0.712	0.544
0.4	0.927	0.957	01.00	0.885	0.855
0.6	0.907	0.962	01.00	0.901	0.769
0.8	0.934	0.979	01.00	0.952	0.877
0.9	0.942	0.992	01.00	0.986	0.918

Table 2-4. Left-hand slope/right-hand slope at T*.

$\omega_1/\omega_2 \backslash \beta_1^2$	0.2	0.4	0.5	0.6	0.8
0.1	0.105 -2.83	0.170 -3.32	0.187 -3.25	0.187 -3.02	0.088 -1.89
0.2	0.218 -4.70	0.252 -4.99	0.179 -4.53	0.002 -3.62	1.60 -1.59
0.4	2.41 -0.681	5.57 -1.44	5.84 -2.17	4.18 -3.20	1.91 -1.86
0.6	1.85 -0.512	2.87 -0.971	2.93 -1.15	2.68 -1.25	1.53 -0.991
0.8	0.468 -0.159	0.693 -0.264	0.721 -0.289	0.683 -0.291	0.439 -0.212
0.9	0.112 -0.042	0.166 -0.066	0.173 -0.070	0.165 -0.069	0.109 -0.048

$$T^* \approx \bar{T} = \pi/(\omega_1 + \omega_2) \approx 0.5\pi/(\omega_2) = 0.5T_{Nyq} \quad (2-33)$$

It is appropriate at this point to recall Kay's result for estimating a covariance function [2-10]. Kay shows that $T = T_{Nyq}/2$ is a necessary and sufficient sampling interval for obtaining estimates of the covariance function with small error variance. This result is a nice complement to Eq. (2-33).

2.6 Zooming In

2.6.1 Phasor Representation

Returning now to Eq. (2-11), we may rewrite Eq. (2-19) as

$$\begin{aligned} R_d(k) &= R_c(kT) = \sum_{i=1}^n \beta_c(i) (e^{\lambda_c(i)T})^k \\ &= \sum_{i=1}^n \beta_d(i) \lambda_d(i)^k \end{aligned} \quad (2-34)$$

Equation (2-34) is valid for any T , namely, it is not restricted to $T < T_{Nyq}$. Thus, one may employ Eq. (2-20) through (2-24) to estimate $\underline{a}(T)$ using Eqs. (2-25) and (2-26), and then solve uniquely for $\{\lambda_d(i)\}$. In this section we shall explore the benefits attainable by abolishing the constraint $T < T_{Nyq}$ and assess the impact of this operation on the estimation of $\{\lambda_c(i)\}$.

We assume here that the covariance sequence $\{R_d(k) = R_c(kT); k = 0, 1, \dots\}$ is available or has been estimated. Note that in the latter case, we abide by the Nyquist rate constraint for sampling the process, or preferably, abide by Kay's recommendation for obtaining good estimates of the covariance sequence, i.e., the process is sampled at least twice the Nyquist rate.

A figurative representation of Eq. (2-34) is via the concept of phasors as follows. Define the i^{th} phasor

$$F(i) = e^{\lambda_c(i)T} = e^{(-|\zeta(i)\omega(i)| + j\omega(i)T)} \quad (2-35)$$

where $i \leq n$, with n even and $\omega(2i) = -\omega(2i-1) > 0$, $i = 1, 2, \dots, n/2$. Namely, the i^{th} phasor rotates (as T varies over R^+) at an angular velocity, $\omega(i)$, around a spiral which collapses at a rate of $e^{-\zeta(i)2\pi}$ per revolution. The assumption of $\omega(2i) = -\omega(2i-1)$ is practical, but not essential for the following discussion. Actually, the clockwise/counterclockwise rotation adds complexity to the solution described below. The phasor interpretation of Eq. (2-34) suggests the choice of T such that the n phasors will be evenly distributed angle-wise, as long as the damping effect does not dominate, i.e., $|F(i)|$ is sufficiently large.

2.6.2 Procedure

Since our objective is the estimation $[\lambda_c(i)]_1$, we can formally write

$$\lambda_c(i) = \frac{1}{T} \ln[F(i)] \quad (2-36)$$

where Eq. (2-35) should be interpreted as

$$T\omega_i \in \left\{ \left| 2\pi k \pm \frac{1}{F(i)} \right| ; k = 0, 1, 2, \dots [T/T_{Nyq}] \right\} \quad (2-37)$$

$$\zeta_i = -\frac{1}{T\omega_i} \ln \left(\left| F(i) \right| \right) \quad (2-38)$$

$|F(i)|$ and $\angle F(i)$ denote the magnitude and angle of $F(i)$, respectively, and $[x]$ is the integer value of x . The ambiguity (nonuniqueness) in Eq. (2-36), as reflected in Eq. (2-37), and thus Eq. (2-38), in the case that $T > T_{Nyq}$, is another way of stating the Nyquist rate constraint. Nevertheless, we propose to use $T > T_{Nyq}$ to achieve high spectral resolution. The procedure that we propose is outlined in the following steps, which we call "zooming in."

Assume the process consists of a single cluster of $n/2$ closely spaced lightly damped modes (i.e., $\zeta_i \ll 1$ $\omega(2i) = -\omega(2i - 1)$ $i = 1 \dots n/2$). The set of modes is resolved as follows:

Step 1: Identify the center frequency of the cluster. This step can be accomplished by one of the following two procedures:

- (1) Plot the FFT of either the data sampled with period $T_1 < T_{Nyq}$ or of the sequence $[R_d(k) = R_c(kT_1)]$.
- (2) Solve Eq. (2-25) and (2-26) in conjunction with Eq. (2-35) using the sequence $[R_c(kT_1)]$ and n_1 such that $R(0, n_1, L)(T_1)$ is well conditioned.

Preferable choice of T_1 is such that

$$T_1 \omega_c \approx \frac{\pi}{2} \quad (2-39)$$

where ω_c is roughly the center frequency of the cluster.

If $n_1 = n$, namely the matrix $R(0, n, L)$ is well-conditioned, then the $n/2$ modes are spaced sufficiently apart to enable their resolution, and thus, Step 1 completes the spectral analysis. If $n_1 < n$, or no prior knowledge is available regarding the number of modes which characterize the signal, proceed to Step 2.

Step 2: Choose $T_2 = \ell \cdot T^*$, where ℓ is an odd integer larger than one, and T^* satisfies Eq. (2-39). Repeat Step 1 using the sequence $\{R(kT_2)\}$. If the parametric method is used, i.e., Eq. (2-25), (2-26), and (2-36)^c to (2-38) are solved, repeat this step, gradually increasing ℓ and determining $n = n(\ell)$ to be the largest integer for which $R(0, n, L)(T_2)$ has full numerical rank (i.e., is well conditioned).

Stop when $n(\ell)$ does not increase for $\ell \geq \ell_1$, or if $n(\ell_1)/2$ is the expected number of modes.

Step 3: Resolve the ambiguity introduced by Eq. (2-36) and (2-37) by selecting the set of modes residing near the center frequency identified in Step 1. Alternatively, use a conventional identification technique for $T < T_{Nyq}$ where the set of identified parameters is the finite set corresponding to the different solutions of these equations. (See also Reference 2-27 for a selection procedure.)

We have earlier stated that $R(0, n, L)(T)$ is least singular if the phasors are evenly distributed. This statement, although correct, should not mislead the reader to believe that T_2 should be so chosen. To achieve even distribution of the phasors we need $T_2/T_{Nyq} \approx \frac{\omega_2}{2(\omega_1 - \omega_2)}$ when we consider two sinusoids. Thus for a 1% frequency separation, a choice of $T_2 \approx 100 T_{Nyq}$ gives least singularity, but at the same time, one has to select among 200 possible frequencies in Step 3 of the procedure.

A practical solution to this dilemma is to choose T_2 as small as possible, while rendering $R(0, n, L)(T_2)$ well-conditioned. This recommendation is further justified when considering "intermingling" as discussed in the following.

The behavior of the ICN for $R(0, n, n)$ and $R(-n+1, n, n)$ (symmetric covariance matrix) for two sinusoids as function of T is illustrated in Figures 2-13 through 2-16.

The above discussion focused on the resolution of a single cluster of modes. In the case of multiclusters, these ideas can be applied using one of the following options.

Option A: Increase T_2 while preventing cluster "intermingling." The problem of intermingling is most simply explained by considering the phasors rotation as in Figure 2-17. The shaded sections A and B represent the two clusters of modes for a given $T < T_{Nyq}$. The phasors in the sectors labelled 1 rotate clockwise and those labelled 2 rotate counterclockwise with T . Intermingling occurs when two shaded sections overlap. Using the information from Step 1, picking T_2 , which gives an intermingling-free phasor distribution, is a simple algebraic exercise. Note that for a large enough T_2 , intermingling can also occur with a single cluster; aliasing being an example of such an occurrence.

Option B: Use frequency decimation to construct two signals, each representing one cluster [2-13, 2-15]. Spectrum analyze each signal separately and recombine.

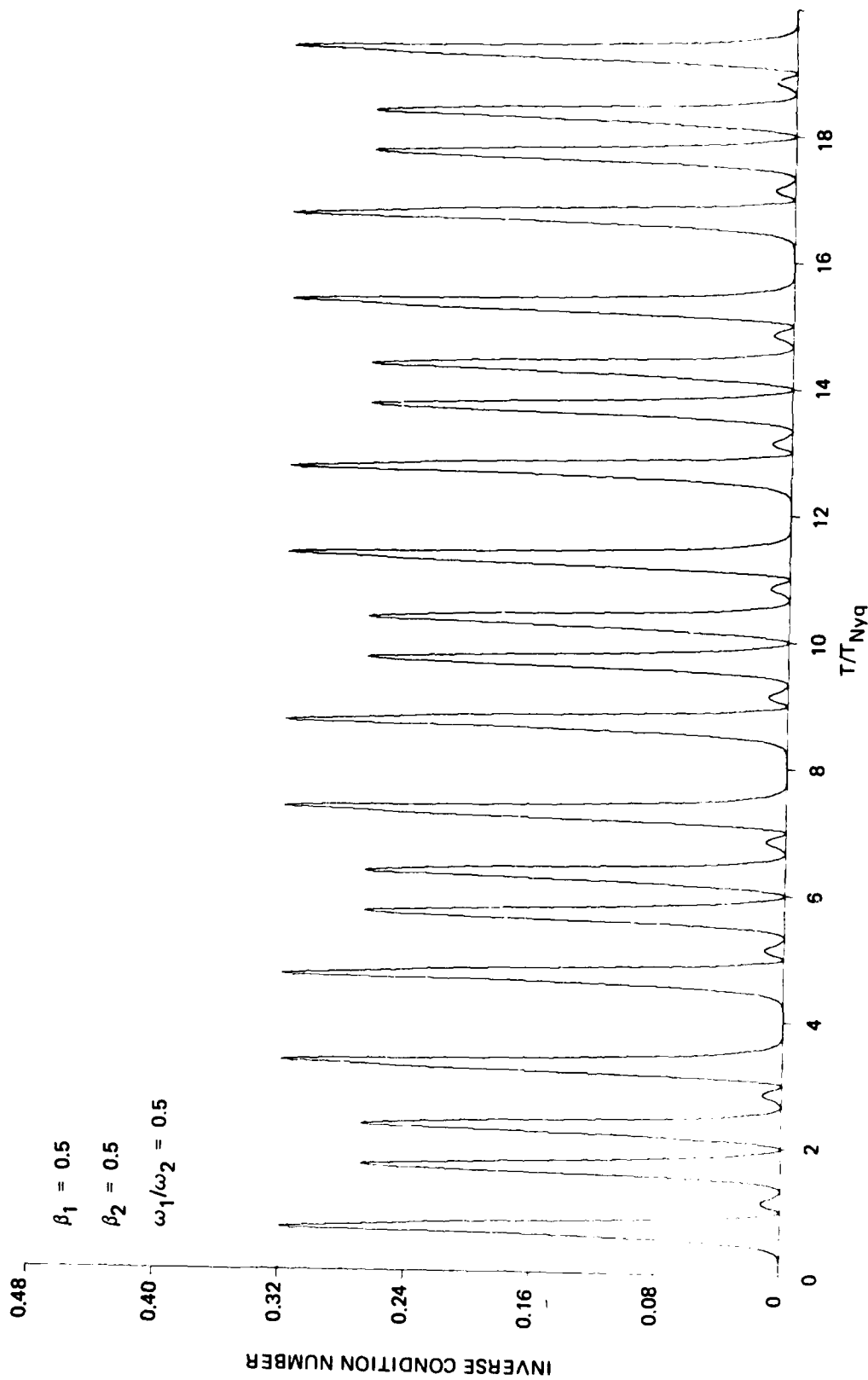


Figure 2-13. ICN vs. T/T_{Nyq} (symmetric covariance matrix).

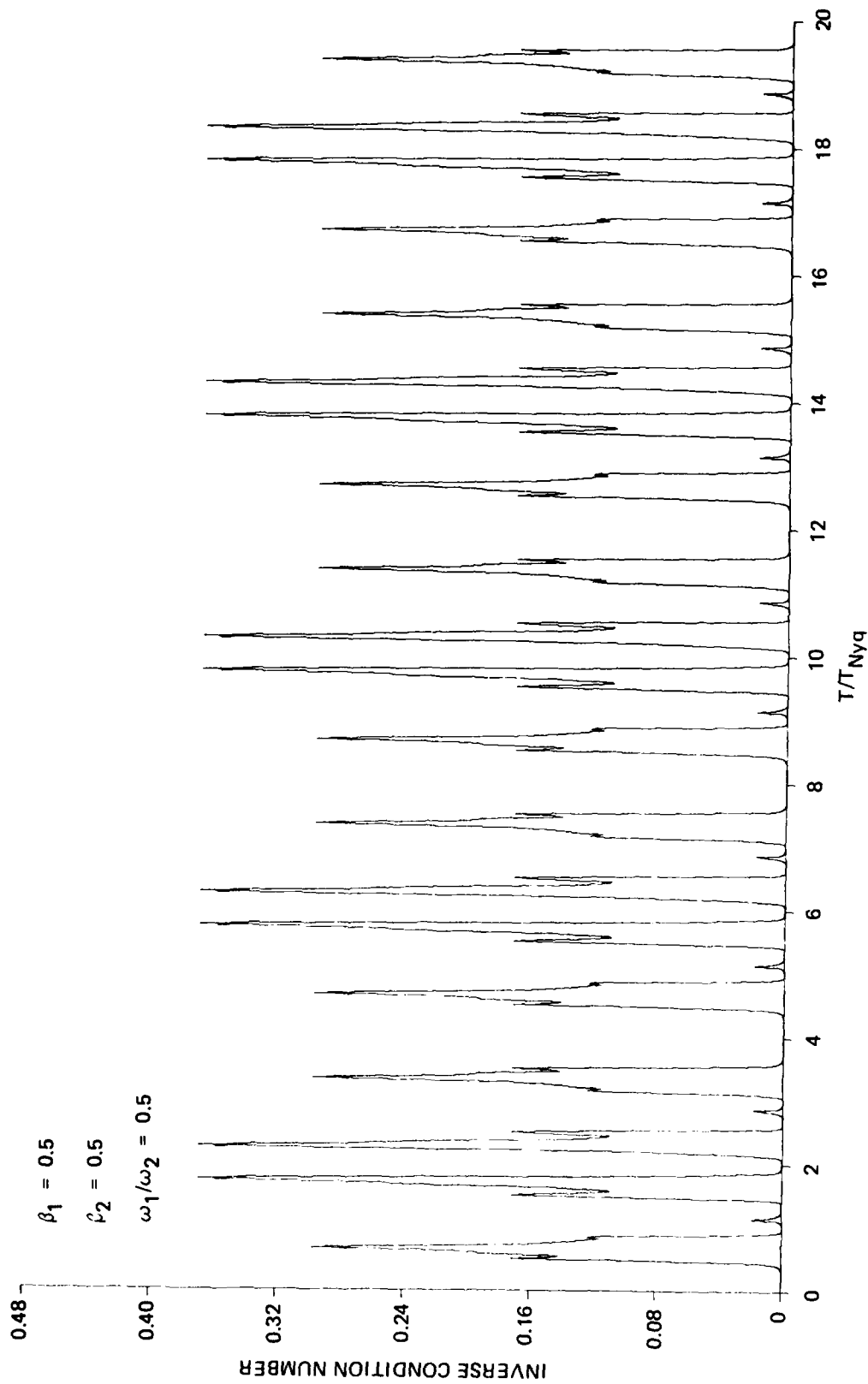


Figure 2-14. ICN vs. T/T_{Nyq} (nonsymmetric covariance matrix).

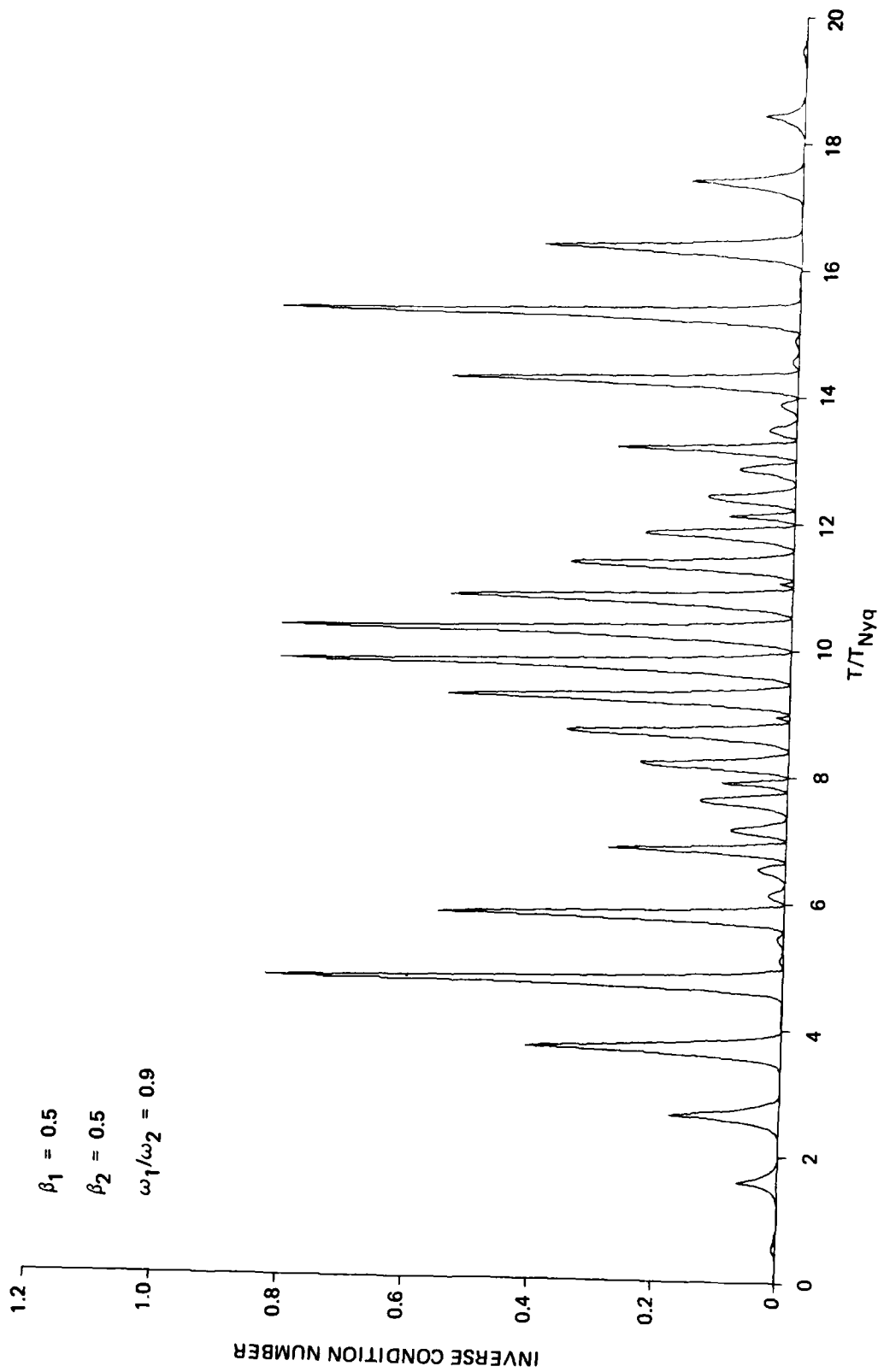


Figure 2-15. ICN vs. T/T_{Nyq} (symmetric covariance matrix).

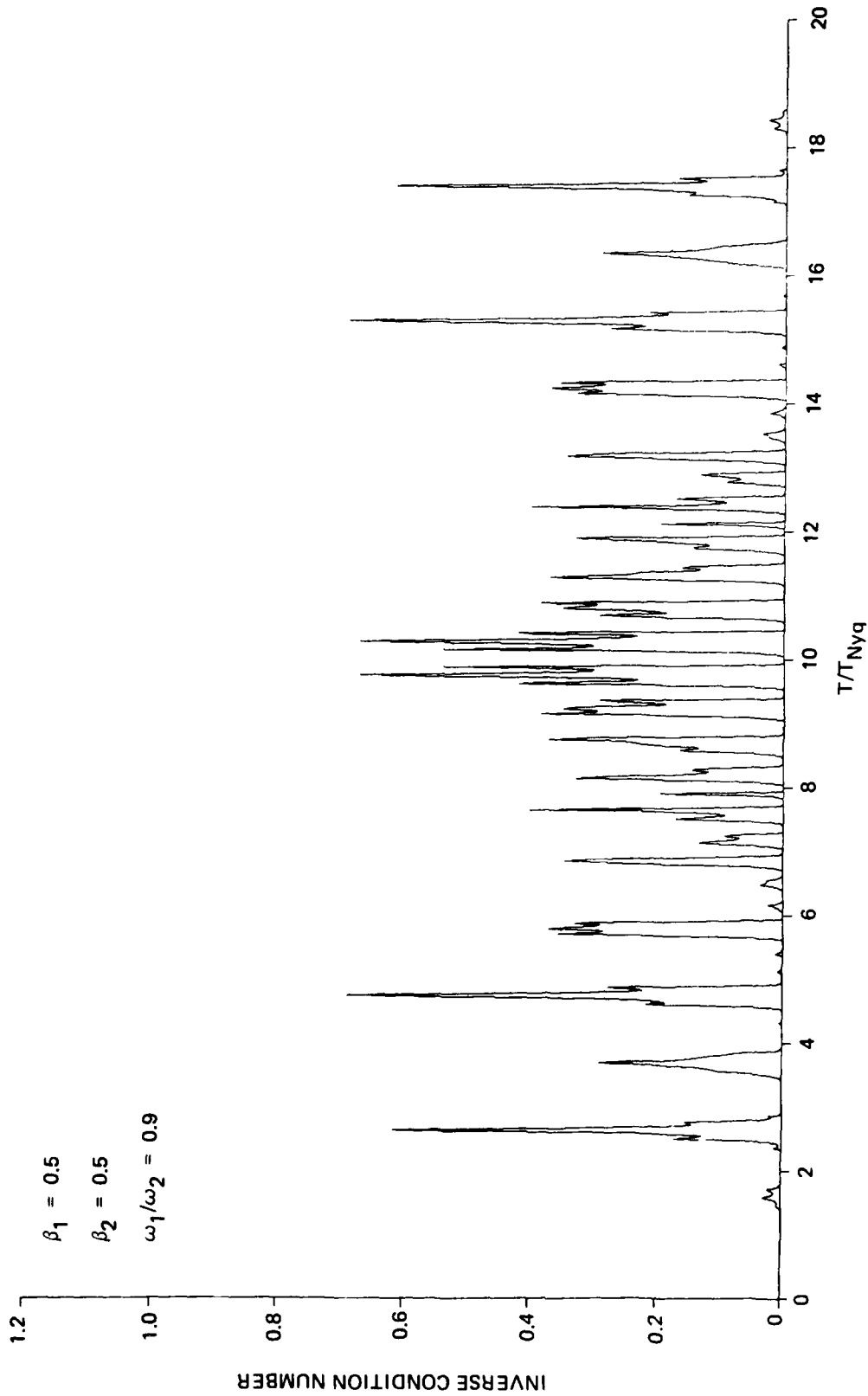


Figure 2-16. ICN vs. T/T_{Nyq} (nonsymmetric covariance matrix).

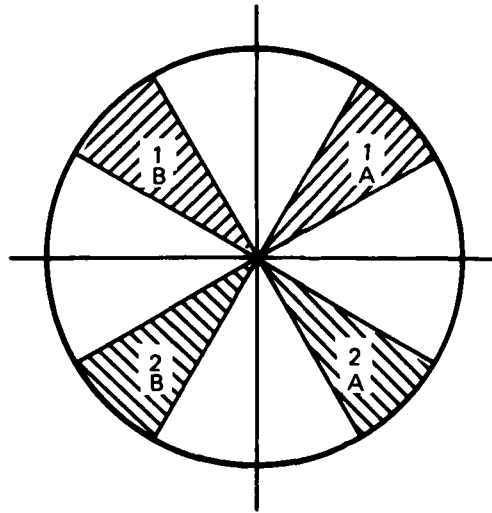


Figure 2-17. Illustration of two-cluster distribution.

2.6.3 Over Parameterization

In the quest for a high spectral resolution algorithm, Cadzow [2-3] and Beex and Scharf [2-2] have proposed over parameterization as one tool for improving algorithms; namely, they have proposed the use of large n in the representation Eq. (2-19) to (2-24). For example, in Reference 2-2, $n = 7$ is used for two sinusoids in white noise (fourth-order system). In Reference 2-3, reasonable success is reported in resolving two sinusoids with a 0 dB signal-to-noise ratio and 7-percent frequency separation using $n = 20$. Actually, the use of over parameterization is quite common in the literature (e.g., [2-18], [2-27], and references therein); however, it has not received sufficient justification.

Let Eq. (2-34) be a correct representation of the covariance sequence and consider the over parameterization via the recursion

$$R_c(kT) = \sum_{i=1}^L a(i)R_c[(k-i)T] \quad k \geq L \quad (2-40)$$

where $T < T_{Nyq}$, and L is an integer larger than n , e.g., $L = 5 \times n$. Then, the solution for the vector $\underline{a} = [a(1), \dots, a(L)]'$ via Eq. (2-25) and (2-26) involves the matrix

$$R [0, 5n, 5n](T) = \begin{bmatrix} R(5n-1) & \dots & R(1) & R(0) \\ \cdot & & \cdot & \cdot \\ \cdot & & \cdot & \cdot \\ \cdot & & \cdot & \cdot \\ R(10n-2) & \dots & R(5n) & R(5n-1) \end{bmatrix} \quad (5n \times 5n)$$

On the other hand, considering Step 2 in our zooming-in procedure with $T_2 = 5T$, we have to solve n linear equations with the coefficient matrix

$$\mathbf{R} [0,n,n](5T) = \begin{bmatrix} R[5(n-1)]\dots & R(5) & R(0) \\ \cdot & \cdot & \cdot \\ \cdot & \cdot & \cdot \\ \cdot & \cdot & \cdot \\ R[10(n-1)]\dots & R[5(n+1)] & R[5(n-1)] \end{bmatrix} \quad (n \times n)$$

that is, $\mathbf{R} [0,n,n](5T)$ is obtained from $\mathbf{R} [0,5n,5n](T)$ by retaining only every fifth column and fifth row. If the representation (Eq. (2-34)) is merely an approximation [2-2], it would be advisable to retain every fifth column of $\mathbf{R} [0,5n,5n]$ and use the covariance least squares as in Eq. (2-25) and (2-26). Now, since the process has order n by assumption, the numerical rank of $\mathbf{R} [0,5n,5n](T)$ is n , provided the numerical rank of $\mathbf{R} [0,n,n](5T)$ is n . Thus, in effect, over parameterization is equivalent to spreading the phasors to increase the numerical rank of the covariance matrix. Using sound numerical procedure in solving $a(5n)$ yields a solution which corresponds to n dominant modes and $(5-1)n$ superfluous modes. This is exactly Beex's and Tuft's observation [2-2, 2-27].

The advantages of our zooming-in procedure are rather obvious. We avoid solving a very high-dimensional ill-conditioned set of equations, thus eliminating the need to use a procedure such as the singular value decomposition (SVD) used by Tufts [2-18] and Cadzow [2-3]. More important, we have to solve only an n^{th} order well-conditioned polynomial for the eigenvalues compared to an L^{th} order polynomial. The penalty paid for these advantages is Step 3 of our procedure.

Finally, we note that using $\ell + 1$ parallel processors, Step 1 and (Step 2) ℓ times can be performed simultaneously, Step 3, recombining the results of the parallel processors. The architecture of such a parallel numerical analyzer is beyond the scope of this section.

2.7 Simulation Results

The effect of sampling within and beyond the Nyquist rate has been extensively tested in simulation. A few examples of the simulation results are given here.

The signals assessed are of the type

$$y(k) = \sum_{i=1}^{n/2} A(i) \exp[-\zeta(i)\omega(i)T_1 k] \cos [\omega(i)T_1 k + \phi(i)] + v(k) \quad (2-41)$$

The frequencies are chosen to generate a closely spaced cluster. We specify for each cluster the frequency separation (FS) (in percent) which is defined as

$$FS = \min \left[2 \frac{|\omega_i - \omega_j|}{(\omega_i + \omega_j)} \cdot 100 \quad i, j = 1 \dots n \quad i \neq j \right] \quad (2-42)$$

$\{v(k)\}$ is a zero mean white Gaussian noise with covariance, V , as specified for each example. We use the equation (see Eq. (2-25) and (2-26))

$$\mathbf{R}(0, n, n)(T_2) \cdot \mathbf{a}(T_2) = \mathbf{R}(n, n)(T_2) \quad (2-43)$$

to estimate $\mathbf{a}(T_2)$. Subsequently, the characteristic polynomial

$$[1, -\mathbf{a}'] \cdot \begin{bmatrix} \lambda_d^n \\ \lambda_d \\ \cdot \\ \cdot \\ \cdot \\ \lambda_d^0 \end{bmatrix} = 0 \quad (2-44)$$

is solved to find $\{\lambda_d(i)(T_2); i=1 \dots n\}$ and Eq. (2-36) to (2-38) are used to estimate $\{\zeta(i), \omega(i)\}$. As entries to the matrices \mathbf{R} and \mathbf{R} , we use the estimated covariances

$$\mathbf{R}(\ell T_2) = \frac{1}{L} \sum_{k=1}^L y(kT_2)y[(k + \ell)T_2] ; \quad \ell = 0 \dots 2n-1 \quad (2-45)$$

where L is fixed and T_2 is chosen such that T_2/T_1 is an integer. The values of L , T_1 , and T_2 are specified for each run. Note that Eq. (2-45) gives the biased estimate of the covariance (see Reference 2-26 for justification). In the tabulated results, we give the estimated frequencies, $\omega(i)$. If $|\lambda_d(i)| \leq 1$, we also give the estimated damping ratios; otherwise, we specify the estimate of $|\lambda_d(i)|$. A * in the tables denotes a failure in estimating the corresponding value. If the estimation failed for $T_2 < T_{Nyg}$, the optimal order and the corresponding estimated system is given in the discussion.

Example 1: Two-sinusoid case.

$\omega(1) = 1.5$ rad/s	$\omega(2) = 1.57$ rad/s	FS = 4.56%
$\zeta(1) = 0$	$\zeta(2) = 0$	
$A(1) = 1.0$	$A(2) = 1.0$	

$$(1) \quad v = 10^{-7} \quad ; \quad T_2 < T_{Nyq}$$

The estimated values are given in Table 2-5. This example demonstrates our observations in Section 2.2. The estimates are reasonably good for the range $0.5T_{Nyq} < T_2 < 0.9T_{Nyq}$. The optimal sampling rate is (see Figure 2-11) $T_2^* = 0.55 T_{Nyq} = 1.1$.

$$(2) \quad v = 10^{-5} \quad ; \quad T_2 < T_{Nyq}$$

The results of the simulations are tabulated in Table 2-6. Here reasonable estimates are obtained for the range $0.5T_{Nyq} < T_2 < 0.8T_{Nyq}$. In case (1), the optimality of $T_2 = T^*$ is obvious. In case (2), $\omega(1)$ is best estimated for $T_2 = T^*$; however, a somewhat better estimate of $\omega(2)$ is obtained for $T_2 = 1.3$.

Both examples consisted of undamped sinusoids, and the error in the estimates of $|\lambda_d(1)|$ did not exceed 6 percent, and was usually considerably smaller. However, attempts to estimate the damping ratios for $\zeta > 0$ have failed for $T_2 < T_{Nyq}$. In the following two examples, we extend the range of T_2 and demonstrate success in estimating the damping ratios and considerable improvement in the estimation of the frequencies compared to the case $T_2 < T_{Nyq}$.

(3) The data is the same as in case (2) except for the damping ratios

$$\zeta(1) = 0.01 \quad \zeta(2) = 0.01$$

(Note that 1 percent is the order of magnitude of material damping--an entity of interest in elasticity and structure engineering.) The results of the simulations are summarized in Table 2-7.

(4) Same as (3) with damping ratios

$$\zeta(1) = 0.05 \quad \zeta(2) = 0.05$$

Results are given in Table 2-8.

Example 1 demonstrates the value of selecting the sampling rate judiciously within the Nyquist rate as well as the improvement that might be gained by zooming in. However, the frequency separation and the noise level in Example 1 are not extreme enough to cause failure of the estimation except for the very poor choice of T_2 . In the following we consider more severe cases.

Example 2

$$\begin{array}{lll} \omega(1) = 1.5543 \text{ rad/s} & \omega(2) = 1.57 \text{ rad/s} & \text{FS} = 1\% \\ \zeta(1) = 0 & \zeta(2) = 0 & \\ A(1) = 1 & A(2) = 1 & \end{array}$$

$$v = 10^{-4}$$

Table 2-5. Estimated two sinusoids $T < T_{Nyq}$.

T_1	T_2	L	$\omega(1)$	$\tau(1)$	$ \lambda_d(1) $	$\omega(2)$	$\tau(2)$	$\lambda_d(2)$
0.2	0.2	128	1.536	0.1113E-1		6.246	0.5773	
0.5	0.5	128	1.4826	0.2831E-1		1.558	0.1602E-1	
1.0	1.0	64	1.504		1.0013	1.5713		1.0048
*1.1	1.1	64	1.4998		1.0013	1.5692		1.0009
1.2	1.2	64	1.498		1.0017	1.5780		1.0007
1.5	1.5	64	1.5004	0.8983E-3		1.5709	0.8376E-3	
1.8	1.8	64	1.509	0.1504E-3		1.5927		1.030
1.9	1.9	64	1.510	0.5548E-2		*	*	*
True Values			1.5	0.0	1.0	1.57	0.0	1.0

Table 2-6. Estimated two sinusoids $T < T_{Nyq}$.

T_1	T_2	L	$\omega(1)$	$\zeta(1)$	$ \lambda_d(1) $	$\omega(2)$	$\zeta(2)$	$\lambda_d(2)$
0.5	0.5	64	1.329	0.2827		1.5396	0.1633E-1	
0.6	0.6	64	1.537	0.1804E-1		1.605	0.4698	
0.7	0.7	64	1.531	0.2171E-1		1.699	0.1156	
0.9	0.9	64	1.521	0.5654E-2		1.597		1.0328
1.0	1.0	64	1.525	0.3338E-2		1.600		1.0684
*1.1	1.1	64	1.499		1.016	1.5599		1.0072
1.3	1.3	64	1.492	0.197E-2		1.564	0.214E-2	
1.5	1.5	64	1.507	0.8296E-2		1.578	0.1139E-1	
1.6	1.6	64	1.518	0.9922E-2		1.614	0.3481E-1	
1.7	1.7	64	1.520	0.6479E-2		1.706	0.8146E-2	
1.8	1.8	64	1.522	0.8154E-2		*	*	*
True Values			1.5	0	1.0	1.57	0	1.0

Table 2-7.

T_1	T_2	L	$\omega(1)$	$\zeta(1)$	$ \lambda_d(1) $	$\omega(2)$	$\zeta(2)$	$ \lambda_d(2) $
1	1	128	1.527	0.6060E-2		1.585		1.059
1	5	128	1.4998	0.1034E-1		1.5702	0.9975E-2	
1	15	128	1.5005	0.8118E-2		1.5699	0.8889E-2	
True Values			1.5	0.1E-1		1.57	0.1E-1	

Table 2-8.

T_1	T_2	L	$\omega(1)$	$\zeta(1)$	$ \lambda_d(1) $	$\omega(2)$	$\zeta(2)$	$ \lambda_d(2) $
1	1	128	1.533	0.2748E-1		1.677		1.245
1	5	128	1.509	0.5174E-1		1.581	0.5059E-1	
1	15	128	1.526	0.2198E-1		1.5701	0.7063E-1	
True Values			1.5	0.5E-1		1.57	0.5E-1	

Table 2-9 summarizes the simulation results. Only one frequency has been identified successfully with $T_2 < T_{Nyq}$, where the optimal order of the recursion is two. The estimation of a second-order recursion yields the estimates $\omega = 1.562$ and $\zeta = 0.12E-2$. We see increasing benefits with larger T_2 . For $T_2 = 35T^*$ perfect estimates of the frequencies are observed.

Example 3: Three sinusoids.

$\omega(1) = 1.5543$	$\omega(2) = 1.57$	$\omega(3) = 1.5857$	FS = 1%
$\zeta(1) = 0.001$	$\zeta(2) = 0.001$	$\zeta(3) = 0.001$	
$A(1) = 1$	$A(2) = 1$	$A(3) = 1$	

$V = 10^{-4}$

Results are summarized in Table 2-10. We have observed failure for $T_2 < 3T_{Nyq}$.

The optimal order of the recursion is $n = 2$, with the estimates $\omega = 1.57$ and $\zeta = 0.6E-2$ when using $T_1 = T_2 = 1$. For $T = 25T^*$, success is registered in estimating the damping ratios and the frequencies.

We have conducted experiments similar to the previous examples for clusters of up to five frequencies with 1-percent frequency separation and similar signal-to-noise ratio. The results were qualitatively identical to those discussed.

We bring as a final example the case studied by Cadzow [2-3] and others. This example culminates a few difficulties. Although the frequency separation (FS = 6.5 percent) is larger than considered in the previous examples, estimation is hampered here by the disparity in the modal amplitudes and by a high noise level (0-dB signal-to-noise ratio).

Example 4

$\omega(1) = 0.4\pi$ rad/s	$\omega(2) = 0.426\pi$ rad/s	FS = 6.5%
$\zeta(1) = 0$	$\zeta(2) = 0$	
$A(1) = 4.47$	$A(2) = 1.414$	

$V = 1.0$

The results of the simulations are given in Table 2-11. For $T_1 = 1$ the optimal order is $n = 3$ with estimates $\omega = 1.266$, $\zeta = 0.3E-2$, and the discrete eigenvalue, $\lambda_d = -0.09$, which does not have a continuous interpretation. Examination of the table reveals the importance of choosing T_2 such that $T_2 = (2\ell + 1)T^*$ for some ℓ (see Step 2). Note that using the estimate, $\omega = 1.266$, T^* can be approximated as $\pi/2\omega = 1.24$. The choice ($T_1 = 1.0$; $T_2 = 5$) does not satisfy the recommended values and yields poor estimates. $T_1 = 1.2$ with $T_2 = 6$ or $T_2 = 18$ approximates this requirement and gives correspondingly good estimates. The choice $T_1 = 1$ and $T_2 = 16 \approx 13 \times 1.24$ also satisfies the recommendation of Step 2 of the zoom-in procedure.

Table 2-9.

T_1	T_2	L	$\omega(1)$	$\zeta(1)$	$ \lambda_d(1) $	$\omega(2)$	$\zeta(2)$	$ \lambda_d(2) $
1.	1.0	128	*	*	*	1.562	0.1246E-2	
1.2	1.2	128	*	*	*	1.562	0.3030E-2	
1.5	1.5	128	*	*	*	1.562	0.3515E-2	
1.0	5.0	128	1.5566	0.3110E-2		1.5778	0.1882E-2	
1.0	15.0	128	1.5538	0.1691E-3		1.5703	0.2491E-3	
1.0	25.0	128	1.5542	0.7900E-4		1.5700	0.1150E-3	
1.0	35.0	128	1.5543	0.2414E-4		1.5700	0.1882E-4	
True Values			1.5543	0		1.57	0	

Table 2-10.

T_1	T_2	L	$\omega(1)$	$\zeta(1)$	$ \lambda_d(1) $	$\omega(2)$	$\zeta(2)$	$ \lambda_d(2) $	$\omega(3)$	$\zeta(3)$	$\lambda_d(3)$
1	1	128	1.520		1.022	1.5728	0.5294E-2		*	*	*
1	5	128	1.5574	0.2933E-2		*	*		1.5837	0.2324E-2	
1	15	128	1.5576	0.1339E-2		1.5633	0.2652E-2		1.5856	0.1783E-2	
1	25	128	1.5543	0.22E-2		1.5702	0.69E-3		1.5856	0.11E-2	
True Values			1.5543	0.1E-2		1.57	0.1E-2		1.5857	0.1E-2	

Table 2-11.

T_1	T_2	L	$\omega(1)$	$\zeta(1)$	$ \lambda_d(1) $	$\omega(2)$	$\zeta(2)$	$ \lambda_d(2) $
1.0	1.0	64	1.2548		1.0039	*	*	
1.0	5.0	64	1.2566		1.108	1.5758	0.467E-1	
1.0	6.0	64	1.259		1.035	1.2973	0.225E-1	
1.2	6.0	64	1.2508	0.155E-2		1.2875	0.597E-1	
0.62	14.0	64	1.264	0.432E-2		1.300	0.280E-1	
1.0	8.0	64	1.252	0.147E-2		1.422	0.326E-1	
1.0	13.0	64	1.258		1.019	1.3439	0.175E-1	1.046
1.0	16.0	64	1.2566		1.002	1.349		
1.2	18.0	64	1.2565		1.008	1.3385	0.398E-2	
True Values			1.2566	0	1.0	1.3383	0	1.0

2.8 General Comments

The benefits of a judicial choice of the sampling rate, as well as our proposed zoom-in procedure, have clearly been demonstrated. Zooming in can be mechanized in various ways. Our approach was to select the group of frequencies closest to the center frequency identified with $T_2 < T_{Nyq}$.

To demonstrate the selection procedure for resolving the ambiguity in the case $T_2 > T_{Nyq}$ (Step 3 of the zoom-in procedure), consider Example 2 with $T_2 = 35T_1^*$. The estimation for $T_2 < T_{Nyq}$ has failed, but estimating the fourth-order data using a second-order model gave the following estimates: frequency estimate = 1.562, damping ratio estimate = 0.26E-2. In Table 2-12, a subset of the 70 frequencies around 1.562 and the damping ratios generated in Step 3 for $T_2 = 35T_1$, $T_1 = 1$ are given. The frequencies marked with * are the closest to 1.562 and are the obvious choice. Note that the estimated frequencies in this case are the exact values (see Table 2-9). This example is the most ambiguous one. In other examples tested, the selection among the different solutions of Eq. (2-35) was even clearer.

2.9 Concluding Remarks

We have established analytically and experimentally in this section the role of the sampling rate in high resolution spectral analysis. Presenting the problem of resolution as a numerical one enabled us to establish desirable sampling rates for high resolution. Moreover, via the phasor interpretation of the covariance function we derived a zoom-in procedure, which is a powerful spectral analysis tool. Although we have concentrated on two procedures for spectral analysis, the FFT and the parametric regression on the covariance sequence, the results of the studies have ramifications to other techniques. The symmetric covariance matrix can be interpreted under certain conditions as the Fisher information matrix [2-6]. The inverse condition number of this matrix is thus an information measure which we have selected for numerical reasons. Maximizing the ICN as a function of the sampling rate thus has ramifications for any statistical estimator.

Although the emphasis of this study was the sampling rate for continuous signals, the results subsume the case of purely discrete time data. In the discrete case, T_1 should be suppressed, say in Eq. (2-41); and thus, $\omega(i) \cdot T_1$ should be replaced by $\omega(i)\varepsilon(0,\pi)$. Correspondingly, T_2 should be replaced in all the expressions by the integer, T_2/T_1 , and the corresponding results follow trivially.

We believe that the algorithm we propose is numerically superior and computationally more efficient than other algorithms proposed recently for improved spectral resolution. Our success can be attributed to the fact that we have addressed the source of the difficulty. Our analysis also extends to other algorithms as discussed in Section 2.6.3.

The simulation results reported in Section 2.7 support our claims.

It should be noted that the zoom-in procedure proposed in Section 2.6 is only applicable for narrow-band signals. If a signal spectrum consists of a set of narrow band signals, frequency decimation and modulation can be employed

before applying the proposed procedure. Wide band signals with no distinct clusters of energy cannot be analyzed via our zoom-in procedure, though our recommendations in Section 2.5 are still valid.

Finally, we would like to give an intuitive, though somewhat ad hoc explanation, of the main features of the high resolution spectral analysis presented in this section. Replacing a very narrow band signal with center frequency ω_c by $\sin(\omega_c t)$, we observe that sampling the signal at intervals

T^* , satisfying Eq. (2-39), generates the sequence $\{\sin(\frac{\pi}{2} \cdot k)\}$. This is the sequence with the maximum variation that can be generated from the sinusoidal function. Since spectral estimation and particularly parametric spectral estimation is concerned with the dynamics of the signal, observing the maximum variation is most beneficial for its estimation. The prism is a classical device for splitting closely spaced colors. Desampling the covariance function while maintaining maximum variation of the signal as in the zoom-in procedure can be viewed as a digital prism in light of the phasor representation.

Table 2-12.

Frequency	Damping	Frequency	Damping
1.0315	0.28E-4	1.0158	0.36E-4
1.1123	0.28E-4	1.1385	0.36E-4
1.2110	0.24E-4	1.1195	0.31E-4
1.3023	0.24E-4	1.3180	0.31E-4
1.3905	0.21E-4	1.3748	0.27E-4
1.4818	0.21E-4	1.4975	0.27E-4
* 1.5700	0.19E-4	1.5543	0.24E-4
1.6613	0.19E-4	1.6770	0.24E-4
1.7495	0.17E-4	1.7338	0.22E-4
1.8409	0.17E-4	1.8566	0.22E-4
1.9291	0.15E-4	1.9134	0.20E-4

Subset of estimated frequencies and damping ratios
 $\omega_c = 1.562$, $T_2 = 35$, $T_1 = 1$.

SECTION 2
LIST OF REFERENCES

- 2-1 Special Issue on Spectral Estimation, Proceedings of the IEEE, Vol. 70, No. 9, September 1982.
- 2-2 Beex, A.A. and L.L. Scharf, "Covariance Sequence Approximation for Parametric Spectrum Modeling," IEEE Trans. Acoust., Speech, Signal Proc., Vol. ASSP-29, No. 5, October 1981, pp. 1042-1052.
- 2-3 Cadzow, J.A., "Spectral Estimation: An Overdetermined Rational Model Equation Approach," Proc. IEEE, Vol. 70, No. 9, September 1982, pp. 907-938.
- 2-4 Bergstrom, A.R., Statistical Inference in Continuous Time Economic Models, North-Holland Pub. Co., 1976.
- 2-5 Åström, K.J., "On the Choice of Sampling Rate in Parametric Identification of Time Series," Information Science, Vol. 1, 1969, pp. 273-278.
- 2-6 Payne, R.L., G.C. Goodwin, and M.B. Zarrop, "Frequency Domain Approach for Designing Sampling Rates for System Identification," Automatica, Vol. 11, pp. 189-191.
- 2-7 Goodwin, G.C. and R.L. Payne, Dynamic System Identification: Experiment Design and Data Analysis, Academic Press, 1977.
- 2-8 Bendat, J.S. and A.G. Piersol, Measurement and Analysis of Random Data, John Wiley & Sons, Inc., New York, 1966.
- 2-9 Iserman, R., "Practical Aspects of Process Identification," Automatica, Vol. 16, No. 5, September 1980.
- 2-10 Kay, S.M., "The Effect of Sampling Rate on Autocorrelation Estimation," IEEE Trans. Acoust., Speech, Signal Proc., Vol. ASSP-29, No. 4, August 1981.
- 2-11 Hewlett-Packard, 3582A Spectrum Analyzer.
- 2-12 Brul & Kjoer, "Narrow Band Analyzer, Type 2031," Technical Review No. 1, B&K Publications, 1979.
- 2-13 Brul & Kjoer, "High Resolution Signal Analyzer, Type 2033," Technical Review No. 2, B&K Publications, 1980.
- 2-14 Perl, J. and L.L. Scharf, "Covariant Invariant Digital Filters," IEEE Trans. Acoust., Speech, Signal Proc., Vol. ASSP-25, No. 2, April 1977, pp.143-151.

SECTION 2
LIST OF REFERENCES (Cont.)

- 2-15 Burg, J.P., "Maximum Entropy Spectral Analysis," presented at the 37th Annual Inter. Meeting, Soc. of Explor. Geophys., Oklahoma City, Oklahoma, October 1967.
- 2-16 Cadzow, J.A., "High Performance Spectral Estimation - A new ARMA Method," IEEE Trans. Acoust., Speech, Signal Proc., Vol. ASSP-28, No. 5, October 1980.
- 2-17 Kay, S.M., "A New ARMA Spectral Estimator," IEEE Trans. Acoust., Speech, Signal Proc., Vol. ASSP-28, No. 5, October 1980.
- 2-18 Tufts, D.W. and R. Kumaresan, "Estimation of Frequencies of Multiple Sinusoids: Making Linear Prediction Perform Like Maximum Likelihood," Proc. of IEEE, Vol. 70, No. 9, September 1982, pp. 975-989.
- 2-19 Young, P.C., "An Instrumental Variable Method for Real-Time Identification of Noisy Process," Automatica, Vol. 6, 1970, pp. 271-287.
- 2-20 Fogel, E., "Total Least Squares for Toeplitz Structures," IEEE Conf. on Decision and Control, December 1982.
- 2-21 Wilkinson, J.H., The Algebraic Eigenvalue Problem, Clarendon Press, Oxford, 1965.
- 2-22 Dongarra, J.J., C.B. Moler, J.R. Bunch, and G.W. Stewart, Linpack User's Guide, SIAM, Philadelphia, 1972.
- 2-23 Golub, G., V. Klema, and G.W. Stewart, "Rank Degeneracy and Least Squares Problems," Report STAN-CS-76-559, Stanford University, 1976.
- 2-24 Golub, G., V. Klema, and S.C. Peters, "Rules and Software for Detecting Rank Degeneracy," J. Econometrics, Vol. 12, 1980, pp. 41-48.
- 2-25 Quirk, M., and B. Liu, "On Narrow-Band Spectrum Calculation by Direct Decimation," Proc. ICASSP, Atlanta, Georgia, 1981.
- 2-26 Kay, S.M., "Noise Compensation for Auto Regressive Spectral Estimation," IEEE Trans. Acoust., Speech, Signal Proc., Vol. ASSP-28, No. 3, June 1980.
- 2-27 Kumaresan, R., D.W. Tufts, and L.L. Scharf, "A Method for Suppressing Spurious Effects and Selecting Order in Linear Prediction," submitted for publication.
- 2-28 ACOSS Eleven Semiannual Technical Report, CSDL-R-1583, August 1982.
- 2-29 ACOSS-16, Final Status Review, Honeywell Systems & Research Center, 29 June 1982.

SECTION 3

CONTROL OF LARGE SPACE STRUCTURES USING ELECTROMECHANICAL ACTUATORS

3.1 Introduction

The published literature on vibration control of large space structures is mainly concerned with the theoretical issues associated with the design of control laws or control strategies. Numerous suggestions have been made regarding the form of suitable control laws and the selection of control law parameters. Such investigations have generally based the design and analysis of control laws solely on the properties of the flexible structure to be controlled and on the vibration control objectives. The important effects of physical transducers, namely actuators and sensors, in achieving the vibration control objectives have generally been ignored. Of course, research has continued on the development of transducer hardware suitable for use in large space structure applications [3-6, 3-7]. The objective of this section is to reconcile the work on vibration control of large space structures (where transducer effects have generally been ignored) with the work on transducers (where application to the particular vibration control objectives have generally been ignored). Although our development will focus solely on the role of actuator transducers, a similar development likely holds with regard to the role of sensors. Thus, our main emphasis in this work is consideration of the role of actuators as an important and necessary part of the problem of vibration control of large space structures. Some recent work [3-2, 3-3] has examined the question of proper placement of actuators, ignoring all effects of actuator dynamics. In this section, the effects of actuator dynamics are examined, while the placement of actuators is assumed fixed.

The overall plan of Section 3 is as follows. In Section 3.2, the important issue of modelling the actuators and large space structure is examined. Section 3.3 takes a specific viewpoint towards the vibration control problem--use of the centralized controller, where both the structural motion and the actuator motions are used for feedback to the actuator inputs, is suggested. An alternative using a decentralized controller consisting of a force controller and actuator controllers, one for each actuator, is considered in Section 3.4. Several examples are presented in Section 3.5. An indication of possible extensions and a summary are given in Section 3.6. Throughout this section there is a dual development for each of two distinct classes of electromechanical actuators mentioned in Section 3.2. In each section, use of a single actuator is initially studied in some detail, and the results are subsequently extended to the case of multiple actuators.

In order for our conclusions to be as general as possible, the detailed nature of actuator hardware is not considered. Rather our interest is in the dynamic effect that the actuators have on the large space structure with respect to the vibration control objectives. Thus the content of the following sections is primarily concerned with the mathematical characterization of the actuators, the large space structure, and the feedback controller. This

generality allows us to develop qualitative insight into the role of actuators in vibration control of large space structures for a wide variety of physical actuator hardware.

3.2 Modelling

3.2.1 Actuators

Actuators are considered to represent the physical devices whereby forces and moments are actually applied to a large space structure. They can also be considered as energy transducers since they transform electrical energy into mechanical energy. Actuators can also be viewed as power amplifiers since they typically require low (electrical) power input while they generate higher (mechanical) power output. Actuator hardware is a necessary ingredient in any actively controlled system [3-8].

An actuator can be characterized in terms of the physical nature of its input and output signals. Throughout, an actuator input will be considered to be a voltage signal. The nature of the actuator output depends on the way in which the actuator is physically connected with the space structure. Although large space structures may consist of plate and shell segments, many large space structures will be truss connections of structural members. In such a case, an actuator may be configured to provide a longitudinal force at a joint connection of several members, an axial force along a member, a moment at a joint, or a bending moment on a member. Since the mathematical characterizations of all of these different physical actuator configurations are equivalent, it suffices in the sequel to consider the output of an actuator to be a suitably defined generalized force applied to the structure.

All electromechanical actuators consist of an electrical subsystem and a mechanical subsystem with some electromechanical interaction. The electrical subsystem is assumed to be of a simple resistive form so that its associated dynamics can be ignored. The mechanical subsystem is assumed to consist of an actuator mass and spring combination which are significant in defining the actuator dynamics. The electromechanical interaction provides a force on the actuator mass of electrical origin. These features are typical of electromechanical actuators where the electromechanical interaction is of magnetic field origin, of electric field origin, or of piezoelectric origin [3-9].

Various devices have been mentioned in the published literature as feasible actuators for vibration control of large space structures: reaction wheels, proof mass actuators, piezoelectric actuators, electronic dampers, voice coil actuators, cable spool actuators, and tendon cable actuators. Each of these electromechanical devices falls within the framework of our subsequent development. Our development does not explicitly include the case of mass expulsion type actuators, control moment gyros, or hydraulic or pneumatic actuators. However, our development may, with some modification, be extended to such cases.

3.2.2 Modelling Assumptions

In this section, the basic assumptions which hold throughout Section 3 are stated. In addition, two classes of actuators are described for detailed examination in the subsequent sections.

Although a large space structure can often be described by a distributed mass model using partial differential equations, our development will make use of a lumped model for a large space structure. Such a model can often be obtained by finite-element methods, even for complex large space structures. Thus the second-order vector differential equation

$$\ddot{M}\mathbf{x} + \dot{D}\mathbf{x} + K\mathbf{x} = B\mathbf{f} \quad (3-1)$$

is chosen to represent the model for structural dynamics. Here \mathbf{x} denotes the n -vector of generalized structural displacements, so that $\dot{\mathbf{x}}$ and $\ddot{\mathbf{x}}$ are structural velocity and acceleration vectors. The $n \times n$ mass matrix M is assumed to be symmetric and positive definite. The $n \times n$ structural stiffness matrix K is assumed to be symmetric. Since our interest is in vibration motion rather than rigid body motion, K is assumed to be positive definite. The $n \times n$ damping matrix D is often rather arbitrarily chosen since there is sparse theory for structural damping available for guidance. In this work, the damping matrix D is assumed to be symmetric and nonnegative definite; the common choice $D = 0$ is allowed. The right-hand side of Eq. (3-1) characterizes the influence of the actuator forces on the structure; the m -vector \mathbf{f} denotes the generalized actuator force vector, while B is an $n \times m$ dimensionless influence matrix. The specific form of the actuator force vector is examined in considerable detail in the following sections.

There are numerous mathematical models that could be used to describe electromechanical actuator dynamics; the literature on actuator dynamics is abundant. Unfortunately, there seems to be no single, tractable model for electromechanical actuator dynamics which is general enough to characterize all of the physical actuators mentioned in the previous section. However, it seems to be the case that each of the physical actuators mentioned does fit into one of two distinct classes of actuators. Hence, our subsequent theory is developed along two separate but parallel lines, corresponding to the two classes of electromechanical actuators considered.

The two electromechanical actuator classes are reaction types and transmission types. Physically, an actuator is a reaction type if the resultant force on the structure is an inertial reaction force; an actuator is a transmission type if the resultant force on the structure is transmitted through a flexible connection. More formally, an actuator is either a reaction type or a transmission type according to the specific form of its mathematical model. In the subsequent sections, detailed mathematical models are developed for each of these two classes of actuators.

Specifically, reaction wheels and proof mass actuators are examples of reaction type actuators, while piezoelectric actuators, electronic dampers, voice coil actuators, cable spool actuators, and tendon cable actuators are

examples of transmission type actuators. Although the literature is vast, References 3-10 through 3-12 examine various examples of reaction type actuators for use in control of elastic systems. References 3-13 through 3-15 examine various examples of transmission type actuators for use in control of elastic systems. This classification of actuators seems natural and is certainly convenient; however, the specific terminology has been chosen by the author and has not been used elsewhere. There is no claim that the classification of electromechanical actuators is exhaustive, but many examples of electromechanical actuators known to the author do seem to fit nicely into one of the two classes. Thus, the classification is suggested as a practical matter whereby mathematically tractable actuator models are obtained.

The structural dynamics, as defined by Eq. (3-1), are defined in terms of a linear differential equation. In the actuator models developed in the next section, the linearity assumption is maintained. But the present work could serve as a framework for development of nonlinear actuator models.

For clarity in the presentation, a mathematical model of a large space structure controlled by a single reaction type actuator is first developed. Next, a mathematical model of a large space structure controlled by a single transmission type actuator is developed. Then the general case where multiple actuators are used to control a large space structure is easily handled.

3.2.3 Single Reaction Type Actuator

In this section, a mathematical model is developed for a large space structure, as described by Eq. (3-1), controlled by a single reaction type actuator.

The basis for our development in this section is the schematic diagram in Figure 3-1. The large space structure is represented by a lumped mass model of which a single mass element is shown. The dynamics of the electromechanical actuator are characterized by an actuator mass, m_a , connected to the structure by a spring and damper in parallel. A reaction type actuator has the property that the electromechanical interaction force, f_a , appears as a reaction pair as shown in this figure. It is claimed that the simple schematic represents the general case of a structure controlled by a single reaction type actuator.

Based on Figure 3-1, equations of motion can be developed using a Lagrangian approach. Introduce the notation

- x = n - vector of generalized structural displacements
- $B^T x$ = scalar generalized displacement of the structure at the actuator location
- z = scalar generalized displacement of the actuator mass relative to the structure

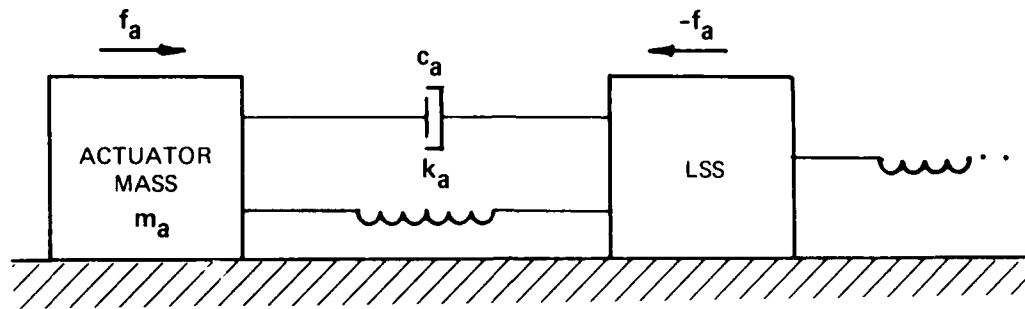


Figure 3-1. Single reaction type actuator.

The actuator/structure Lagrangian is given by

$$L = \frac{1}{2} \dot{x}^T M \dot{x} + \frac{1}{2} m_a \left| \dot{z} + B^T \dot{x} \right|^2 - \frac{1}{2} x^T K x - \frac{1}{2} k_a |z|^2 \quad (3-2)$$

where M and K are $n \times n$ matrices as in Eq. (3-1), B is actuator influence vector, and $m_a > 0$, $k_a > 0$ define the actuator mass and stiffness. From Lagrange's equations obtain

$$M \ddot{x} + m_a B (B^T \ddot{x} + \ddot{z}) + Kx = Q_1 \quad (3-3)$$

$$m_a (B^T \ddot{x} + \ddot{z}) + k_a z = Q_2 \quad (3-4)$$

The generalized forces are

$$Q_1 = -D\dot{x} \quad (3-5)$$

and

$$Q_2 = c_a \dot{z} + f_a \quad (3-6)$$

where f_a represents the electromechanical interaction force given by

$$f_a = b_a u \quad (3-7)$$

Here, u is actuator input voltage, and $b_a > 0$ is actuator servo constant; $c_a > 0$ represents actuator damping coefficient. The choice of coordinates with z defined as a relative displacement results in Q_2 depending explicitly on the reaction force f_a , while Q_1 does not.

In summary, the actuator/structure model obtained is

$$M \ddot{x} + D \dot{x} + Kx = -B m_a (\ddot{z} + B^T \ddot{x}) \quad (3-8)$$

$$m_a (\ddot{z} + B^T \ddot{x}) + c_a \dot{z} + k_a z = b_a u \quad (3-9)$$

These equations are inherently coupled through the actuator inertial term. The effective actuator force on the structure is given by

$$f = -m_a (\ddot{z} + B^T \ddot{x}) \quad (3-10)$$

which can be viewed as a force in reaction to the acceleration of the actuator mass. It is this view that motivates the designation of the actuator as being a reaction type. Note that Eq. (3-8), (3-9), and (3-10) have a transmission zero at $s = 0$. Thus, a reaction type actuator cannot be used to control rigid body motion; the actuator cannot excite the rigid body motion.

There are two approximations that are commonly made, since the actuator/structure dynamics are considerably simplified. The approximation is based on the "no loading assumption" that the acceleration of the structure at the actuator location is negligible compared with the acceleration of the actuator mass, i.e.

$$|B^T \ddot{x}| \ll |\ddot{z}| \quad (3-11)$$

The result is

Approximation Model I

$$M\ddot{x} + D\dot{x} + Kx = -B m_a \ddot{z} \quad (3-12)$$

$$m_a \ddot{z} + c_a \dot{z} + k_a z = b_a u \quad (3-13)$$

This approximation essentially decouples the actuator motion from the structural motion. A further simplification that is often made is to assume that "actuator inertial terms are dominant" in that

$$|k_a z| \ll |m_a \ddot{z}| \quad (3-14)$$

The result is

Approximation Model II

$$M\ddot{x} + D\dot{x} + Kx = -B m_a \ddot{z} \quad (3-15)$$

$$m_a \ddot{z} + c_a \dot{z} = b_a u \quad (3-16)$$

Approximation Model II is often employed to characterize reaction wheel dynamics, since in that case, $k_a = 0$.

The preceding approximation models should be recognized as specific assumed simplifications of the general model described by Eq. (3-8) and (3-9). There is often no a priori reason for accepting the "no loading assumption"; thus, in the subsequent developments, the exact equations (3-8) and (3-9) are used. Of course, all our subsequent results are substantially simplified if one of the above approximations is employed.

3.2.4 Single Transmission Type Actuator

A mathematical model for a large space structure controlled by a single transmission type actuator is now developed.

The basis for the development in this section is the schematic diagram in Figure 3-2. As before, the large space structure is represented by a lumped mass model, of which a single mass element is shown. The dynamics of the electromechanical actuator are characterized by an actuator mass, m_a , connected to the structure by a spring with a damper. A transmission type actuator has the property that the electromechanical interaction force, f_a , acts only on the actuator mass as shown in this figure. It is claimed that the simple schematic of Figure 3-2 represents the general case of a structure controlled by a single transmission type actuator.

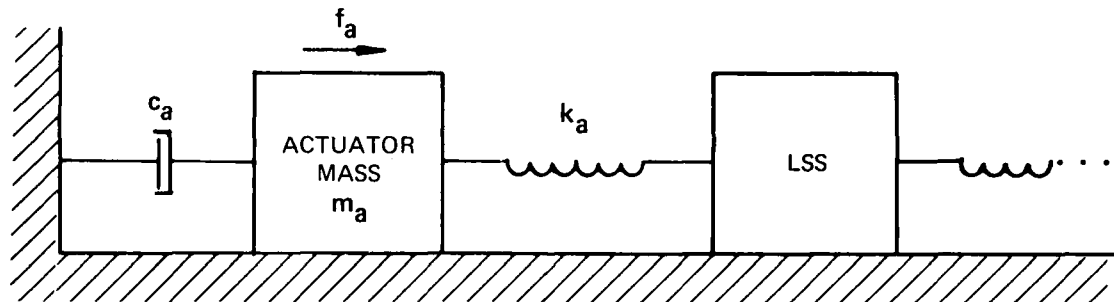


Figure 3-2. Single transmission type actuator.

Based on Figure 3-2, equations of motion can be developed using a Lagrangian approach. Introduce the notation

x = n - vector of generalized structural displacements

$B^T x$ = scalar generalized displacement of the structure at the actuator location

z = scalar generalized displacement of the actuator mass

The actuator/structure Lagrangian is given by

$$L = \frac{1}{2} \dot{x}^T M \dot{x} + \frac{1}{2} m_a \dot{z}^2 - \frac{1}{2} x^T K x - \frac{1}{2} k_a \left| z - B^T x \right|^2 \quad (3-17)$$

where M and K are $n \times n$ matrices as in Eq. (3-1), B is an actuator influence vector, and $m_a > 0$, $k_a > 0$ define the actuator mass and stiffness. From Lagrange's equations obtain

$$M\ddot{x} + Kx - B k_a (z - B^T x) = Q_1 \quad (3-18)$$

$$m_a \ddot{z} + k_a (z - B^T x) = Q_2 \quad (3-19)$$

The generalized forces are

$$Q_1 = -D\dot{x} \quad (3-20)$$

and

$$Q_2 = -c_a \dot{z} + f_a \quad (3-21)$$

where f_a represents the electromechanical interaction force given by

$$f_a = b_a u \quad (3-22)$$

Here u is actuator input voltage, $b_a > 0$ is the actuator servo constant, and $c_a > 0$ is the actuator damping coefficient.

In summary, the actuator/structure model obtained is

$$M\ddot{x} + D\dot{x} + Kx = B k_a (z - B^T x) \quad (3-23)$$

$$m_a \ddot{z} + c_a \dot{z} + k_a (z - B^T x) = b_a u \quad (3-24)$$

These equations are inherently coupled through the actuator flexibility term. The effective actuator force on the structure is given by

$$f = k_a (z - B^T x) \quad (3-25)$$

which can be viewed as a force transmitted from the actuator mass to the structure. It is this view that motivates the designation of the actuator as being a transmission type.

Two approximations of the preceding equations are now mentioned; the resulting actuator/structure dynamics are considerably simplified. The first approximation is based on the "no loading assumption," that the displacement of the structure at the actuator location is negligible compared with the displacement of the actuator mass, i.e.

$$|B^T x| \ll |z| \quad (3-26)$$

The result is

Approximation Model III

$$\ddot{M}x + \dot{D}x + Kx = B k_a z \quad (3-27)$$

$$m_a \ddot{z} + c_a \dot{z} + k_a z = b_a u \quad (3-28)$$

This approximation essentially decouples the actuator motion from the structural motion. A further approximation that is often made is to assume that "actuator flexibility terms are dominant" so that

$$|m_a z| \ll |k_a z| \quad (3-29)$$

The result is

Approximation Model IV

$$\ddot{M}x + \dot{D}x + Kx = B k_a z \quad (3-30)$$

$$c_a \dot{z} + k_a z = b_a u \quad (3-31)$$

The above approximation models should be recognized as specific assumed simplifications of the general model described by Eq. (3-23) and (3-24). There is often no a priori reason for accepting the "no loading assumption"; thus, in the subsequent developments, the exact equations (3-23) and (3-24) are used. All of our subsequent results are substantially simplified if one of the above approximations is employed.

3.2.5 Multiple Actuators

In this section, a mathematical model for a large space structure controlled by multiple actuators is developed. It is assumed that there are a total of m actuators, ordered so that the first p actuators are reaction type and the last $m - p$ actuators are transmission type. The notation used in the previous sections is maintained, so that the actuators/structure Lagrangian is given by

$$L = \frac{1}{2} \dot{x}^T M \dot{x} + \sum_{i \in I_1} \frac{1}{2} m_a^i \left| \dot{z}_i + B_1^T x \right|^2 + \sum_{i \in I_2} \frac{1}{2} m_a^i \left| \dot{z}_i \right|^2 - \frac{1}{2} x^T K x$$

$$-\frac{1}{2} \sum_{i \in I_1} k_a^i |z_i|^2 - \frac{1}{2} \sum_{i \in I_2} k_a^i |z_i - B_i^T x|^2 \quad (3-32)$$

where

$$I_1 = \{1, \dots, p\}$$

$$I_2 = \{p+1, \dots, m\}$$

The parameters $m_a^i > 0$, $k_a^i > 0$ represent the i^{th} actuator mass and stiffness values, and B_i represents the i^{th} actuator influence vector, $i = 1, \dots, m$.

From Lagrange's equations obtain

$$Mx + Kx + \sum_{i \in I_1} B_i m_a^i (z_i + B_i^T x) - \sum_{i \in I_2} B_i k_a^i (z_i - B_i^T x) = Q_1 \quad (3-33)$$

$$m_a^i (B_i^T x + z_i) + k_a^i z_i = Q^i, \quad i \in I_1 \quad (3-34)$$

$$m_a^i z_i + k_a^i (z_i - B_i^T x) = Q^i, \quad i \in I_2 \quad (3-35)$$

The generalized forces are

$$Q_1 = -D\dot{x} \quad (3-36)$$

$$Q^i = -c_a^i \dot{z}_i + f_a^i, \quad i = 1, \dots, m \quad (3-37)$$

where

$$f_a^i = b_a^i u_i, \quad i = 1, \dots, m \quad (3-38)$$

In summary the actuators/structure model obtained is

$$Mx + D\dot{x} + Kx = - \sum_{i \in I_1} B_i m_a^i (z_i + B_i^T x) + \sum_{i \in I_2} B_i k_a^i (z_i - B_i^T x) \quad (3-39)$$

$$m_a^i z_i + c_a^i \dot{z}_i + k_a^i z_i = -m_a^i B_i^T x + b_a^i u_i, \quad i \in I_1 \quad (3-40)$$

$$m_a^i z_i + c_a^i \dot{z}_i + k_a^i z_i = k_a^i B_i^T x + b_a^i u_i, \quad i \in I_2 \quad (3-41)$$

These coupled equations provide the basic model for the actuators/structure. It is observed that Eq. (3-39) takes on the form of Eq. (3-1) where the actuator force vector $f = (f_1, \dots, f_m)$ is given by

$$\begin{aligned} f_i &= -m_a^i (z_i + B_i^T x) , \quad i \in I_1 \\ f_i &= k_a^i (z_i - B_i^T x) , \quad i \in I_2 \end{aligned} \quad (3-42)$$

and

$$B = (B_1, \dots, B_m) \quad (3-43)$$

is $n \times m$ influence matrix.

Actuator approximations, as indicated in the previous sections, can be made. The resulting simplifications are straightforward.

3.3 Centralized Control Design Viewpoint

In Sections 3.3 and 3.4, two viewpoints toward control design for an actuators/structure interconnection are expressed and developed. In this section, the viewpoint of a centralized controller is examined, where feedback of both the structural motion and the actuator motion is possible, with no a priori restriction on the controller form. A certain decentralized control design viewpoint is taken in Section 3.4, where only local feedback of the actuator motion is allowed. This leads to a natural partition of the controller into a force controller which depends on the feedback of the structural motion and actuator servo controllers, one for each actuator, which depend on feedback of the local actuator motion only. This latter control design viewpoint is natural in the case where a force controller is developed by completely ignoring all actuator effects, and internal compensation for each actuator is used to justify that assumption.

Although these two viewpoints have not been explicitly stated in the published literature, they have been implicitly followed in two cases where actuator dynamics have been examined. In Reference 3-16, the actuator dynamics were included as part of the plant for purposes of controller design; this is characteristic of the centralized control design viewpoint. In Reference 3-17 a controller is developed, ignoring actuator dynamics, and the effects of actuator dynamics on the closed loop is evaluated; this is characteristic of the decentralized control design viewpoint.

Consideration of the two control design viewpoints does seem useful since, depending on the context, the role of the actuators in the two cases does differ. These two viewpoints are conceptual. A given controller for an actuator/structure cannot be classified as necessarily having been developed using a particular viewpoint; however, the different viewpoints do lead naturally to certain controller configurations that are discussed in this section and in Section 3.4.

3.3.1 Approach

A large space structure with associated actuators can be viewed as a single plant. This is a natural viewpoint since the mathematical equations which describe the actuators and structure, e.g., Eq. (3-39), (3-40), and (3-41), are inherently coupled. Since there is no reason to distinguish between the actuators and structure in defining the plant, a centralized controller is based on feedback of both the actuator motion and the structural motion. A schematic of a closed loop, incorporating a centralized controller, is shown in Figure 3-3. The actuators and structure are indicated separately for conceptual reasons. The centralized control design viewpoint is defined by the feedback system in Figure 3-3.

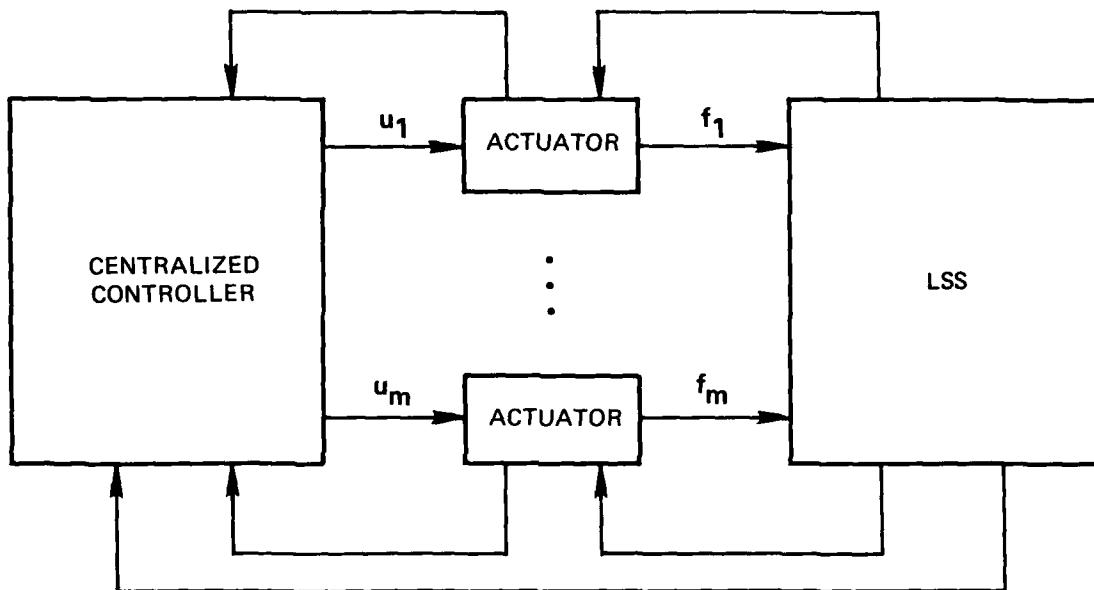


Figure 3-3. Centralized control representation.

3.3.2 Single Reaction Type Actuator

Centralized control using the scheme shown in Figure 3-3 is applied to a large space structure controlled by a single reaction type actuator. The development is based on Eq. (3-8) and (3-9) for the actuator/structure combination. They can be written in compact form as

$$M \ddot{q} + D \dot{q} + K q = B u \quad (3-44)$$

where $q = (x, z)$ and M, D, K, B are partitioned matrices

$$M = \begin{bmatrix} M + m_a B B^T & m_a B \\ m_a B^T & m_a \end{bmatrix} \quad (3-45)$$

$$D = \begin{bmatrix} D & 0 \\ 0 & 0 \end{bmatrix} \quad (3-46)$$

$$K = \begin{bmatrix} K & 0 \\ 0 & k_a \end{bmatrix} \quad (3-47)$$

and

$$B = \begin{bmatrix} 0 \\ b_a \end{bmatrix} \quad (3-48)$$

It is important to recognize that the mathematical form of the augmented Eq. (3-44) is the same as the mathematical form of the large space structure Eq. (3-1) alone, in the sense that the $(n + 1) \times (n + 1)$ matrices, M , D , K , are symmetric with M , K positive definite, and D nonnegative definite. The practical implications of this observation are great: all control design procedures developed explicitly for large space structure equations are formally applicable to the actuator/structure combination. Thus, there is a wide range of design and analysis procedures which are directly applicable to Eq. (3-44). A few simple results are mentioned.

To illustrate the centralized control design viewpoint consider the use of direct velocity feedback.

In the most general case, both the actuator velocity and the structural velocity can be used for feedback control. In this case, the controller is given by

$$u = -\frac{c_f}{b_a} \dot{z} + \frac{C_d^T}{b_a} \dot{x} \quad (3-49)$$

In this case, the second term in Eq. (3-49) is assumed to have a positive coefficient in order to characterize positive damping. The constant scalar, c_f , and vector, C_d , represent the feedback gains. In this case, the closed loop is described by equations

$$M \ddot{q} + D_c \dot{q} + K q = 0 \quad (3-50)$$

where

$$D_c = \begin{bmatrix} D & 0 \\ -C_d & c \end{bmatrix} \quad (3-51)$$

$$D = \begin{bmatrix} D & 0 \\ 0 & c_a \end{bmatrix} \quad (3-46)$$

$$K = \begin{bmatrix} K & 0 \\ 0 & k_a \end{bmatrix} \quad (3-47)$$

and

$$B = \begin{bmatrix} 0 \\ b_a \end{bmatrix} \quad (3-48)$$

It is important to recognize that the mathematical form of the augmented Eq. (3-44) is the same as the mathematical form of the large space structure Eq. (3-1) alone, in the sense that the $(n + 1) \times (n + 1)$ matrices, M , D , K , are symmetric with M , K positive definite, and D nonnegative definite. The practical implications of this observation are great: all control design procedures developed explicitly for large space structure equations are formally applicable to the actuator/structure combination. Thus, there is a wide range of design and analysis procedures which are directly applicable to Eq. (3-44). A few simple results are mentioned.

To illustrate the centralized control design viewpoint consider the use of direct velocity feedback.

In the most general case, both the actuator velocity and the structural velocity can be used for feedback control. In this case the controller is given by

$$u = -\frac{c_f}{b_a} \dot{z} + \frac{C_d^T}{b_a} \dot{x} \quad (3-49)$$

In this case, the second term in Eq. (3-49) is assumed to have a positive coefficient in order to characterize positive damping. The constant scalar, c_f , and vector, C_d , represent the feedback gains. In this case, the closed loop is described by equations

$$M \ddot{q} + D_c \dot{q} + K q = 0 \quad (3-50)$$

where

$$D_c = \begin{bmatrix} D & 0 \\ -C_d & c \end{bmatrix} \quad (3-51)$$

with $c = c_a + c_f$. In this case, the matrix D_c is not symmetric, in fact, the skew-symmetric part of D_c represents the usual gyroscopic type terms [3-18]. The closed-loop system (Eq. (3-50)) is stable if and only if each eigenvalue of Eq. (3-50) has negative real part. A simple sufficient condition for the stability of Eq. (3-50), based on results in Reference 3-18, is the following. Any choice of feedback gains for which the symmetric matrix $D_c + D_c^T$ is positive definite guarantees that the closed loop defined by Eq. (3-50) is stable. Suppose D is positive definite; the closed loop can be stabilized for any actuator velocity gain $c_f > 0$ if the structural velocity gain, C_d , is sufficiently small.

One special case of Eq. (3-49) of particular interest is

$$u = -\frac{c_f}{b_a} \dot{z} \quad (3-52)$$

where only actuator velocity is used for feedback. In this case, the closed loop can be viewed as the feedback connection of the positive real transfer function

$$s B^T [M s^2 + D s + K]^{-1} B \quad (3-53)$$

and the feedback gain, $\frac{c_f}{b_a}$. Hence, based on the results of Reference 3-19, the closed-loop system, Eq. (3-50), with $C_d = 0$, is stable if $c_f > 0$. Moreover, as shown in Reference 3-19, the closed loop has certain desirable robustness properties.

Even the simplest case of Eq. (3-49), corresponding to open-loop control

$$u = 0 \quad (3-54)$$

may be a feasible control strategy. The closed loop system (Eq. (3-50)) with $c_f = 0$, $C_d = 0$, is stable if D is positive definite and $c_a > 0$. This simple control configuration corresponds to the case where the reaction actuator is used as a passive damper [3-20].

The above example control strategies are only illustrative of the centralized design approach applied to a large space structure with a single reaction type actuator.

3.3.3 Single Transmission Type Actuator

Consider Eq. (3-24) and (3-25) developed previously to describe the dynamics for a large space structure controlled by a single transmission type actuator. Those equations can be written in the augmented form

$$\mathbf{M} \ddot{\mathbf{q}} + \mathbf{D} \dot{\mathbf{q}} + \mathbf{K} \mathbf{q} = \mathbf{B} \mathbf{u} \quad (3-55)$$

where $\mathbf{q} = (x, z)$ and \mathbf{M} , \mathbf{D} , \mathbf{K} , \mathbf{B} are partitioned matrices

$$\mathbf{M} = \begin{bmatrix} \mathbf{M} & 0 \\ 0 & m_a \end{bmatrix} \quad (3-56)$$

$$\mathbf{D} = \begin{bmatrix} \mathbf{D} & 0 \\ 0 & c_a \end{bmatrix} \quad (3-57)$$

$$\mathbf{K} = \begin{bmatrix} \mathbf{K} + k_a \mathbf{B} \mathbf{B}^T & -k_a \mathbf{B} \\ -k_a \mathbf{B}^T & k_a \end{bmatrix} \quad (3-58)$$

and

$$\mathbf{B} = \begin{bmatrix} 0 \\ b_a \end{bmatrix} \quad (3-59)$$

In this case, it is recognized that the mathematical form of the augmented Eq. (3-55) is the same as the mathematical form of the large space structure Eq. (3-1) alone, in the sense that the $(n+1) \times (n+1)$ matrices \mathbf{M} , \mathbf{D} , \mathbf{K} are symmetric with \mathbf{M} , \mathbf{K} positive, and \mathbf{D} nonnegative definite. The practical implication of this observation is that any control design procedure developed for large space structure equations is directly applicable to the actuator/structure combination. Thus, there are many design and analysis procedures that can be applied to Eq. (3-55). A few such results are now mentioned.

Direct velocity feedback is again used to illustrate the centralized control design viewpoint in this case.

Assuming both actuator velocity and structural velocity are used for feedback, consider the controller given by

$$\mathbf{u} = -\frac{c_f}{b_a} \dot{z} - \frac{C_d^T}{b_a} \dot{x} \quad (3-60)$$

where c_f and C_d are feedback gains. The closed loop is described by equation

$$M \ddot{q} + D_c \dot{q} + K q = 0 \quad (3-61)$$

where

$$D_c = \begin{bmatrix} D & 0 \\ C_d^T & c \end{bmatrix} \quad (3-62)$$

with $c = c_a + c_f$. Comparing Eq. (3-60) through (3-62) to Eq. (3-49) through (3-51), the discussion following Eq. (3-51) applies here verbatim.

3.3.4 Multiple Actuators

In this section, centralized control of a large space structure controlled by multiple actuators is considered; the assumptions made in Section 3.2.5 are continued so that the actuators/structure are described by Eq. (3-39), (3-40), and (3-41). The augmented variables $z = (z_1, \dots, z_m)$, $q = (x, z)$, and $u = (u_1, \dots, u_m)$ are introduced so that Eq. (3-40), (3-41), and (3-42) can be written as

$$M \ddot{q} + D \dot{q} + K q = B u \quad (3-63)$$

where M , D , K , B are defined by the $(n + m) \times (n + m)$ partitioned matrices

$$M = \begin{bmatrix} M_{11} & M_{12} & 0 \\ M_{12}^T & M_{22} & 0 \\ 0 & 0 & M_{33} \end{bmatrix} \quad (3-64)$$

where

$$M_{11} = M + \sum_{i \in I_1} m_a^i B_i B_i^T \quad (3-65)$$

$$M_{12} = [m_a^1 B_1, \dots, m_a^p B_p] \quad (3-66)$$

$$M_{22} = \text{diag} (m_a^1, \dots, m_a^p) \quad (3-67)$$

$$M_{33} = \text{diag} (m_a^{p+1}, \dots, m_a^m) \quad (3-68)$$

and

$$\mathbf{D} = \begin{bmatrix} \mathbf{D} & 0 \\ 0 & \mathbf{D}_a \end{bmatrix} \quad (3-69)$$

where

$$\mathbf{D}_a = \text{diag} (c_a^1, \dots, c_a^m) \quad (3-70)$$

and

$$\mathbf{K} = \begin{bmatrix} \mathbf{K}_{11} & 0 & \mathbf{K}_{13} \\ 0 & \mathbf{K}_{22} & 0 \\ \mathbf{K}_{13}^T & 0 & \mathbf{K}_{33} \end{bmatrix} \quad (3-71)$$

where

$$\mathbf{K}_{11} = \mathbf{K} + \sum_{i \in I_2} k_a^i \mathbf{B}_i \mathbf{B}_i^T \quad (3-72)$$

$$\mathbf{K}_{13} = (-k_a^{p+1} \mathbf{B}_{p+1}, \dots, -k_a^m \mathbf{B}_m) \quad (3-73)$$

$$\mathbf{K}_{22} = \text{diag} (k_a^1, \dots, k_a^p) \quad (3-74)$$

$$\mathbf{K}_{33} = \text{diag} (k_a^{p+1}, \dots, k_a^m) \quad (3-75)$$

and

$$\mathbf{B} = \begin{bmatrix} 0 \\ \mathbf{B}_a \end{bmatrix} \quad (3-76)$$

where

$$\mathbf{B}_a = \text{diag} (b_a^1, \dots, b_a^m) \quad (3-77)$$

In this general case, the mathematical form of the augmented Eq. (3-63) is the same as the mathematical form of the structure of Eq. (3-1) alone in the sense that the $(n + m) \times (n + m)$ matrices M , D , K are symmetric with M , K positive definite, and D nonnegative definite. Again, the implication of this observation is that all control design procedures developed for large space structure equations are directly applicable to the actuators/structure combination.

Obviously, there are innumerable possible control configurations in the case of multiple actuators. A few cases are considered using feedback of the actuator velocities and the structural velocities.

Consider the feedback controller

$$u = -B_a^{-1} (C_f \dot{z} + C_d \dot{x}) \quad (3-78)$$

where C_f is $m \times m$ gain matrix and C_d is $m \times n$ gain matrix.

The closed loop is described by

$$M \ddot{q} + D_c \dot{q} + K q = 0 \quad (3-79)$$

where

$$D_c = \begin{bmatrix} D & 0 \\ C_d & D_a + C_f \end{bmatrix} \quad (3-80)$$

The nonsymmetric matrix includes gyroscopic terms as before. The closed-loop system, Eq. (3-79), is stable if and only if each eigenvalue of Eq. (3-79) has a negative real part. A simple sufficient condition, based on results in Reference 3-18 is that: any choice of feedback gains for which the symmetric matrix $D_c + D_c^T$ is positive definite guarantees that the closed loop defined by Eq. (3-79) is stable. Suppose D is positive definite. The closed loop can be stabilized for any symmetric, positive definite actuator velocity gain matrix, C_f , if the structural velocity gain matrix, C_d , is sufficiently small.

One special case of the control Eq. (3-78) is

$$u = -B_a^{-1} C_f \dot{z} \quad (3-81)$$

where feedback control depends only on the actuator velocities. In this case, the closed loop can be viewed as the feedback connection of the positive real transfer function matrix

$$s \mathbf{B}^T (\mathbf{M} s^2 + \mathbf{D} s + \mathbf{K})^{-1} \mathbf{B} \quad (3-82)$$

and the feedback gain matrix $\mathbf{B}_a^{-1} \mathbf{C}_f \mathbf{B}_a^{-1}$. Hence, based on results in Reference 3-19, the closed-loop, Eq. (3-63), with $\mathbf{C}_d = 0$, is stable if \mathbf{C}_f is symmetric and positive definite. Moreover, as shown in Reference 3-19, the closed loop has certain desirable robustness properties.

The case where all actuators are used as passive dampers corresponds to

$$\mathbf{u} = 0$$

The closed loop, Eq. (3-63), with $\mathbf{C}_f = 0$, $\mathbf{C}_d = 0$, is stable if \mathbf{D} is positive definite and $\mathbf{C}_a^i > 0$, $i = 1, \dots, m$.

These constant gain velocity feedback strategies are illustrative of the centralized design approach applied to a large space structure controlled by multiple electromechanical actuators.

3.3.5 Comments

The centralized control design approach is to impose no a priori constraints on the controller configuration. This approach is natural when the actuators and structure are viewed as a "plant" and there is no necessary distinction between feedback of the actuators motion and the structural motion.

The advantage of this control design viewpoint is its generality. Since no a priori control constraints are imposed, selection of a particular control configuration can be made with freedom. Furthermore, any particular controller design obtained on the basis of the augmented model, e.g., Eq. (3-63), has explicitly obtained closed-loop properties. In other words, Eq. (3-63) represents a complete model of the actuators and structure.

The disadvantage of designing a controller on the basis of Eq. (3-63) lies in the fact that it contains $n + m$ modes, i.e., $2(n + m)$ state variables. This increase in model order, due to inclusion of the actuator dynamics, may increase the computational difficulty in achieving a good control design. Model order reduction methods have been commonly employed as a way of achieving a reduced-order large space structure model of tractable order [3-4, 3-5]. Our suggestion is that it is preferable to perform any model order reduction on the basis of Eq. (3-63), which includes the actuator dynamics, rather than performing order reduction on the large space structure model alone and subsequently incorporating the actuator dynamics.

3.4 Decentralized Control Design Viewpoint

3.4.1 Approach

A natural approach to the design of a controller is to develop a controller for the large space structure alone, ignoring all actuator dynamics. It is then necessary to provide local compensation for each actuator as a means of justifying the original assumption. The controller is thus separated into two parts: a force controller, typically based on the structural dynamics only, and an actuator servo controller for each actuator. This a priori assumed controller configuration is referred to here as a decentralized controller. A schematic of a closed loop, incorporating a decentralized controller, is shown in Figure 3-4.

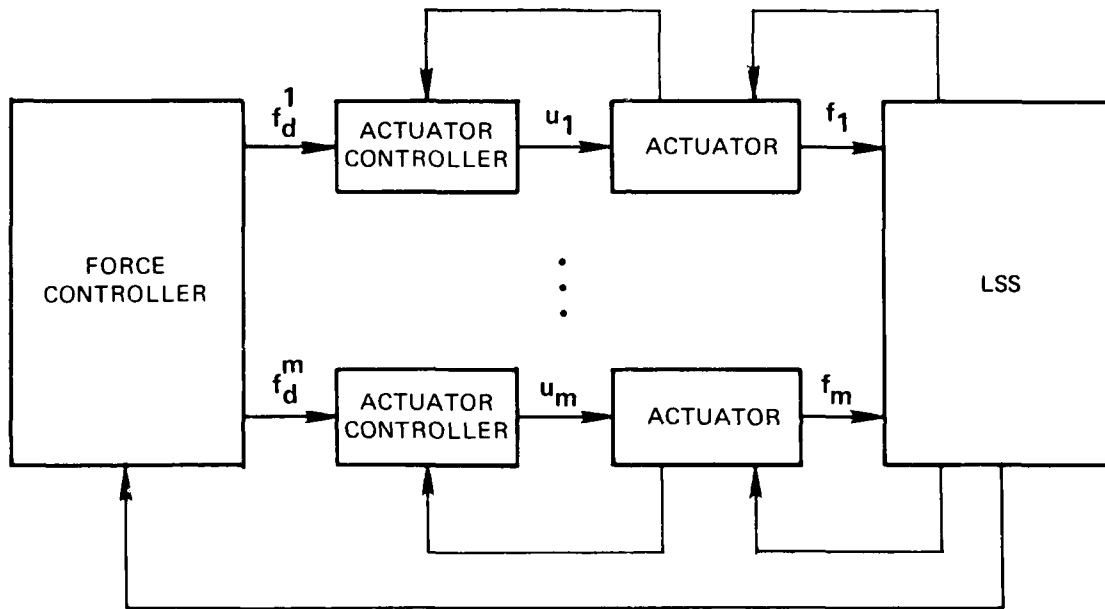


Figure 3-4. Decentralized control representation.

Our objective is to consider a general class of procedures for designing such decentralized control schemes. Since much attention has been focused on the design of force controllers, this issue is generally ignored here. For purposes of illustration, a force controller which depends on structural velocity feedback only is subsequently employed. Our main attention is focused on design of the actuator controllers.

This decentralized control design approach is conceptually appealing. However, the equations which describe the large space structure and actuators, e.g., Eq. (3-40), (3-41), and (3-42), are inherently coupled. This inability to completely separate structural dynamics from actuator dynamics makes the design of a decentralized controller with guaranteed closed-loop properties difficult. Hence, some attention is given to methods for evaluating closed-loop stability, where the loop is closed using a decentralized controller.

3.4.2 Single Reaction Type Actuator

In this section, a decentralized control scheme as shown in Figure 3-4 is developed for the case of a large space structure controlled by a single reaction type actuator.

Let f_d denote the output force of the force controller. The special force controller form

$$f_d = -c_d B^T \dot{x} \quad (3-83)$$

is assumed, where $B^T \dot{x}$ represents the structural velocity feedback and c_d is the feedback gain. Development of the actuator controller characteristics do not strongly depend on the force controller, so subsequent results can easily be generalized if a different force controller form is assumed.

Our objective now is to develop insight into methods for choosing a suitable actuator controller. Since the actuator dynamics cannot be separated from the structural dynamics, care must be taken. The first task is to determine the transfer function from u to f , based on Eq. (3-8) and (3-9), where the actuator force, f , on the structure is given by Eq. (3-10). To this end, define the scalar transfer function

$$G_s(s) = B^T (Ms^2 + Ds + K)^{-1} B \quad (3-84)$$

which represents the influence of the force, f , on the displacement, $B^T x$, of the structure at the location of the actuator. It can be shown that

$$\frac{F(s)}{U(s)} = G_a(s) = \frac{-b_a}{1 + \frac{c_a s + k_a}{m_a s^2} + G_s(c_a s + k_a)} \quad (3-85)$$

Thus $G_a(s)$ represents the effective actuator transfer function, where the structural loading effects on the actuator are taken into account. An actuator controller can be developed using this actuator transfer function, Eq. (3-85).

The actuator controller is supposed to servo the actuator so that the actuator force, f , tracks the desired force, f_d . This is achieved through actuator velocity feedback plus a suitable dynamic interface between f_d and the actuator input voltage, u . Formally, the actuator controller should be realizable and, as closely as is possible, represent the system inverse of $G_a(s)$. It is also desirable for the actuator controller not to depend explicitly on properties of the structure. Such constraints are severe.

One form for the actuator controller, which represents a realizable approximation to the actuator inverse, is given by

$$U(s) = -\frac{1}{b_a} \left(1 + \frac{c}{m_a s}\right) F_d(s) - \frac{c_f}{b_a} s Z(s) \quad (3-86)$$

where $c = c_a + c_f$. This actuator controller depends on actuator velocity feedback plus dynamic (integral) forward compensation. The resulting transfer function from f_d to f is

$$\frac{F(s)}{F_d(s)} = G_f(s) = \frac{1}{1 + \frac{k_a + m_a s^2 (cs + k_a) G_s}{m_a s^2 + cs}} \quad (3-87)$$

where $G_f(s)$ represents the effective actuator controller transfer function. This dimensionless transfer function characterizes the total effect of the actuator and actuator controller dynamics on the structure.

The actuator controller, Eq. (3-86), is a reasonable choice, but other actuator controller forms could be selected. In Eq. (3-86), the actuator controller output voltage, u , depends on feedback of the velocity of the actuator mass; it is also proportional to f_d and to its integral. Clearly, the actuator controller described by Eq. (3-86) is realizable. In the case that f_d is given by Eq. (3-83), the actuator controller output, u , can be expressed directly in terms of the structural displacement and velocity, thereby avoiding need for explicit integration.

The effective actuator transfer function, $G_f(s)$, can be represented as a feedback connection of

$$\frac{m_a s(cs + k_a)}{m_a s^2 + cs + k_a}$$

and

$$sG_s$$

Each of these transfer functions is positive real, with the former strictly positive real if $c > 0$. Using the result in Reference 3-19, the actuator/actuator controller system defined by Eq. (3-87) is stable if $c > 0$. Thus, a reaction type actuator cannot be destabilized when connected to any elastic structure in an open-loop configuration.

The closed-loop configuration of Figure 3-4 is now examined, where the force controller is given by Eq. (3-83), the actuator controller is given by Eq. (3-86), and the actuator/large space structure is described by Eq. (3-8) and (3-9). The closed-loop system is defined by

$$\mathbf{M} \ddot{\mathbf{q}} + \mathbf{D} \dot{\mathbf{q}} + \mathbf{K} \mathbf{q} = \mathbf{0} \quad (3-88)$$

where $\mathbf{q} = (x, z)$ and \mathbf{M} , \mathbf{D} , \mathbf{K} are defined by the partitioned matrices

$$\mathbf{M} = \begin{bmatrix} \mathbf{M} + m_a \mathbf{B} \mathbf{B}^T & m_a \mathbf{B} \\ m_a \mathbf{B}^T & m_a \end{bmatrix} \quad (3-89)$$

$$\mathbf{D} = \begin{bmatrix} \mathbf{D} & \mathbf{0} \\ -\mathbf{B}^T c_d & c \end{bmatrix} \quad (3-90)$$

$$\mathbf{K} = \begin{bmatrix} \mathbf{K} & \mathbf{0} \\ -\frac{c}{m_a} \mathbf{B}^T c_d & k_a \end{bmatrix} \quad (3-91)$$

This set of closed-loop equations does not have the symmetric properties of the structural Eq. (3-1); the matrices \mathbf{D} and \mathbf{K} are not generally symmetric. But Eq. (3-88) could form the basis for analysis of the closed loop.

An alternative description of the closed loop can be given in terms of transfer functions. The return difference function is given by

$$1 + G_f(s) G_p(s) \quad (3-92)$$

where the controller/structure transfer function

$$G_p(s) = C_d s \mathbf{B}^T (\mathbf{M} s^2 + \mathbf{D} s + \mathbf{K})^{-1} \mathbf{B} \quad (3-93)$$

Stability of the closed loop is critical. The following conditions are well known. The closed loop, defined by Eq. (3-88), is stable if and only if each eigenvalue of Eq. (3-88) has a negative real part. Equivalently, the closed loop is stable if and only if each zero of Eq. (3-92) has a negative real part. Such necessary and sufficient conditions for closed-loop stability give little insight into the effect of the actuator dynamics.

From the viewpoint of decentralized control, the key issue is whether the effective actuator dynamics, defined by Eq. (3-87), destabilize the closed loop. Recently developed tests [3-17, 3-22] are particularly suitable in this case since they characterize the robustness of the closed loop explicitly in terms of the effective actuator dynamics. The conditions are sufficient for stability of the closed loop. In the present context the following is obtained.

Suppose that each zero of

$$1 + G_p(s) \quad (3-94)$$

has a negative real part. If

$$|G_f(j\omega) - 1| < |1 + G_p^{-1}(j\omega)| \quad (3-95)$$

holds for all $\omega > 0$, the closed loop is stable.

The hypothesis of Eq. (3-94) is that the closed loop, ignoring actuator dynamics, is stable; this hypothesis is satisfied in the particular case, Eq. (3-93), if $c_d > 0$ [3-18, 3-19]. The frequency condition, Eq. (3-95), has a simple interpretation: the left-hand side represents the frequency response magnitude of the actuator error, while the right-hand side is the frequency response magnitude of the nominal inverse return difference. The inequality Eq. (3-95) can easily be checked using graphical procedures. Use of this robustness test is illustrated in a subsequent example in Section 3.5.

In this case, as a partial justification for the decentralized control design approach, consider the following property. Suppose a force controller is chosen so that the closed loop, ignoring actuator dynamics, is stable. There are actuator parameters, $m_a > 0$, $c > 0$, $k_a > 0$, such that the closed loop, including actuator dynamics, is stable. In other words, it is always possible to determine an actuator and actuator controller of the form of Eq. (3-86) so that the closed loop is stable.

A few general remarks can be made regarding selection of the actuator parameters for a reaction type actuator. The actuator mass parameter, m_a , should be selected so that the inertial effects of the actuator are dominant over the frequency range of interest. The actuator stiffness parameter, k_a , should be chosen as small as possible.

3.4.3 Single Transmission Type Actuator

Decentralized control of a large space structure as shown in Figure 3-4 is now examined where the structure is controlled by a single transmission type actuator.

A force controller given by

$$f_d = -c_d B^T x \quad (3-96)$$

is once again assumed for simplicity, where c_d is the feedback gain constant.

A basis for choosing an actuator controller is now developed. The transfer function for the actuator relates the actuator voltage, u , to the actuator force, f . Using the structural transfer function, G_s , defined by

$$G_s = B^T(Ms^2 + Ds + K)^{-1}B \quad (3-97)$$

and Eq. (3-23) and (3-24) for a transmission type actuator, the actuator input voltage, u , and actuator force, f , defined by Eq. (3-25) can be related by

$$\frac{F(s)}{U(s)} = G_a(s) = \frac{b_a}{1 + \frac{m_a s^2 + c_a s}{k_a} + G_s(m_a s^2 + c_a s)} \quad (3-98)$$

Here, $G_a(s)$ represents the effective actuator transfer function, where the structural loading effects on the actuator are taken into account. An actuator controller can be developed using this actuator transfer function.

As mentioned previously, the actuator controller should be chosen to represent a realizable approximation to the actuator inverse. One suitable form for the actuator controller, in this case, is given by

$$U(s) = \frac{1}{b_a} \left(1 + \frac{cs}{k_a}\right) F_d(s) - \frac{c_f}{b_a} s Z(s) \quad (3-99)$$

where $c = c_a + c_f$. This actuator controller depends on actuator velocity feedback plus dynamic (derivative) forward compensation. The resulting transfer function from f_d to f is

$$\frac{F(s)}{F_d(s)} = \frac{1}{1 + \frac{m_a s^2 + (m_a s^2 + cs)k_a G_s}{cs + k_a}} \quad (3-100)$$

where $G_f(s)$ represents the effective actuator and actuator controller transfer function.

The actuator controller form Eq. (3-99) is one choice, where the actuator controller output, u , depends on feedback of the velocity of the actuator mass and it is proportional to f_d and its derivative. In the case that f_d is given by Eq. (3-96), the actuator controller output, u , can be expressed directly in terms of the structural velocity and acceleration, thereby avoiding need for explicit differentiation.

The effective actuator transfer function, $G_f(s)$, can be represented as a feedback connection of

$$\frac{k_a (m_a s + c)}{m_a s^2 + c s + k_a}$$

and

$$sG(s)$$

Each of these transfer functions is positive real, with the former strictly positive real if $c > 0$. Using results from Reference 3-19, the actuator/actuator controller system defined by Eq. (3-100) is stable if $c > 0$. Consequently, a transmission type actuator can not be destabilized when connected to any elastic structure in an open-loop configuration.

The closed-loop configuration of Figure 3-4 is now examined, where the force controller is given by Eq. (3-96), the actuator controller is given by Eq. (3-99), and the actuator/large space structure is given by Eq. (3-23) and (3-24). The closed-loop system can be described by

$$M \ddot{q} + D \dot{q} + K q = 0 \quad (3-101)$$

where $q = (x, z)$ and M, D, K are defined by the partitioned matrices

$$M = \begin{bmatrix} M & 0 \\ \frac{c}{k_a} B^T c_d & m_a \end{bmatrix} \quad (3-102)$$

$$D = \begin{bmatrix} D & 0 \\ -B^T c_d & c \end{bmatrix} \quad (3-103)$$

$$K = \begin{bmatrix} K + k_a B B^T & -k_a B \\ -k_a B^T & k_a \end{bmatrix} \quad (3-104)$$

The set of closed-loop equations (Eq. (3-101)) does not have the symmetry properties of the structural equation (Eq. (3-1)); the matrices M, D are not generally symmetric. But Eq. (3-101) could form the basis for analysis of the closed loop.

Another description of the closed loop can be given using transfer functions. The return difference function is given by

$$1 + G_f(s) G_p(s) \quad (3-105)$$

where the controller/structure transfer function

$$G_p(s) = c_d s B^T [Ms^2 + Ds + K]^{-1} B \quad (3-106)$$

Stability of the closed loop is easily determined as follows. The closed loop, defined by Eq. (3-101), is stable if and only if each eigenvalue of Eq. (3-101) has a negative real part. Equivalently, the closed loop is stable if and only if each zero of Eq. (3-105) has a negative real part. Simpler conditions which give explicit insight into the effect of actuator dynamics are also available using the robustness tests of References 3-17 and 3-22.

Suppose that each zero of

$$1 + G_p(s) \quad (3-107)$$

has a negative real part. If

$$|G_f(j\omega) - 1| < |1 + G_p^{-1}(j\omega)| \quad (3-108)$$

holds for all $\omega > 0$, the closed loop is stable.

As stated previously, the general hypothesis of Eq. (3-107) is that the closed loop, ignoring the actuator dynamics, is stable; the hypothesis is satisfied in the special case, Eq. (3-106), if $c_d > 0$ [3-18, 3-19]. The frequency condition, Eq. (3-108), has a simple interpretation and can be easily checked graphically. Use of these robustness tests is illustrated by a subsequent example in Section 3.5.

As a partial justification for the decentralized control design approach, in this case, consider the following property. Suppose a force controller is chosen so that the closed loop, ignoring actuator dynamics, is stable. There are actuator parameters, $m_a > 0$, $c > 0$, $k_a > 0$, such that the closed loop, including actuator dynamics, is stable. In other words, it is always possible to determine an actuator and actuator controller of the form of Eq. (3-99) so that the closed loop is stable.

A few remarks can be made regarding selection of the actuator parameters for a transmission type actuator. The actuator stiffness parameter, k_a , should be selected so that flexibility effects of the actuator are dominant over the frequency range of interest. The actuator mass parameter, m_a , should be chosen as small as possible.

3.4.4 Multiple Actuators

In this section, decentralized control of a large space structure controlled by multiple actuators is considered; the assumptions made in Section 3.2.5 are continued so that the actuators/structure are described by Eq. (3-40), (3-41), and (3-42).

A force controller is assumed to be of the form

$$f_d = -C_d B^T x \quad (3-109)$$

where

$$f_d = (f_d^1, \dots, f_d^m) \quad (3-110)$$

$$B = (B_1, \dots, B_m)$$

and C_d is $m \times m$ feedback gain matrix.

Actuator controllers for each actuator are used as in the previous sections. On the basis of the previous developments, the actuator controllers are assumed to be given by

$$U_i(s) = -\frac{1}{b_a^i} \left(1 + \frac{c_i}{m_a^i s}\right) F_d^i(s) - \frac{c_f^i}{b_a^i} s Z_i(s), \quad i \in I_1 \quad (3-111)$$

$$U_i(s) = \frac{1}{b_a^i} \left(1 + \frac{c_i s}{k_a^i}\right) F_d^i(s) - \frac{c_f^i}{b_a^i} s Z_i(s), \quad i \in I_2 \quad (3-112)$$

where $c_i = c_a^i + c_f^i$, $i = 1, \dots, m$. Each actuator controller depends on actuator velocity feedback plus dynamic forward compensation. The resulting $m \times m$ effective actuator and actuator controller transfer function matrix $G_f(s)$ defined by

$$F(s) = G_f(s) F_d(s) \quad (3-113)$$

is given by

$$G_f(s) = (I + Q_1(s) + Q_2(s) G_s(s))^{-1} \quad (3-114)$$

where

$$Q_1(s) = \text{diag} \left(\frac{k_a^1}{m_a^1 s^2 + c_1 s}, \dots, \frac{m_a^{p+1} s^2}{c_{p+1} s + k_a^{p+1}}, \dots \right) \quad (3-115)$$

$$Q_2(s) = \text{diag} \left(\frac{m_a^1 s^2 (c_1 s + k_a^1)}{m_a^1 s^2 + c_1 s}, \dots, \frac{k_a^{p+1} (m_a^{p+1} s^2 + c_{p+1} s)}{c_{p+1} s + k_a^{p+1}}, \dots \right) \quad (3-116)$$

and

$$G_s(s) = B^T (Ms^2 + Ds + K)^{-1} B \quad (3-117)$$

This actuator/actuator controller transfer function, $G_f(s)$, is not in general diagonal due to the presence of the general nondiagonal structural transfer function, $G_s(s)$, in Eq. (3-114). In the case where multiple actuators are used to control a large space structure, the effective actuator dynamics involve crossfeed between the actuation channels, where the cross feed effects are explicitly due to structural loading of the actuators.

The effective actuator transfer function, $G_f(s)$, can be represented as a feedback connection of

$$[I + Q_1(s)]^{-1} \frac{Q_2(s)}{s}$$

and

$$sG_s(s)$$

Each of these transfer function matrices are positive real, with the former strictly positive real if $c_i > 0$, $i = 1, \dots, m$. From the results in References 3-18 and 3-19, the actuator/actuator controller system defined by Eq. (3-114) is stable if $c_i > 0$, $i = 1, \dots, m$. Consequently, multiple actuators of the reaction and transmission types cannot be destabilized when connected to any elastic structure in an open-loop configuration.

The closed-loop configuration of Figure 3-4 is now examined, where the force controller is given by Eq. (3-109), the actuator controllers are given by Eq. (3-111) and (3-112) and the actuator/large space structure is described by Eq. (3-40), (3-41), and (3-42). The closed-loop system can be described by

$$M \ddot{q} + D \dot{q} + K q = 0 \quad (3-118)$$

where $q = (x, z_1, \dots, z_m)$ and M , D , K are defined by $(n + m) \times (n + m)$ partitioned matrices

$$\mathbf{M} = \begin{bmatrix} \mathbf{M}_{11} & \mathbf{M}_{12} & 0 \\ \mathbf{M}_{12}^T & \mathbf{M}_{22} & 0 \\ \mathbf{M}_{31} & 0 & \mathbf{M}_{33} \end{bmatrix} \quad (3-119)$$

where

$$\mathbf{M}_{11} = \mathbf{M} + \sum_{i \in I_1} m_a^i \mathbf{B}_i \mathbf{B}_i^T \quad (3-120)$$

$$\mathbf{M}_{12} = (m_a^1 \mathbf{B}_1, \dots, m_a^p \mathbf{B}_p) \quad (3-121)$$

$$\mathbf{M}_{22} = \text{diag} (m_a^1, \dots, m_a^p) \quad (3-122)$$

$$\mathbf{M}_{33} = \text{diag} (m_a^{p+1}, \dots, m_a^m) \quad (3-123)$$

$$\mathbf{M}_{31}^T = \left(\frac{c_{p+1}}{k_a^{p+1}} \mathbf{B}_d^{p+1}, \dots, \frac{c_m}{k_a^m} \mathbf{B}_d^m \right) \quad (3-124)$$

and the feedback gain matrix

$$\mathbf{C}_d^T = [c_d^1, \dots, c_d^m] \quad (3-125)$$

and

$$\mathbf{D} = \begin{bmatrix} \mathbf{D}_{11} & 0 & 0 \\ \mathbf{D}_{21} & \mathbf{D}_{22} & 0 \\ \mathbf{D}_{31} & 0 & \mathbf{D}_{33} \end{bmatrix} \quad (3-126)$$

where

$$\mathbf{D}_{11} = \mathbf{D} \quad (3-127)$$

$$\mathbf{D}_{22} = \text{diag} (c_1, \dots, c_p) \quad (3-128)$$

$$\mathbf{D}_{33} = \text{diag} (c_{p+1}, \dots, c_m) \quad (3-129)$$

$$D_{21}^T = (-BC_d^1, \dots, -BC_d^p) \quad (3-130)$$

$$D_{31}^T = (BC_d^{p+1}, \dots, BC_d^m) \quad (3-131)$$

and

$$K = \begin{bmatrix} K_{11} & 0 & K_{13} \\ K_{21} & K_{22} & 0 \\ K_{13}^T & 0 & K_{33} \end{bmatrix} \quad (3-132)$$

where

$$K_{11} = K + \sum_{i \in I_2} k_a^i B_i B_i^T \quad (3-133)$$

$$K_{22} = \text{diag} (k_a^1, \dots, k_a^p) \quad (3-134)$$

$$K_{33} = \text{diag} (k_a^{p+1}, \dots, k_a^m) \quad (3-135)$$

$$K_{13} = [-k_a^{p+1} B_{p+1}, \dots, -k_a^m B_m] \quad (3-136)$$

$$K_{21}^T = \left[\frac{c_1}{m_a^1} BC_d^1, \dots, -\frac{c_p}{m_a^p} BC_d^p \right] \quad (3-137)$$

This set of closed-loop equations does not have the symmetry properties of the structural equation (Eq. (3-1)), but Eq. (3-118) could form the basis for analysis of the closed loop.

An alternative description of the closed loop can be given in terms of transfer functions. The return difference function is given by

$$\det [I + G_f(s) G_p(s)] \quad (3-138)$$

where the controller/structure transfer function

$$G_p(s) = C_d^T (Ms^2 + Ds + k)^{-1} B \quad (3-139)$$

Stability of the closed loop is an essential property and can be characterized as follows. The closed loop, defined by Eq. (3-118), is stable if and only if each eigenvalue of Eq. (3-118) has a negative real part. Equivalently, the closed loop is stable if and only if each zero of Eq. (3-138) has a negative real part. Such necessary and sufficient conditions for closed-loop stability are so complicated that little insight into the effect of the actuator dynamics is obtained.

Simpler conditions, which do give explicit insight into the effect of actuator dynamics on closed-loop stability, can be developed using the results of References 3-17 and 3-22. Suppose that each zero of

$$\det[1 + G_p(s)] \quad (3-140)$$

has a negative real part. If

$$\bar{\sigma}[G_f(j\omega) - 1] < \underline{\sigma}[1 + G_p^{-1}(j\omega)] \quad (3-141)$$

holds for all $\omega > 0$, the closed loop is stable. Here $\bar{\sigma}[G]$ and $\underline{\sigma}[G]$ denote the maximum and minimum singular values of a matrix G , respectively.

The general hypothesis of Eq. (3-140) is that the closed loop, ignoring all actuator dynamics, is stable; the hypothesis is satisfied in the special case in Eq. (3-139) if C_d is symmetric and positive definite (Eq. [3-18]). The frequency condition, Eq. (3-141), has a simple interpretation and can be checked graphically.

In the case where multiple actuators are used to control a large space structure, it can be shown that it is always possible to determine actuators and actuator controllers of the form of Eq. (3-111) and (3-112) so that the closed loop is stable. Suppose a force controller is chosen so that the closed loop, ignoring actuator dynamics, is stable. There are actuator parameters, $m_a^i > 0$, $c_i > 0$, $k_a^i > 0$, $i = 1, \dots, m$, such that the closed loop, including actuator dynamics, is stable. Explicit guidelines for selection of the actuator parameters are difficult to obtain. As in the previous sections, it appears desirable to choose large $m_a^i > 0$ and small $k_a^i > 0$, $i = 1, \dots, p$ for the reaction actuator parameters and small $m_a^i > 0$ and large $k_a^i > 0$, $i = p + 1, \dots, m$ for the transmission actuator parameters. Substantial trial and error may be required to select the actuator parameters effectively in a particular case.

3.4.5 Comments

The decentralized control design approach is to impose the a priori constraint that the controller consists of a force controller and a set of actuator controllers, one for each actuator, as shown in Figure 3-4. This approach is natural when the structure is viewed as the "plant" and the actuator

AD-A135 675

ACROSS ELEVEN (ACTIVE CONTROL OF SPACE STRUCTURES)
VOLUME 1(U) CHARLES STARK DRAPER LAB INC CAMBRIDGE MA
E FOGEL ET AL. JUL 83 CSDL-R-1598-VOL-1

2/2

UNCLASSIFIED

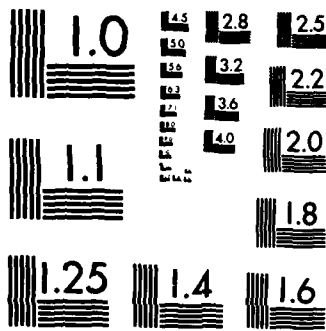
RADC-TR-83-158-VOL-1 F30602-81-C-0180

F/G 22/1

NL

END

FORMED
144
1110



MICROCOPY RESOLUTION TEST CHART
NATIONAL BUREAU OF STANDARDS-1963-A

dynamics are ignored; a controller obtained on the basis of this assumption is essentially a force controller. The actuator controllers can be subsequently developed.

The main advantage of this control design viewpoint is that, since all actuator dynamics are ignored in developing a force controller, there is a reduction in dimensionality and hence complexity of the control design problem. Such an order of reduction is often desirable as a means of obtaining a computationally tractable control design problem. Specifically, this decentralized approach depends on obtaining a force controller based on n structural modes, plus m single-loop actuator controllers, as opposed to the use of $n + m$ modes, i.e., $2(n + m)$ state variables if the centralized control design approach is taken.

The major disadvantage with this approach is that there can be no guarantee of specific closed-loop properties, e.g., stability. As shown in Reference 3-23 and elsewhere, there is the possibility that a closed-loop system with controllers chosen to stabilize the closed loop, ignoring actuator dynamics, may, in fact, be destabilized by actuator dynamics. Thus closed-loop characteristics, where the controller is obtained using the decentralized design approach, should always be carefully analyzed. As indicated, a complete eigenvalue analysis of the closed loop can be performed using, for example, Eq. (3-118). An alternative that often gives insight into the specific importance of the actuator parameters is to make use of the robustness test as discussed.

3.5 Examples

3.5.1 Control of Single-Mode Structure Using Single Reaction Type Actuator

Our objective here is to illustrate the theory developed for reaction type actuators by examining in some detail the simplest case of a single-mode structure controlled by a single reaction type actuator.

From Eq. (3-8) and (3-9), the mathematical model for the structure/actuator is

$$M\ddot{x} + D\dot{x} + Kx = -m_a(\ddot{x} + \ddot{z}) \quad (3-142)$$

$$m_a(\ddot{z} + \ddot{x}) + c_a\dot{z} + k_a z = b_a u \quad (3-143)$$

where $M > 0$, $D > 0$, and $K > 0$ are structural mass, damping, and stiffness parameters, and $m_a > 0$, $c_a > 0$, $k_a > 0$, and $b_a > 0$ are actuator mass, damping, stiffness, and input parameters; x denotes the scalar displacement of the structure.

It is convenient to introduce the parameters

$$\rho = \frac{m_a}{M}, \quad \omega_s^2 = \frac{K}{M}, \quad 2\zeta_s \omega_s = \frac{D}{M}, \quad \omega_a^2 = \frac{k_a}{m_a} \quad (3-144)$$

in the analysis to follow. Several different control laws are now examined.

First, consider feedback control using only actuator velocity feedback as given by

$$u = -\frac{c_f}{b_a} \dot{z} \quad (3-145)$$

If the definition

$$2\zeta_a \omega_a = \frac{c_a + c_f}{m_a} \quad (3-146)$$

is used, the closed-loop characteristic equation can be written as

$$1 + \frac{2\zeta_a \omega_a s [(1 + \rho)s^2 + 2\zeta_s \omega_s s + \omega_s^2]}{(s^2 + 2\zeta_s \omega_s s + \omega_s^2)(s^2 + \omega_a^2) + \rho s^2 \omega_a^2} = 0 \quad (3-147)$$

It is easily shown that the closed-loop system defined by Eq. (3-142), (3-143), and (3-144), is always stable for any $\zeta_a > 0$, $\zeta_s \geq 0$. Thus, the structure can be stabilized by using only actuator velocity feedback or by using the actuator as a passive damper. A root locus plot for Eq. (3-147) for the indicated parameter values is shown in Figure 3-5; dependence of the closed-loop poles on the actuator damping parameter, ζ_a , is indicated. Although the structure is stabilized by the actuator, there is a modest amount of closed-loop damping that can be achieved using the feedback control Eq. (3-145). The maximum damping ratio for the dominant pole pair is 0.12, corresponding to the selection of $\zeta_a = 0.68$.

Consequently, the centralized control viewpoint suggests use of the controller

$$u = -\frac{c_f}{b_a} \dot{z} + \frac{c_c}{b_a} \dot{x} \quad (3-148)$$

where both the actuator velocity and the structural velocity are fed back. If the definition

$$2\zeta_c \omega_s = \frac{c_c}{M} \quad (3-149)$$

is used, the closed-loop characteristic equation can be written as

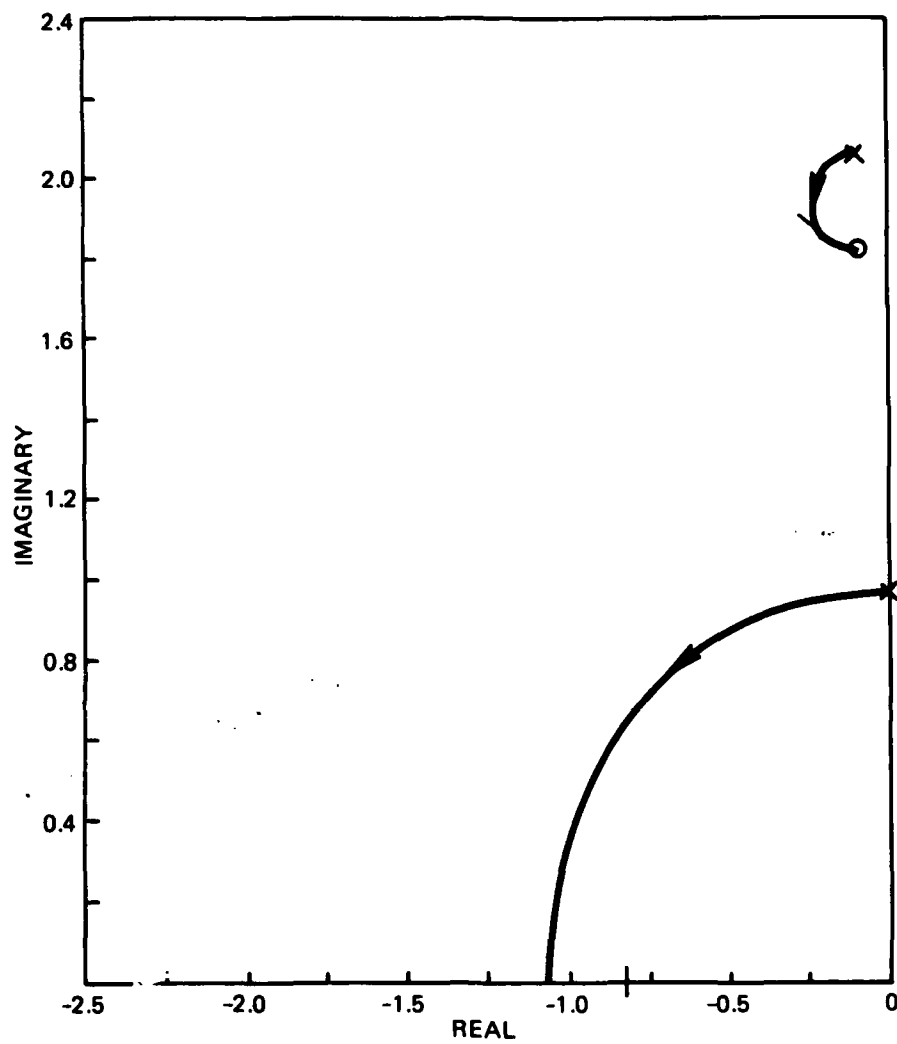


Figure 3-5. Closed-loop root locus.
 Type: Reaction Actuator
 Feedback: Actuator only
 Parameter: ζ_a
 Data: $\rho = 0.2$, $\omega_a^2 = 1.0$, $\omega_s^2 = 4.0$, $\zeta_s = 0.05$

$$1 + \frac{(2\zeta_c \omega_s s) s^2}{(s^2 + 2\zeta_s \omega_s s + \omega_s^2)(s^2 + 2\zeta_a \omega_a s + \omega_a^2) + \rho s^2(2\zeta_a \omega_a s + \omega_a^2)} = 0 \quad (3-150)$$

The closed-loop system, defined by Eq. (3-142), (3-143), and (3-148), is stable for any $\zeta_a > 0$ and for ζ_c , not exceeding some bound. A root locus plot for Eq. (3-150) for the particular value $\zeta_a = 0.68$ obtained in Figure 3-5 is shown in Figure 3-6; dependence of the closed-loop poles on the structural damping parameter, ζ_c , is indicated. In this case, significant additional damping can be obtained by using the feedback control Eq. (3-148). Note that Figure 3-6 indicates that there is a limit to the closed-loop damping that can be achieved; the maximum damping ratio for the dominant pole pair is 0.25 corresponding to the choice $\zeta_c = 0.19$. If the structural velocity feedback gain is too large so that $\zeta_c > 1.0$, the closed loop is unstable.

The decentralized control viewpoint suggests use of the force controller

$$f_d = -c_d \dot{x} \quad (3-151)$$

together with the actuator controller defined by

$$U(s) = -\frac{1}{b_a} \left(1 + \frac{c}{m_a s}\right) F_d(s) - \frac{c_f}{b_a} s Z(s) \quad (3-152)$$

where $c = c_a + c_f$. As mentioned previously, these expressions can be combined to obtain the expression

$$u = -\frac{c_f}{b_a} \dot{z} - \frac{c_d}{b_a} \dot{x} + \frac{cc_d}{bm_a} x \quad (3-153)$$

which can be compared with Eq. (3-145) and (3-148); an extra displacement feedback term appears in Eq. (3-153). Hence, the actuator controller Eq. (3-152) in conjunction with structural velocity feedback for the force controller is equivalent to the controller Eq. (3-153). The effective actuator transfer function using Eq. (3-87) is

$$G_f(s) = \frac{(s^2 + 2\zeta_a \omega_a s)(s^2 + 2\zeta_s \omega_s s + \omega_s^2)}{(s^2 + 2\zeta_s \omega_s s + \omega_s^2)(s^2 + 2\zeta_a \omega_a s + \omega_a^2) + \rho s^2(2\zeta_a \omega_a s + \omega_a^2)} \quad (3-154)$$

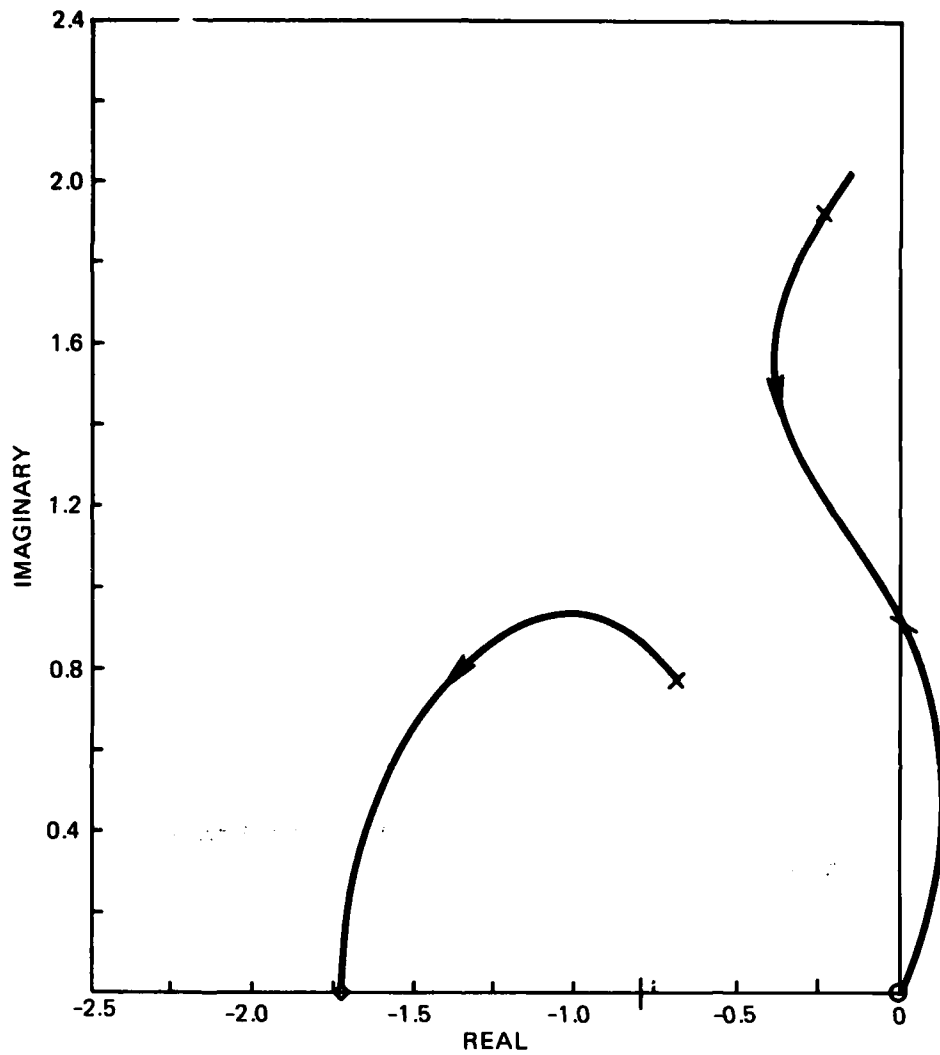


Figure 3-6. Closed-loop root locus.
 Type: reaction actuator
 Feedback: centralized
 Parameter: ζ_c
 Data: $\rho_2 = 0.2$, $\omega_a^2 = 1.0$, $\omega_s^2 = 4.0$, $\zeta_a = 0.68$

Using the control Eq. (3-153), if the definitions

$$2\zeta_d \omega_s = \frac{c_d}{M} \quad (3-155)$$

and

$$G_p(s) = \frac{2\zeta_d \omega_s}{s^2 + 2\zeta_s \omega_s s + \omega_s^2} \quad (3-156)$$

are introduced, the closed-loop characteristic equation can be written as

$$1 + G_f(s) G_p(s) = 0 \quad (3-157)$$

The closed-loop system defined by Eq. (3-142), (3-143), (3-151), and (3-152) is stable for all values $\zeta_a > 0$ and $\zeta_d > 0$. A root locus plot of Eq. (3-157), for the particular value of $\zeta_a = 0.68$ obtained in Figure 3-5, is shown in Figure 3-7. Dependence of the closed-loop poles on the structural damping parameter, ζ_d , is indicated. In this case, significant additional damping can be obtained by using the force controller Eq. (3-151) and the actuator controller Eq. (3-152). Figure 3-7 indicates that there is a limit to the closed-loop damping that can be achieved. For example, if $\zeta_d = 0.25$, the damping ratios for the two pole pairs are 0.47 and 0.48.

As an alternative to a direct analysis of the closed-loop poles, the robustness test of Eq. (3-95) can be used. One procedure would be to plot the frequency response of the actuator error, $|G_f(j\omega) - 1|$, which does not depend on the force controller. Then the force controller could be adjusted to guarantee satisfaction of the robustness inequality Eq. (3-95). In this particular example, the frequency response for the actuator error function, $|G_f(j\omega) - 1|$, is indicated in Figure 3-8; and for any $\zeta_d > 0$, the robustness inequality Eq. (3-95) is satisfied. To illustrate the procedure, the frequency response for the inverse return difference function, $|1 + G_p^{-1}(j\omega)|$, is indicated in Figure 3-8 for the value $\zeta_d = 0.25$. Certain conclusions can be drawn from the figure based on the robustness test, Eq. (3-95). First, it is clear that for $\zeta_d = 0.25$, and in fact for any $\zeta_d > 0$, the actuator dynamics do not destabilize the closed loop using the force controller Eq. (3-151). Second, since the separation between $|1 + G_p^{-1}(j\omega)|$ and $|G_f(j\omega) - 1|$ is an indication of the stability margin, Figure 3-8 can be used to assess qualitative characteristics of the closed loop. In particular, the closed loop would be most sensitive to disturbances at a frequency near 2.0 rad/s, where the "loading peak" for the actuator error occurs. Further, the high frequency margins are large since the actuator error is small. At low frequencies, the actuator errors are relatively large, but good margin is maintained due to the force controller characteristic. These qualitative conclusions should be typical of a large space structure controlled by a single reaction type actuator, using a properly chosen force controller.

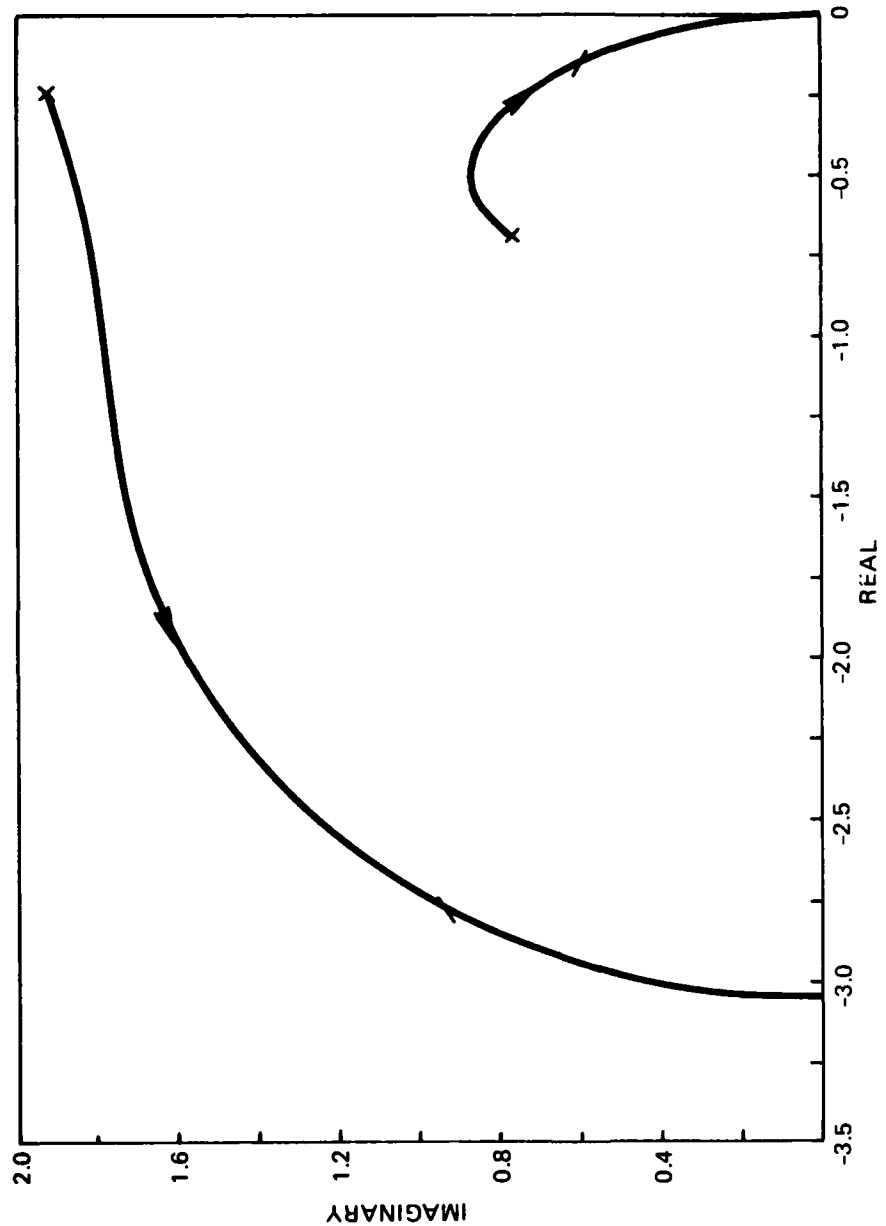


Figure 3-7. Closed-loop root locus.
 Type: reaction actuator
 Feedback: decentralized
 Parameter: ζ_d
 Data: $\rho_2 = 0.2, \omega_a^2 = 1.0, \omega_s^2 = 4.0, \zeta_s = 0.5, \zeta_a = 0.68$

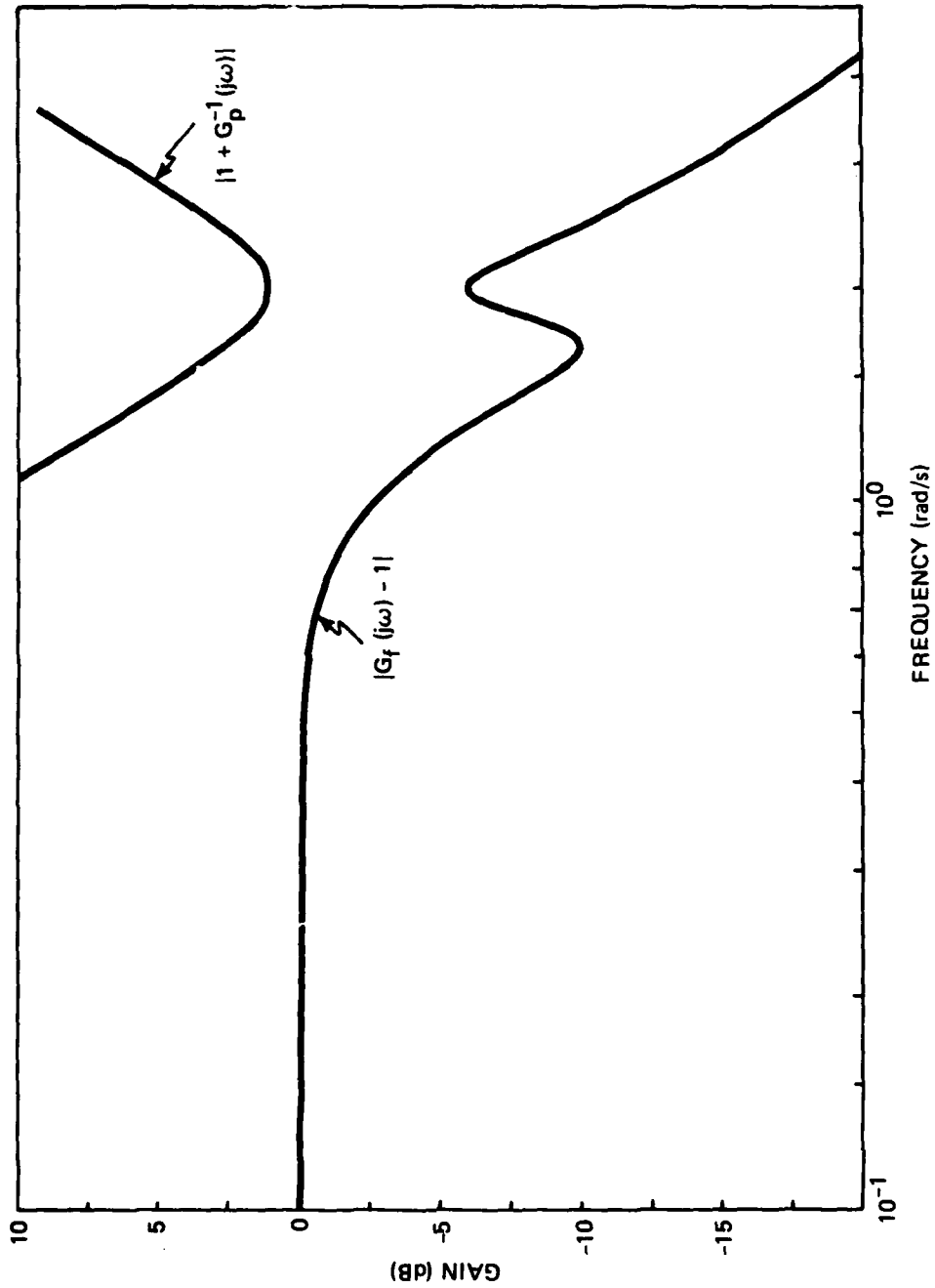


Figure 3-8. Robustness test (Eq. (3-95))

Type: reaction actuator
 Feedback: decentralized

Data: $\rho_2 = 0.2$, $\omega_a^2 = 1.0$, $\omega_s^2 = 4.0$, $\zeta_s = 0.05$, $\zeta_a = 0.68$,
 $\zeta_\alpha = 0.25$

Experience has indicated that the magnitude of the loading peak for the actuator error is strongly affected by the assumption regarding open-loop structural damping. In particular, the robustness inequality of Eq. (3-95) may not be satisfied if the open-loop structural damping is assumed too low.

3.5.2 Control of a Single-Mode Structure Using Single Transmission Type Actuator

The previously developed theory is now illustrated by examining in some detail the simplest case of a single-mode structure controlled by a single transmission type actuator.

The mathematical model for the actuator/structure is based on Eq. (3-23) and (3-24), which in this case can be written as

$$M\ddot{x} + D\dot{x} + Kx = k_a(z - x) \quad (3-158)$$

$$m_a\ddot{z} + c_a\dot{z} + k_a(z - x) = b_a u \quad (3-159)$$

where $M > 0$, $D > 0$, and $K > 0$ are structural mass, damping, and stiffness parameters and $m_a > 0$, $c_a > 0$, $k_a > 0$, and $b_a > 0$ are actuator mass, damping, stiffness, and input parameters; and x denotes the scalar displacement of the structure.

It is convenient to introduce the parameters

$$\rho = \frac{k_a}{K}, \quad \omega_s^2 = \frac{K}{M}, \quad 2\zeta_s\omega_s = \frac{D}{M}, \quad \omega_a^2 = \frac{k_a}{m_a} \quad (3-160)$$

in this case. Several different control laws, each based on some form of velocity feedback, are now examined.

First, consider feedback control using only actuator velocity feedback as given by

$$u = -\frac{c_f}{b_a} \dot{z} \quad (3-161)$$

Define the actuator damping parameter ζ_a from

$$2\zeta_a\omega_a = \frac{c_a + c_f}{m_a} \quad (3-162)$$

The closed-loop characteristic equation can be written as

$$1 + \frac{2\zeta_a \omega_a s [s^2 + 2\zeta_s \omega_s s + (1 + \rho)\omega_s^2]}{(s^2 + 2\zeta_s \omega_s s + \omega_s^2)(s^2 + \omega_a^2) + \rho s^2 \omega_s^2} = 0 \quad (3-163)$$

Using this characteristic equation, it is easily shown that the closed-loop system defined by Eq. (3-158), (3-159), and (3-161) is always stable for any $\zeta_a > 0$. The structure can always be stabilized by using only actuator velocity feedback or by using the actuator as a passive damper. A root locus plot for Eq. (3-163) for a particular case is shown in Figure 3-9; dependence of the closed-loop poles on the actuator damping parameter, ζ_a , is indicated. The structure can be stabilized in this manner, but only modest damping of the closed loop can be achieved using feedback of the actuator velocity only. The maximum damping ratio for the dominant pole pair is 0.12, corresponding to the selection of $\zeta_a = 0.78$.

In order to achieve additional structural damping, the centralized control viewpoint suggests feedback of both actuator and structural velocity as given by the controller

$$u = -\frac{c_f}{b_a} \dot{z} - \frac{c_c}{b_a} \dot{x} \quad (3-164)$$

Define the structural damping parameter, ζ_c , from

$$2\zeta_c \omega_s = \frac{c_c}{M} \quad (3-165)$$

the closed-loop characteristic equation can be written as

$$1 + \frac{(2\zeta_c \omega_s) \omega_a^2}{(s^2 + 2\zeta_s \omega_s s + \omega_s^2)(s^2 + 2\zeta_a \omega_a s + \omega_a^2) + \rho \omega_s^2 (s^2 + 2\zeta_a \omega_a s)} = 0 \quad (3-166)$$

The closed-loop system, defined by Eq. (3-158), (3-159), and (3-164), is stable for any $\zeta_a > 0$ and for ζ_c not exceeding some bound. A root locus plot for Eq. (3-166) for the particular value $\zeta_a = 0.78$ obtained in Figure 3-9 is shown in Figure 3-10; dependence of the closed-loop poles on the structural damping parameter ζ_c is indicated. It is clear from Figure 3-10 that substantial additional closed-loop damping can be achieved by feedback of both actuator and structural velocities. In particular, a maximum damping ratio of 0.21 can be achieved for the dominant pole pair, corresponding to $\zeta_c = 0.21$. If the structural velocity feedback gain is too large so that $\zeta_c > 1.3$, the closed loop is unstable.

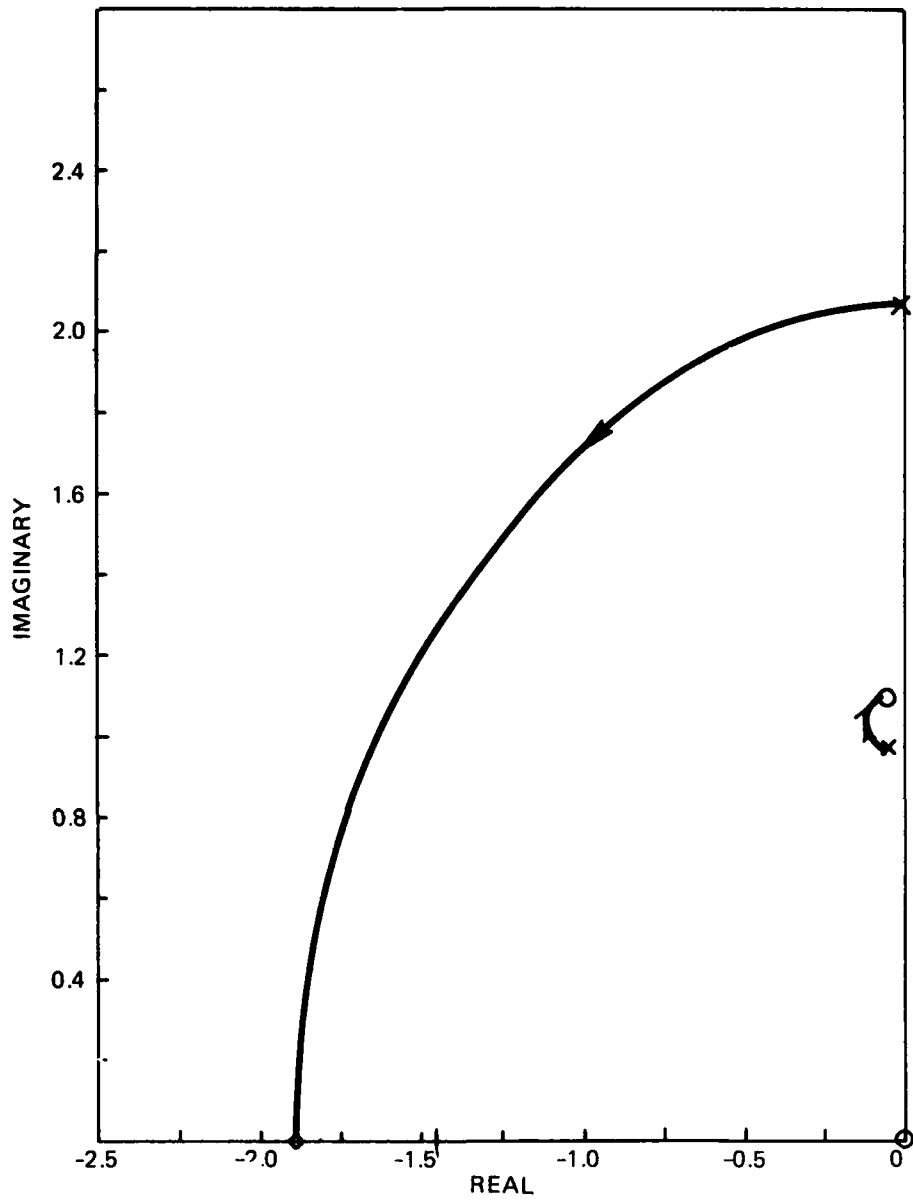


Figure 3-9. Closed-loop root locus
 Type: transmission actuator
 Feedback: actuator only
 Parameter: ζ_a
 Data: $\rho_2 = 0.2$, $\omega_s^2 = 4.0$, $\omega_s^2 = 1.0$, $\zeta_s = 0.05$

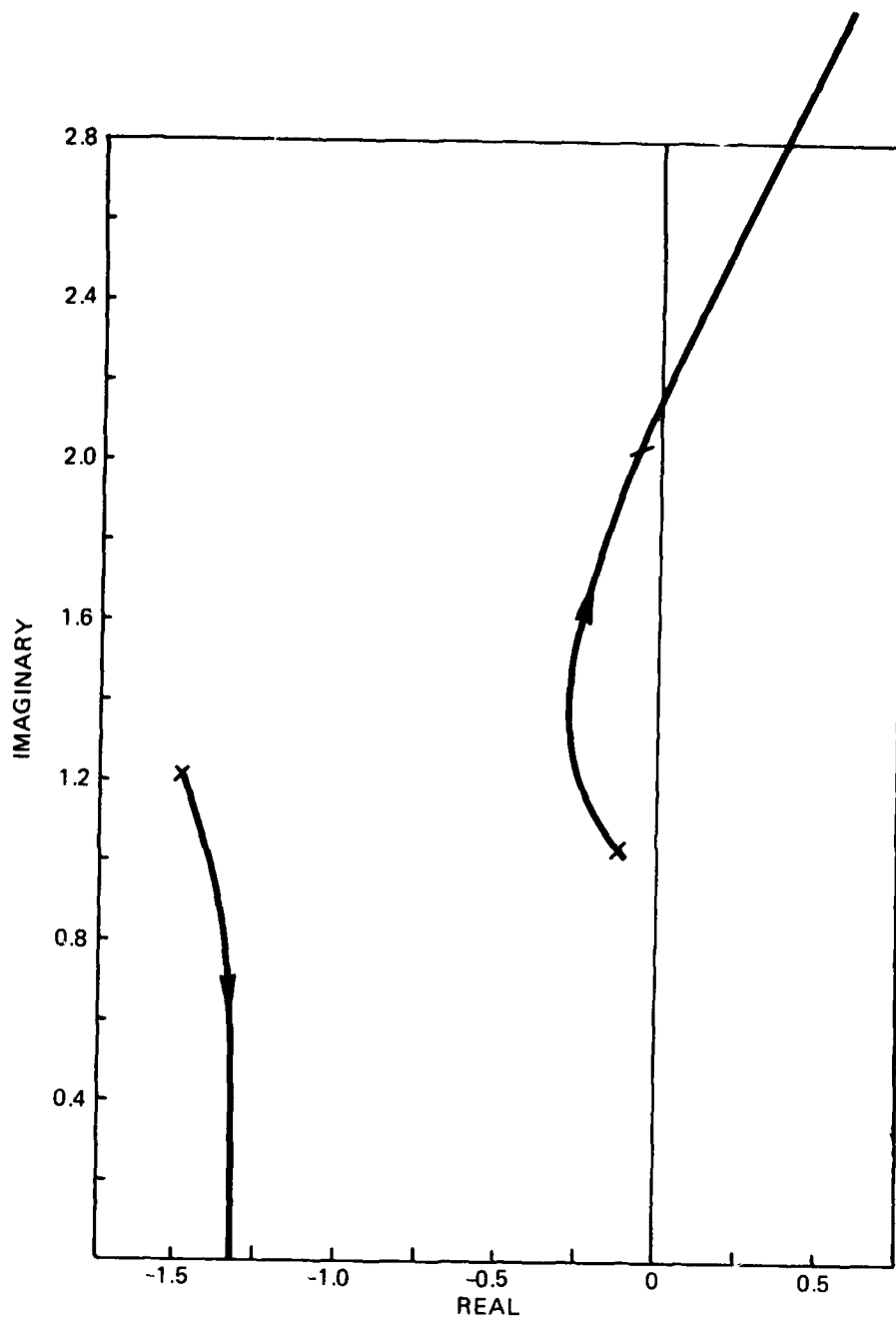


Figure 3-10. Closed-loop root locus
 Type: transmission actuator
 Feedback: centralized
 Parameter: ζ_c
 Data: $\rho_2 = 0.2$, $\omega_a^2 = 4.0$, $\omega_s^2 = 1.0$, $\zeta_s = 0.05$, $\zeta_a = 0.78$

The decentralized control viewpoint suggests use of the force controller

$$f_d = -c_d \dot{x} \quad (3-167)$$

together with the actuator controller defined by

$$U(s) = \frac{1}{b_a} \left(1 + \frac{cs}{k_a} \right) F_d(s) - \frac{c_f}{b_a} sZ(s) \quad (3-168)$$

where $c = c_a + c_f$. The force controller and the actuator controller can be combined to obtain the equivalent control expression

$$u = -\frac{c_f}{b_a} \dot{z} - \frac{c_d}{b_a} \dot{x} - \frac{c c_d}{k_a} \ddot{x} \quad (3-169)$$

which can be compared with Eq. (3-161) and (3-164); this form for the controller involves an extra acceleration feedback term. The effective actuator transfer function based on Eq. (3-100) is given by

$$G_f(s) = \frac{(2\zeta_a \omega_a s + \omega_a^2)(s^2 + 2\zeta_s \omega_s s + \omega_s^2)}{(s^2 + 2\zeta_s \omega_s s + \omega_s^2)(s^2 + 2\zeta_a \omega_a s + \omega_a^2) + \rho \omega_s^2 (s^2 + 2\zeta_a \omega_a s)} \quad (3-170)$$

For the control Eq. (3-169), define the structural damping parameter, ζ_d , by

$$2\zeta_d \omega_s = \frac{c_d}{M} \quad (3-171)$$

and define

$$G_p(s) = \frac{2\zeta_d \omega_s s}{s^2 + 2\zeta_s \omega_s s + \omega_s^2} \quad (3-172)$$

The closed-loop characteristic equation is

$$1 + G_f(s) G_p(s) = 0 \quad (3-173)$$

The closed-loop system, defined by Eq. (3-158), (3-159), (3-167), and (3-168), is stable for any $\zeta_a > 0$ and any $\zeta_d \geq 0$. A root locus plot of Eq. (3-173) for the particular value of $\zeta_a = 0.78$ obtained in Figure 3-9 is shown in Figure 3-11; dependence of the closed-loop poles on the structural damping parameter ζ_d is indicated. It is clear that significant damping can be obtained using the force control Eq. (3-167) and the actuator control Eq. (3-168). As seen from Figure 3-11, there is a limit to the closed-loop damping that can

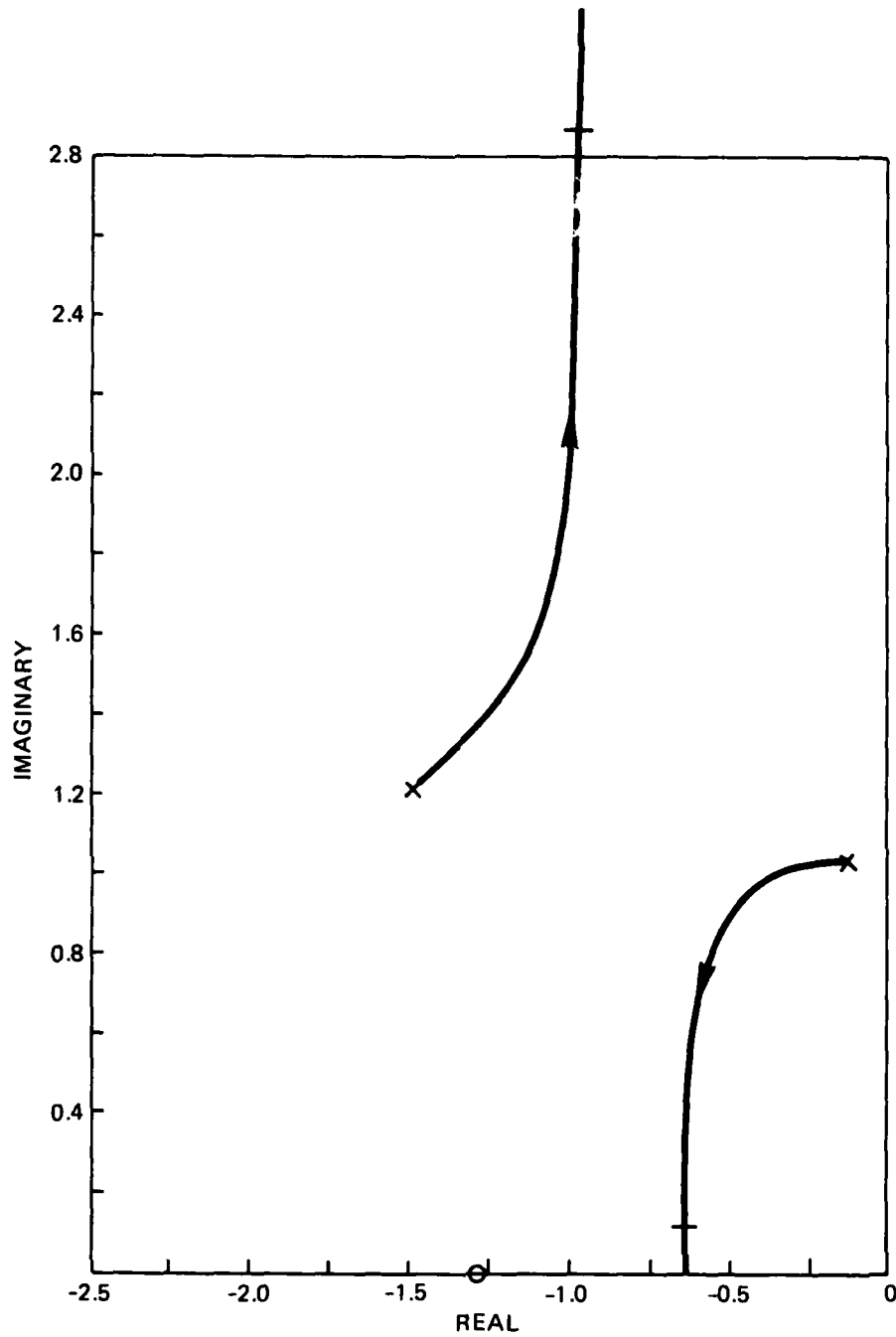


Figure 3-11. Closed-loop root locus
 Type: transmission actuator
 Feedback: decentralized
 Parameter: ζ_d
 Data: $\rho_2 = 0.2$, $\omega_a^2 = 4.0$, $\omega_s^2 = 1.0$, $\zeta_s = 0.05$, $\zeta_a = 0.78$

be achieved. If $\zeta_d = 0.32$, the damping ratios for the two pole pairs are 0.50 and 0.58.

Instead of a direct analysis of the closed-loop poles, an analysis of the closed loop using the robustness test, Eq. (3-108), can be used. In this particular example, the frequency response for the actuator error function, $|G_f(j\omega) - 1|$, is indicated in Figure 3-12; for any $\zeta_d > 0$ the robustness inequality of Eq. (3-108) is satisfied. As an illustration, the frequency response for the inverse return difference function, $|1 - G_p^{-1}(j\omega)|$, is also indicated in Figure 3-12 for the value $\zeta_d = 0.32$. Certain conclusions can be drawn from Figure 3-12, based on the robustness test in Eq. (3-108). First, for the specific case where $\zeta_d = 0.32$ as shown in Figure 3-12, and, in fact, for any $\zeta_d > 0$, the actuator dynamics do not destabilize the closed loop using the force controller Eq. (3-167). Also, the closed loop is most sensitive to disturbances with a frequency near 1.0 rad/s, where the "loading peak" for the actuator error occurs. The low-frequency margins are large since the actuator error is small. At high frequencies, the actuator errors are relatively large but a good margin is maintained due to the force controller characteristic. These qualitative conclusions should be typical of a large space structure controlled by a single transmission type actuator using a properly chosen force controller. Experience has indicated that the magnitude of the loading peak for the actuator error is strongly affected by the assumption regarding open-loop structural damping; the robustness inequality of Eq. (3-108) may not be satisfied if the open-loop structural damping is assumed too low.

3.5.3 Comments

The two simplest possible examples have been considered, where the large space structure can be described by a single vibration mode. Caution must be exercised in making general conclusions on the basis of two examples but the following comments are suggested by the examples.

It is possible to add damping to a structure by operating an electro-mechanical actuator as a passive damper, or by using actuator velocity feedback only. It appears that this control approach can add only a modest amount of damping to a structure, however. In order to increase the closed-loop damping, controls developed using the centralized and decentralized viewpoint have been developed and analyzed. A centralized controller, where both actuator and structural velocities are fed back, can substantially increase the system damping. The feedback gains must be carefully selected so that the closed loop is stable with good response characteristics. A decentralized controller with the force controller based on structural velocity feedback can also substantially increase the system damping.

Our analysis of the closed-loop characteristics has been based on direct evaluation of the closed-loop poles. Such a direct approach is generally difficult to use as a method for design or modification of a force controller. In the case of decentralized control, use of a robustness test has been demonstrated as a way of evaluating the effects of the actuator dynamics on the closed loop. This robustness condition may prove effective as a basis for design or modification of a force controller.

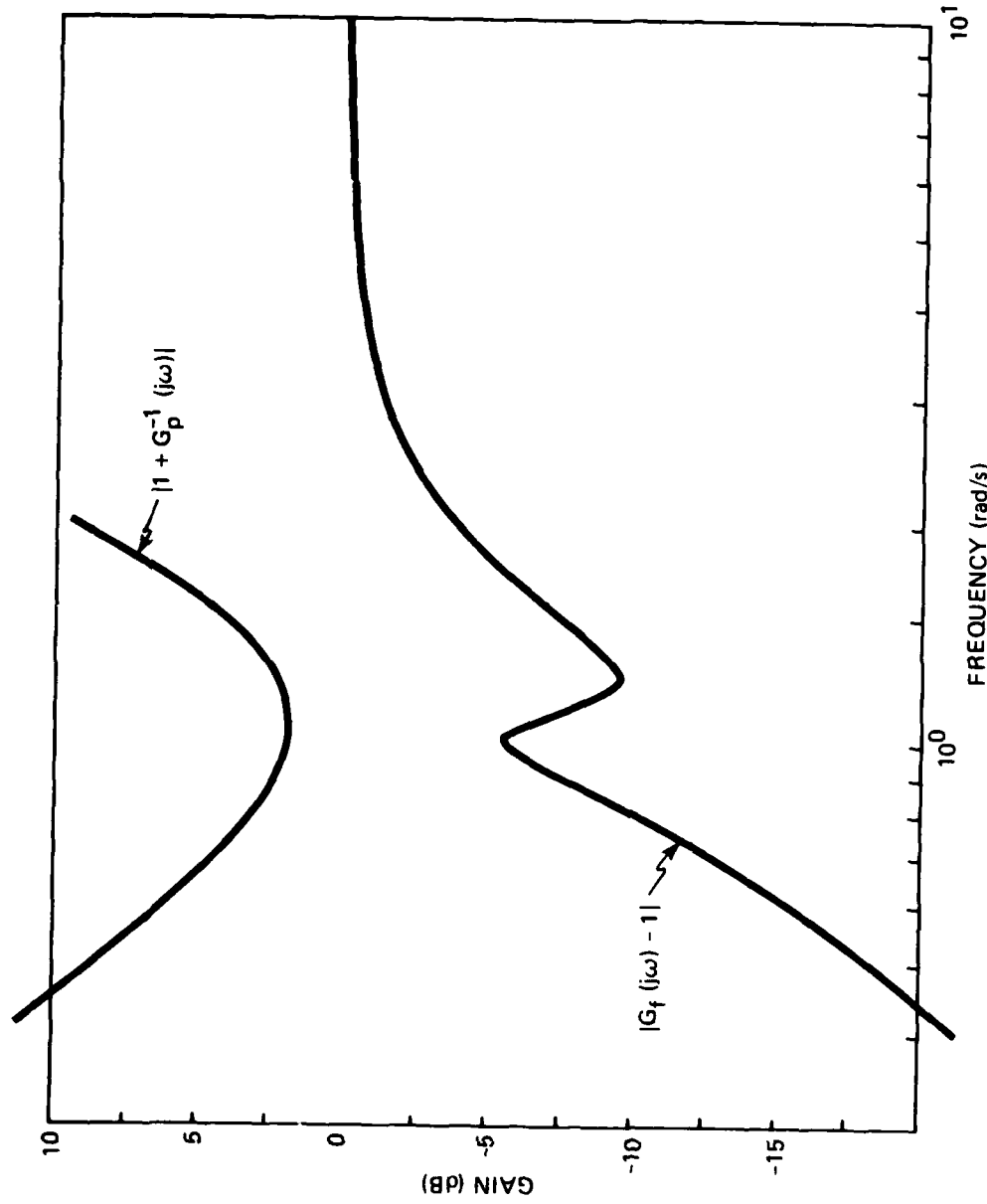


Figure 3-12. Robustness test (Eq. (3-108)).

Type: transmission actuator

Feedback: decentralized

Data: $\rho_2 = 0.2$, $\omega_a^2 = 4.0$, $\omega_s^2 = 1.0$, $\zeta_s = 0.05$, $\zeta_a = 0.78$,
 $\zeta_d = 0.32$

Although the two examples do not demonstrate it, in more complicated cases, there is the possibility for closed-loop instability unless the force controller and actuator controller are carefully selected. The robustness demonstrated in the two examples is a consequence of the use of a force controller defined in terms of constant gain structural velocity feedback.

3.6 Conclusions

3.6.1 Extensions

A rather detailed theory has been developed for large space structures controlled by certain classes of electromechanical actuators. This theory has been based on rather specific assumptions about the actuator characteristics and the assumed controller forms. The specifics of these assumptions are not critical and extensions in several directions can be indicated.

Our development has been based on specific assumptions about reaction type actuators and transmission type actuators, as characterized by the schematics in Figures 3-1 and 3-2. Although it appears that many physical actuators do fall within one of these two classes, there is no doubt that a parallel theory could be developed for electromechanical actuators where slightly different assumptions are required. It should be clear that the qualitative system theoretic characteristics of reaction type actuators and transmission type actuators are similar; their characteristics differ only in detail. Hence our development can be viewed as indicating qualitative system characteristics of any electromechanical actuator.

Development of the material in Section 3.3 on centralized control was illustrated solely through the use of a constant gain actuator and structural velocity feedback. Such a simple control form is natural where the objective is augmentation of system damping. However, in many cases other variables, e.g., displacements and accelerations, may be available for feedback. Further, control laws based on use of optimal linear-quadratic-Gaussian theory may be desired, where a filter or observer is incorporated as part of the controller. Each of these cases represents a viable procedure for developing a centralized control law. The key idea is that, no matter what control design procedures are used, the design model is assumed to include both structural and actuator dynamics.

Extension of the material in Section 3.4 on decentralized control is possible, in the sense that modifications to the developed forms for both force controller and actuator controllers can be made. The development was illustrated by considering a force controller defined in terms of constant gain structural velocity feedback. The form of the actuator controllers suggested is consistent with that class of force controllers. However, other classes of force controllers could be used, including other output feedback forms or control based on optimal linear-quadratic-Gaussian theory. In principle, the actuator controllers specified in Section 3.4 could be used in conjunction with any force controller; the only limitation arises from the fact that the force controller and actuator controllers must be realizable. Thus there are many extensions to the developments in Section 3.4 that could be

made. The key idea is that the force controller be chosen to suitably control the structure, ignoring actuator dynamics, and the actuator controllers be chosen to suitably suppress the actuator dynamics.

3.6.2 Summary

There has been substantial research into the problems of active control of large space structures. Many issues have been carefully addressed and a coherent theory is evolving.

With few exceptions, the effects of actuator dynamics as part of the closed-loop control scheme have been ignored. It is the premise of this work that actuator dynamics may play an important role in the feedback control of large space structures. Specifically, if actuator dynamics are ignored in the control design process, their presence in an actual closed-loop system may tend to be destabilizing due to neglected actuator phase shifts. Such an undesirable possibility is thought to be more likely precisely in the class of control problems considered, namely where a lightly damped elastic structure is coupled to actuators with damped oscillatory dynamics. There is also the possibility that actuator dynamics play a desirable role in the closed loop. Their filtering effect provides gain roll-off at low frequencies and at high frequencies; thus, electromechanical actuators tend to suppress coupling with low-frequency rigid body modes and with high-frequency unmodelled modes. In any event, the presence of actuators in the closed loop should be carefully taken into account.

Our objective has been to develop a framework for the control design process where effects of actuator dynamics are not completely ignored. Two different viewpoints have been suggested. It is impossible to select either the centralized design viewpoint or the decentralized design viewpoint as preferable; each approach should have sufficient flexibility to allow development of suitable control strategies for a large space structure with multiple electromechanical actuators.

A detailed examination has been made of the control problems, associated with each of these design viewpoints. It is hoped that this work will serve to focus additional attention on the role of actuators and other instrumentation as a critical part of closed-loop control of large space structures.

SECTION 3
LIST OF REFERENCES

- 3-1 Actively Controlled Structures Theory - Final Report, Vol. 1, CSDL Report R-1338, December 1979.
- 3-2 Active Control of Space Structures - Final Report, CSDL Report R-1454, February 1981.
- 3-3 ACOSS Eleven Semiannual Technical Report, Vol. 2, CSDL Report R-1536, February 1982.
- 3-4 Balas, M.J., "Trends in Large Space Structure Control Theory: Fondest Hopes, Wildest Dreams," IEEE Trans. Automatic Control, Vol. AC-27, No. 3, June 1982, pp. 522-535.
- 3-5 Skelton, R., "Control Design of Flexible Spacecraft," (to appear).
- 3-6 Hardy, J.W., "Active Optics: A New Technology for the Control of Light," Proceedings IEEE, Vol. 66, No. 6, June 1978, pp. 651-697.
- 3-7 Murugeson, "An Overview of Electric Motors for Space Applications," IEEE Trans. Indus. Electronics and Control Instrumentation, Nov. 1981, pp. 260-265.
- 3-8 Grabbe, E.M., et al., ed., Handbook of Automation, Computation, and Control, Vol. 3, Chapter 22, John Wiley, New York, 1961.
- 3-9 Meisel, J., Principles of Electromechanical Energy Conversion, McGraw-Hill, 1966.
- 3-10 Aubrun, J.N., J.A. Berkwell, and G.J. Chambers, "Experimental Results for Active Structural Control," Proceedings of 20th IEEE Conference on Decision and Control, San Diego, California, 1981, pp. 706-709.
- 3-11 Lund, R.A., "Active Damping of Large Structures in Wind," Structural Control, H.H.E. Leipholz, ed., North-Holland, 1980, pp. 459-470.
- 3-12 Roberts, J.W. and M.C. Borgohain, "Active System for Neutralization of Vibratory Force Interactions in Structures," Structural Control, H.H.E. Leipholz, ed., North-Holland, 1980, pp. 613-627.
- 3-13 Khalil, W., and A. Liegeois, "The Dynamics of Electrically-Actuated and Cable Driven Manipulators," Dynamics of Multibody Systems, K. Magnus, ed., Springer-Verlag, 1978, pp. 120-132.
- 3-14 Taft, C.K., and B.M. Herrick, "A Proportional Piezoelectric Electro-Fluidic Pneumatic Valve Design," J. Dynamic Systems, Measurement and Control, Vol. 103, Dec. 1981, pp. 361-367.

SECTION 3
LIST OF REFERENCES (Cont.)

- 3-15 Roorda, J., "Tendon Control in Tall Structures," ACSE J. of the Structural Division, Vol. 101, No. ST3, 1975, pp. 505-521.
- 3-16 Iwens, R.P., "Challenges in Stable and Robust Control System Design for Large Space Structures," Proceedings of 19th IEEE Conference on Decision and Control, Albuquerque, New Mexico, 1980, pp. 999-1002.
- 3-17 Kosut, R.L., "Stability and Robustness of Control Systems for Large Space Structures," 3rd AIAA/VPI Symposium on the Dynamics and Control of Large Flexible Spacecraft, Blacksburg, Virginia, June 1981.
- 3-18 Hughes, P.C., and R.E. Skelton, "Stability, Controllability and Observability of Matrix Second Order Systems," Proceedings of Joint Automatic Control Conference, June 1979, pp. 56-62.
- 3-19 Benhabib, R.J., R.P. Iwens, and R.L. Jackson, "Stability of Distributed Control for Large Flexible Structures Using Positivity Concepts," Proceedings of the AIAA Guidance and Control Conference, Paper No. 79-1780, August 1979, Boulder, Colorado.
- 3-20 Hughes, P.C., "Passive Damper Analysis for Reducing Attitude Controller/Flexibility Interaction," J. Spacecraft and Rockets, Vol. 13, No. 5, May 1976, pp. 271-274.
- 3-21 Van de Vegte, J., "Optimal Dynamic Absorbers for Plate Vibration Control," J. Dynamic Systems, Measurement and Control, Dec. 1975, pp. 432-438.
- 3-22 Doyle, J.C., "Robustness of Multi-Loop Linear Feedback Systems," Proceedings of IEEE 17th Conference on Decision and Control, San Diego, California, 1979.
- 3-23 McClamroch, N.H., and J. Serakos, "Displacement Control of Elastic Structures: Integral Control with a Robustness Property," Proceedings of 1st American Control Conference, Arlington, Virginia, 1982.

SECTION 4

MODAL-SPRING PLUS MODAL-DASHPOT DESIGN OF OUTPUT FEEDBACK VIBRATION CONTROLLERS

A modal-spring plus modal-dashpot design of displacement and velocity output feedback vibration controllers was performed for the 20-mode VCOSS example model. Only the 10 primary modes (those modes which contribute the most to the RMS line-of-sight errors) were considered in the design process, but all 20 modes were used in the evaluation. The 20-mode closed-loop system is as stable as expected (see Reference 4-1), and each of the 20 modes has an increase in frequency or damping ratio or both.

The purpose of the design was to increase the frequency of some primary modes by "modal springs" and the damping ratio of some other primary modes by "modal dashpots". In other words, it was desired to have some closed-loop poles with larger imaginary parts, and some others to have more negative real parts. As in the preceding sections, the nine collocated actuator/sensor pairs were used. The rows of the 10×9 modal actuator influence matrix (and equivalently, the columns of the 9×10 modal sensor influence matrices) were very dependent on each other. Since it had been observed that high feedback gains would result in large spillover, one design criterion was to restrain them from extremely high gains. Feedback gains for both displacement and velocity feedback can be greatly reduced by requiring the rows of the modal actuator influence matrix (and the columns of the modal sensor influence matrices) to have a high degree of linear independence. A sequential "Gramian test" was then developed and implemented in PL/I which would choose the most linearly independent rows (or columns). The Gramian test indicated that only 5 to 6 of the 10 primary modes should be used in the design, since their modal actuator/sensor influences were most independent.

The displacement and velocity feedback gain matrices, G_D and G_V , respectively, were computed using the pseudoinverses that were initially considered by Canavin for modal dashpots. Damping was added to modes 9, 14, 22, 23, 33, and 34, while frequency increases were applied to modes 7, 9, 12, 22, and 23. The desired damping ratio, ζ_{id} , and the desired frequency, ω_{id} , for these modes are shown in Table 4-1. The resulting gain matrices, G_D and G_V , are shown in Tables 4-2 and 4-3, respectively.

These two feedback gain matrices were simultaneously put into the 20-mode model and the closed-loop poles were evaluated. Table 4-4 lists the real and imaginary parts of the poles, their frequencies, and damping ratios. Recall that all 20 modes are assumed to have an inherent damping ratio $\zeta_{i0} = 0.001$. The corresponding open-loop modes are also indicated in the table. Linking the closed-loop modes to the open-loop modes was accomplished by tracing the root locus when the gain matrices were gradually scaled down. Specifically, the gain matrices, G_D and G_V , were first replaced by γG_D and γG_V , respectively; the closed-loop poles were then computed for discrete samples of γ between 0 and 1. When $\gamma = 1$, the poles correspond to the closed-loop modes, and when $\gamma = 0$, they correspond to the open-loop modes. Figure 4-1 shows such a portion of the root locus.

Table 4-1. Desired damping ratios and frequencies.

Mode	ζ_{id}	ω_{id}
7	---	3.3
9	0.103	3.3
12	---	4.36
14	0.261	---
22	0.707	14.77
23	0.707	35.59
33	0.036	---
34	0.026	---

Table 4-2. Displacement output feedback gain matrix, G_D .

	1	2	3	4	5	6	7	8	9
1	1.95E + 10	5.29E + 10	1.53E + 10	2.92E + 09	-1.13E + 10	1.27E + 10	2.42E + 10	-9.21E + 07	9.27E + 07
2	5.29E + 10	2.68E + 11	8.05E + 10	9.83E + 08	-3.75E + 10	4.37E + 10	1.07E + 11	-4.47E + 08	4.47E + 08
3	1.58E + 10	8.05E + 10	2.44E + 10	1.54E + 08	-1.12E + 10	1.31E + 10	3.22E + 10	-1.37E + 08	1.37E + 08
4	2.93E + 09	9.83E + 08	1.54E + 08	8.79E + 08	-1.30E + 09	1.38E + 09	1.29E + 09	-1.22E + 06	1.24E + 06
5	-1.13E + 10	-3.75E + 10	-1.12E + 10	-1.30E + 09	6.93E + 09	-7.88E + 09	-1.63E + 10	6.46E + 07	-6.46E + 07
6	1.27E + 10	4.37E + 10	1.30E + 10	1.38E + 09	-7.88E + 09	8.97E + 09	1.88E + 10	-7.51E + 07	7.50E + 07
7	2.42E + 10	1.07E + 11	3.22E + 10	1.29E + 09	-1.63E + 10	1.88E + 10	4.40E + 10	-1.81E + 08	1.81E + 08
8	-9.21E + 07	-4.47E + 08	-1.37E + 08	-1.21E + 06	6.46E + 07	-7.51E + 07	-1.81E + 08	8.59E + 05	-8.57E + 05
9	9.21E + 07	4.47E + 08	1.37E + 08	1.24E + 06	-6.46E + 07	7.50E + 07	1.81E + 08	-8.57E + 05	8.57E + 05

Table 4-3. Velocity output feedback gain matrix, G_V .

	1	2	3	4	5	6	7	8	9
1	1.34E + 09	-5.16E + 08	6.50E + 07	7.34E + 08	-1.64E + 08	5.43E + 07	9.92E + 07	3.19E + 06	-3.18E + 06
2	-5.16E + 08	1.99E + 08	-2.70E + 07	-2.80E + 08	6.42E + 07	-2.18E + 07	-3.85E + 07	-1.23E + 06	1.22E + 06
3	6.30E + 07	-2.70E + 07	9.26E + 06	2.98E + 07	-1.01E + 07	4.60E + 06	5.50E + 06	1.56E + 05	-1.55E + 05
4	7.34E + 08	-2.80E + 08	2.98E + 07	4.04E + 08	-8.80E + 07	2.81E + 07	5.36E + 07	1.74E + 06	-1.73E + 06
5	-1.64E + 08	6.42E + 07	-1.01E + 07	-8.80E + 07	2.10E + 07	-7.42E + 06	-1.25E + 07	-3.92E + 05	3.91E + 05
6	5.43E + 07	-2.18E + 07	4.60E + 06	2.81E + 07	-7.42E + 06	2.89E + 06	4.29E + 06	1.31E + 05	-1.30E + 05
7	9.92E + 07	-3.85E + 07	5.50E + 06	5.36E + 07	-1.25E + 07	4.29E + 06	7.45E + 06	2.36E + 05	-2.36E + 05
8	3.19E + 06	-1.23E + 06	1.56E + 05	1.74E + 06	-3.92E + 05	1.31E + 05	2.36E + 05	8.17E + 03	-8.06E + 03
9	-3.18E + 06	1.22E + 06	-1.55E + 05	-1.73E + 06	3.91E + 05	-1.30E + 05	-2.36E + 05	-8.06E + 03	8.12E + 03

Table 4-4. Closed-loop poles.

Real Part	Imaginary Part	Frequency	Damping Ratio	Corresponding Open-Loop Mode
-0.54D + 06	0.0			45
-0.44D + 03	0.66D + 04	0.66D + 04	0.67D - 01	62
-0.44D + 03	-0.66D + 04	0.66D + 04	0.67D - 01	
-0.16D + 04	0.00			47
-0.48D + 01	0.72D + 03	0.72D + 03	0.66D - 02	56
-0.48D + 01	-0.72D + 03	0.72D + 03	0.66D - 02	
-0.29D + 01	0.13D + 03	0.13D + 03	0.23D - 01	48
-0.29D + 01	-0.13D + 03	0.13D + 03	0.23D - 01	
-0.17D + 01	0.10D + 03	0.10D + 03	0.16D - 01	40
-0.17D + 01	-0.10D + 03	0.10D + 03	0.16D - 01	
-0.32D + 00	0.78D + 02	0.78D + 02	0.41D - 02	34
-0.32D + 00	-0.78D + 02	0.78D + 02	0.41D - 02	
-0.11D + 01	0.58D + 02	0.58D + 02	0.19D - 01	37
-0.11D + 01	-0.58D + 02	0.58D + 02	0.19D - 01	
-0.36D + 01	0.42D + 02	0.43D + 02	0.85D - 01	33
-0.36D + 01	-0.42D + 02	0.43D + 02	0.85D - 01	
-0.65D + 01	0.39D + 02	0.39D + 02	0.17D + 00	15
-0.65D + 01	-0.39D + 02	0.39D + 02	0.17D + 00	
-0.17D + 01	0.29D + 02	0.29D + 02	0.59D - 01	24
-0.17D + 01	-0.29D + 02	0.29D + 02	0.59D - 01	
-0.13D + 02	0.00			47
-0.13D + 00	0.13D + 02	0.13D + 02	0.97D - 02	23
-0.13D + 00	-0.13D + 02	0.13D + 02	0.97D - 02	
-0.81D - 02	0.73D + 01	0.73D + 01	0.11D - 02	22
-0.81D - 02	-0.73D + 01	0.73D + 01	0.11D - 02	
-0.74D - 03	0.72D + 00	0.72D + 00	0.10D - 02	7
-0.74D - 03	-0.72D + 00	0.72D + 00	0.10D - 02	
-0.26D - 01	0.00			45
-0.12D - 01	0.41D + 01	0.41D + 01	0.29D - 02	16
-0.12D - 01	-0.41D + 01	0.41D + 01	0.29D - 02	
-0.13D - 01	0.41D + 01	0.41D + 01	0.33D - 02	14
-0.13D - 01	-0.41D + 01	0.41D + 01	0.33D - 02	
-0.47D - 01	0.38D + 01	0.38D + 01	0.12D - 01	13
-0.47D - 01	-0.38D + 01	0.38D + 01	0.12D - 01	
-0.53D - 02	0.36D + 01	0.36D + 01	0.15D - 02	12
-0.53D - 02	-0.36D + 01	0.36D + 01	0.15D - 02	
-0.43D - 02	0.33D + 01	0.33D + 01	0.13D - 02	10
-0.43D - 02	-0.33D + 01	0.33D + 01	0.13D - 02	
-0.29D + 00	0.32D + 01	0.32D + 01	0.89D - 01	9
-0.29D + 00	-0.32D + 01	0.32D + 01	0.89D - 01	

It should be noted even though many poles other than those used in design also moved due to spillover, the closed-loop system is stable. The reduced-order design of modal-spring/modal-dashpot type of output feedback controllers can guarantee full-order closed-loop stability, as was proved analytically and demonstrated numerically by a simple free-free beam in Reference 4-1. This result is again demonstrated numerically by this rather complicated example.

SECTION 4
LIST OF REFERENCES

- 4-1 Lin, J.G., "Augmentation of Damping, Stiffness and Stability to Large Space Structures by Modal Dashpots and Modal Springs," Active Control of Space Structures - Final Report, Section 4, Report R-1454, The Charles Stark Draper Laboratory, Inc., February 1981.

SECTION 5

A CONTROLLED EXPERIMENT FOR ACOSS DESIGN

5.1 Motivation

Attempts to synthesize an active control strategy for ACOSS Model No. 2 that is stable, that accommodates the effects of a broadband disturbance, and that meets stringent specifications on the error in line-of-sight (LOS) rotation have so far been unsuccessful. Early synthesis efforts using several different, but complementary, approaches to the controller design appeared promising at the level of a 10-mode design model [5-1]. Subsequent evaluation of these designs on a 20-mode evaluation model proved disappointing, exhibiting spillover-induced instability. Further attempts to modify the designs so as to obtain the desired stability, disturbance accommodation, and LOS performance were similarly unsuccessful. Except in isolated instances in which unrealistic assumptions were invoked, the various designs either failed to meet LOS performance specifications at the design model level, or proved unstable in evaluation. It is not our intent to give the details of these attempted designs here. Rather, the purpose of the present section is to outline a new approach to the process of synthesizing active controllers that holds high promise for success in the sense described above.

At least two reasonable alternatives come to mind at this point. One is to try to answer the question: "What went wrong?" That is, to focus on discovering why the synthesis attempts so far have not succeeded, employing available analysis tools to suggest ways of improving and reapplying the approaches already tried. Another is to try to answer the question: "What is going on?" That is, to reexamine carefully and systematically all the principal steps in the synthesis process, not just the controller design itself, and allowing what is observed to suggest new approaches to the synthesis process.

There is a growing conviction that the latter alternative is the course that should be followed, principally because it is the more fundamental one. Since it subsumes the former, it is certain to take longer, but can be expected to provide a much deeper understanding of the synthesis process, and suggest answers to questions that perhaps have not arisen yet. This conviction has been reaffirmed through a recent editorial by a well-known expert in the field of control, who has proposed a major and intentional effort in "experimental control science" [5-2].

5.2 Preliminary Observations

In order to set the stage properly for the approach to be presented, a few preliminary observations are needed.

There are at least four principal elements that make up the complete process of synthesizing an active control strategy for a complicated structure such as ACOSS Model No. 2. First is the selection of a basic structural design to work with. In the case of Model No. 2, the original design has been substantially revised several times. In the present discussion, the reasons

for, or the details of, these revisions are not as important as the recognition that most of them have substantial influence upon the control synthesis process. Second is the selection of two or more distinct mathematical models of the structure, one for design, and one or more for evaluation of the design. Essentially, this may reduce to a (nontrivial) decision as to which modes of the original (finite element) structural model to retain for the various purposes. Third is a selection of active devices (sensors and actuators) to implement the control and observation strategies. Fourth is a selection of an algorithm for determining the feedback structure of the controller.

It is important to note in passing that, whereas each of these elements when viewed separately is quite amenable to sophisticated mathematical analysis, the entire synthesis process that incorporates the interactions between these elements is not nearly so amenable, if at all. This fact represents a substantial obstacle to obtaining a satisfactory synthesis.

In the designs attempted to date, attention has focused overwhelmingly on the fourth element: algorithms for determining the controller feedback structure. Selections of the first two elements (structural design and reduced-order model selection) have been made with a certain arbitrariness, principally for simplicity and convenience, and the third element (active devices) has been selected with certain somewhat arbitrary restrictions (e.g., no nodal actuators). These three selections have remained fixed through all of the attempts at determining an appropriate controller feedback structure. The results suggest that in so doing, the overall synthesis problem has been overconstrained. Either a solution does not exist, or the process of finding it has an unacceptably low probability of success. In particular, there appears to be a strong possibility that the reduced-order models (design and evaluation) and the active device selections are mutually incompatible.

We propose to approach this impasse by conducting a "controlled experiment" in which each principal element in the overall synthesis process is systematically examined. Essential features of the experiment are that:

- (1) Experiment "variables" are adjusted only one at a time.
- (2) The effect of adjusting any experiment "variable" is assessed by conducting a complete end-to-end synthesis attempt.
- (3) Results of each synthesis attempt are analyzed and, as appropriate, taken into account in subsequent stages of the experiment.

5.3 Definition of a "Controlled Experiment"

"Variables" of the controlled experiment identify important features of each of the principal elements in the complete synthesis process. They are:

a: The basic structural design.

b \equiv (b₁, b₂, b₃): Reduced-order models.

b₁: The criterion for ranking of structural modes.

b_2 : The basis for retaining modes in the design model.

b_3 : The basis for retaining modes in an evaluation model.

$c \equiv (c_1, c_2, c_3)$: Active devices (sensors and actuators).

c_1 : The types of active devices to be allowed (e.g., axial only).

c_2 : The criterion for selecting locations of active devices.

c_3 : The class of reduced-order models to be considered in selecting active devices.

d : The algorithm for determining controller feedback structure.

To clarify these variable definitions, we note that the following assignment of initial values to these variables describes the design process with ACOSS Model No. 2 as it has developed to date

$$a + a^{(0)}, \quad b + b^{(0)}, \quad c + c^{(0)} \quad (5-1)$$

where

$a^{(0)} \triangleq$ Revision 3 of ACOSS Model No. 2, incorporating details of the interaction between certain rigid components and the associated flexible supports, and lightweighting of nodal connecting elements

$b_1^{(0)} \triangleq$ the root-mean-square (RMS) LOS-error induced by the deflection of a mode (ignoring interactions with other modes) in response to the broadband disturbance (Reference 5-1, Section 5.2.1)

$b_2^{(0)} \triangleq$ the first 10 modes, ranked according to criterion $b_1^{(0)}$

$b_3^{(0)} \triangleq$ the first 20 modes, ranked according to criterion $b_1^{(0)}$

$c_1^{(0)} \triangleq$ only node-connecting elements (e.g., member-dampers, axial-motion sensors)

$c_2^{(0)} \triangleq$ a best approximation (in the least-squares sense) to each component of the modal representation (or modal coefficient) of the LOS-rotation vector by linear combinations of node shapes corresponding to a candidate selection of active devices (Reference 5-1, Section 3)

$c_3^{(0)} \triangleq$ the modal representation of the LOS-rotation vector in criterion $c_2^{(0)}$ reflects only those modes included in design model $b_2^{(0)}$

Variable "d" has assumed a number of values in the various design attempts, including

- $d^{(0)} \triangleq$ basic disturbance rejection control (DRC) design in which complete knowledge of the disturbance statistics is assumed (Reference 5-1, Section 4)
- $d^{(1)} \triangleq$ linear quadratic optimal control design, in which no explicit knowledge of the disturbance statistics is assumed (Reference 5-1, Section 5)
- $d^{(2)} \triangleq$ algorithm $d^{(1)}$ augmented by the incorporation of measures to alleviate spillover (Reference 5-1, Section 6)

among others.

In the initial phase of the experiment, we propose to fix the values of variables "a" and "d", and focus on the effects of changes in variables "b" and "c"--particularly the interaction between them. The fixed values chosen for variables "a" and "d" are

$$a + a^{(00)} \quad , \quad d + d^{(0)}$$

where

$a^{(00)} \triangleq$ Revision 1 of ACOSS Model No. 2, a stiffer structural design which does not contain the lightweighting feature of design $a^{(0)}$

A pictorial representation of the overall synthesis process is shown in Figure 5-1. A most significant feature of this process is the interaction of variables "b" and "c", which has not been given sufficient attention in previous design attempts.

Specific classes of values for variables "b" and "c" that appear to be of interest include those listed below. These listings are most conveniently expressed as functions of other experiment variables and of additional variables n_C, n_R that may be considered parameters of the experiment.

$b_1^{(1)} \triangleq$ criterion $b_1^{(0)}$ augmented by specific a priori information on physical or modal deformations

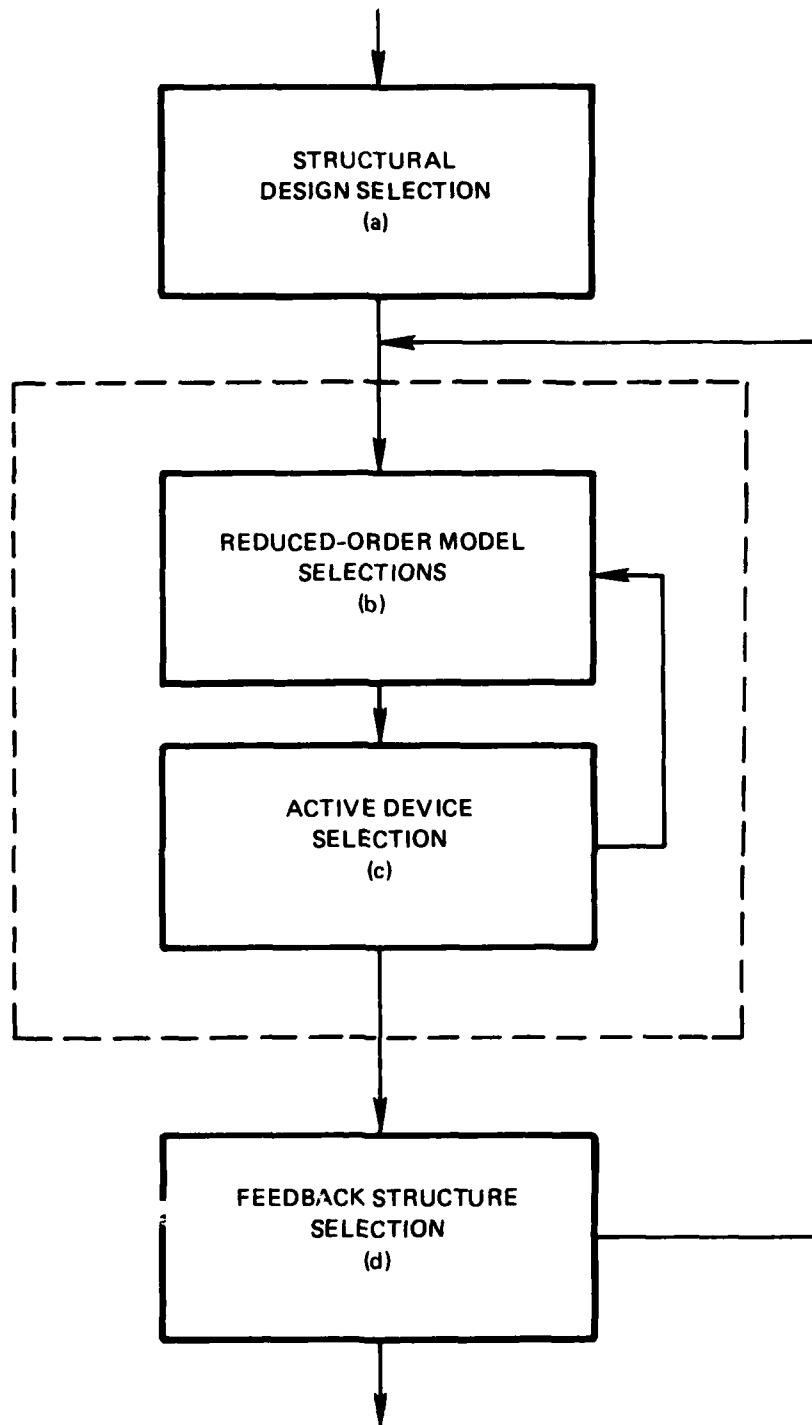


Figure 5-1. Process for active control synthesis.

- $b_2^{(1)}(n_C, b_1) \triangleq$ the first n_C modes, ranked according to criterion b_1 (i.e., the value being defined for b_2 is a function of whatever value has been selected for variable b_1)
- $b_2^{(2)}(n_C, b_1) \triangleq$ the modes selected by criterion $b_2^{(1)}(n_C, b_1)$ augmented by all modes whose natural frequencies lie in the range associated with those selections (i.e., not allowing an interlacing of controlled and residual nodes)
- $b_3^{(1)}(n_R, b_1) \triangleq$ the first n_R modes ($n_R > n_C$), ranked according to criterion b_1
- $b_3^{(2)}(n_R, b_1) \triangleq$ the modes selected by criterion $b_3^{(1)}(n_R, b_1)$ augmented by all modes whose natural frequencies lie in the range associated with those selections
- $c_1^{(1)} \triangleq$ devices $c_1^{(0)}$ together with devices located at nodes and capable of translational action only
- $c_1^{(2)} \triangleq$ devices $c_1^{(1)}$ augmented with a rotational action capability at nodes
- $c_2^{(1)} \triangleq$ criterion $c_2^{(0)}$ augmented by specific a priori information on physical or modal deformations
- $c_3^{(1)}(c_2, b_2) \triangleq$ the modal representation of the LOS rotation vector in criterion c_2 reflects all modes included in design model b_2
- $c_3^{(2)}(c_2, b_3) \triangleq$ the modal representation of the LOS rotation vector in criterion c_2 reflects all modes included in evaluation model b_3

A pictorial representation of typical stages of the experiment in terms of experiment variables is shown in Table 5-1. Each column represents an end-to-end attempt of the entire synthesis process. The succession from one column to the next (from left to right) involves changing only one variable.

5.4 Expected Outcome

It is expected that the conduct of this experiment will lead to a deeper understanding of the complete process of active control synthesis. It is especially important to understand more clearly the essential elements of selecting appropriate reduced-order models, selecting active devices for actuation and sensing, and the nature of the relationship between them. In

Table 5-1. Typical stages of a controlled experiment.

Variables	Benchmark	Model Selection Trials			Active Device Selection Trials		
<u>Structure (a)</u>	Revision 1 $a^{(0)}$	→					
<u>Models (b)</u>	RMS LOS $b^{(0)}$	*	*	*	Best preliminary selection of reduced-order models		
Ranking Criteria (b_1)							
Design Model (b_2)	First 10 modes $b_2^{(0)}$	First 20; gaps $b_2^{(1)}(20, b_1^{(0)})$	First 20; no gaps $b_2^{(2)}(20, b_1^{(0)})$...			
Evaluation Model (b_3)	First 20 modes $b_3^{(0)}$	First 50; gaps $b_3^{(1)}(50, b_1^{(0)})$	First 50; no gaps $b_3^{(2)}(50, b_1^{(0)})$	*			
<u>Active Devices (c)</u>	Members Only $c_1^{(0)}$	*	*	*	Members & Nodes (trans.) $c_1^{(1)}$	Members & Nodes (trans. & rot.) $c_1^{(2)}$	*
Types (c_1)							
Selection Criteria (c_2)	RMS LOS $c_2^{(0)}$	*	*	*			*
Model Influence (c_3)	Design Model $c_3^{(0)}$	Design Model $c_3^{(1)}(c_2, b_2^{(1)}(20, b_1^{(0)}))$	Design Model $c_3^{(2)}(c_2, b_2^{(2)}(20, b_1^{(0)}))$	Design Model $c_3^{(3)}(c_2, b_2^{(3)}(20, b_1^{(0)}))$			Evaluation Model $c_3^{(2)}(c_2, b_3^{(2)}(n_g, b_1^{(0)}))$
<u>Controller (d)</u>	Basic DRC $d^{(0)}$	→					

particular, it is expected that the results of the experiment will generate a process by which a reduced-order design model and a set of active devices which are mutually compatible can be found. Such mutual compatibility is the key to successful synthesis for active control.

SECTION 5
LIST OF REFERENCES

- 5-1 R. Strunce, et al., ACOSS Eleven Second Semiannual Technical Report, Volume 2: Active Controller Designs, Report CSDL-R-1583, Charles Stark Draper Laboratory, Cambridge, MA, August 1982.
- 5-2 Ho, Y.-C., "Is It Application or Is It Experimental Science?" (Editorial), IEEE Trans. Automatic Control, Vol. AC-27, No. 6, December 1982, p. 1142.

RADC/DAP GRIFFISS AFB NY 13441	2	3
RADC/TSLD GRIFFISS AFB NY 13441	1	
ADMINISTRATOR DEF TECH INF CTR ATTN: DTIC-DDA CAMERON STA BG 5 ALEXANDRIA VA 22314	12	5
Charles Stark Draper Lab 555 Technology Square Cambridge, MA 02139	5	3
Charles Stark Draper Lab Attn: Dr. Keto Soosaar 555 Technology Square M.S. -95 Cambridge, MA 02139	1	4
NASA Headquarters ATTN: Mr. J. B. Dahlgren Code RTH-6 Washington, DC 20546	1	5
Charles Stark Draper Lab Attn: Mr. R. Strunce 555 Technology Square M.S. -60 Cambridge, MA 02139	1	6
Charles Stark Draper Lab Attn: Dr. Daniel R. Hegg 555 Technology Square M.S. -60 Cambridge, MA 02139	1	7
ARPA/STO Attn: Lt Col A. Herzberg 1400 Wilson Blvd Arlington, VA 22209	1	8
ARPA/STO Attn: Maj E. Dietz 1400 Wilson Blvd Arlington, VA 22209	1	9

Riverside Research Institute Attn: Mr. A. DeVilliers 1701 N. Ft. Myer Drive, Suite 711 Arlington, VA 22209	2	10
Riverside Research Attn: HALO Library, Mr. Bob Passut 1701 N. Ft. Myer Drive Arlington, VA 22209	1	11
Itek Corp Optical Systems Division 10 Maguire Rd. Lexington, MA 02173	1	12
Perkin Elmer Corp Attn: Mr. H. Levenstein Electro Optical Division Main Avenue Norwalk, CT 06856	1	13
Hughes Aircraft Company Attn: Mr. George Speak M. S. B_156 Culver City, CA 09230	1	14
Hughes Aircraft Company Attn: Mr. Ken Beale Centinela Teale Sts Culver City, CA 90230	1	15
Air Force Flight Dynamics Lab Attn: Dr. Lynn Rogers Wright Patterson AFB, OH 45433	1	16
AFWL/FIBG Attn: Mr. Jerome Pearson Wright Patterson AFB, OH 45433	1	17
Air Force Wright Aero Lab. FIGC Attn: Siva S. Banda Wright Patterson AFB, OH 45433	1	18

Air Force Institute of Technology Attn: Prof. R. Calico/ENY Wright Patterson AFB, OH 45433	1	19
Aerospace Corp. Attn: Dr. G.T. Tseng 2350 E. El Segundo Blvd El Segundo, CA 90245	2	20
Aerospace Corp. Attn: Mr. J. Mosich 2350 E. El Segundo Blvd El Segundo, CA 90245	1	21
Aerospace Corp/Bldg 125/1054 Attn: Mr. Steve Burrin Advanced Systems Tech Div. 2400 E El Segundo Blvd El Segundo, CA 90245	1	22
SD/SD/YLVS Attn: Mr. Lawrence Weeks P.O. Box 92960 Worldway Postal Center Los Angeles CA 90009	1	23
SD/YCD Attn: YCPT/Capt Gajewski P.O. Box 92960 Worldway Postal Center Los Angeles, CA 90009	1	24
Grumman Aerospace Corp Attn: Dr. A. Mendelson South Oyster Bay Road Bethpage, NY 11714	1	25
OUSDR&E/DS Attn. Mr. A. Bertapelli Room 3D136 Pentagon, Washington, DC 20301	1	26
Jet Propulsion Laboratory Dr. S. Szermay 4800 Oak Grove Drive Pasadena, CA 91103	2	27

MIT/Lincoln Laboratory Attn: S. Wright P. O. Box 73 Lexington, MA 02173	1	28
MIT/Lincoln Laboratory Attn: Dr. D. Hyland P. O. Box 73 Lexington, MA 02173	1	29
MIT/Lincoln Laboratory Attn: Dr. N. Smith P. O. Box 73 Lexington, MA 02173	1	30
Control Dynamics Co. Attn: Dr. Sherman Seltzer Suite 1414 Executive Plaza 555 Sparkman Drive Huntsville, AL 35805	1	31
Lockheed Space Missile Corp. Attn: A. A. Woods, Jr., O/62-E6 p. O. Box 504 Sunnyvale, California 94088-3504	5	32
Lockheed Missiles Space Co. Attn: Mr. Paul Williamson 3251 Hanover St. Palo Alto, CA 94304	1	33
General Dynamics Attn: Ray Halstenberg Convair Division 5001 Keary Villa Rd San Diego, CA 92123	1	34
STI Attn: Mr. R. C. Stroud 20065 Stevens Creek Blvd. Cupertino, CA 95014	1	35
NASA Langley Research Ctr Attn: Dr. Earle K. Huckins III Dr. M. F. Card Langley Station, Bldg 1293B, MS 230 Hampton, VA 23665	2	36

NASA Johnson Space Center Attn: Robert Piland Ms. EA Houston, TX 77058	1	37
McDonald Douglas Corp Attn: Mr. Read Johnson Douglas Missile Space Systems Div 3301 Bulsa Ave Huntington Beach, CA 92607	1	38
Integrated Systems Inc. Attn: Dr. N. K. Gupta and M. G. Lyons 151 University Avenue, Suite 400 Palo Alto, California 94301	2	39
TRW Defense Space Sys Group Inc. Attn: Ralph Iwens Bldg 82/2054 One Space Park Redondo Beach, CA 90278	1	40
TRW Attn: Mr. Len Pincus Bldg R-5, Room 2031 Redondo Beach, CA 90278	1	41
Department of the NAVY Attn: Dr. K. T. Alfriend Naval Research Laboratory Code 7920 Washington, DC 20375	1	42
Airesearch Manuf. Co. of Calif. Attn: Mr. Oscar Buchmann 2525 West 190th St. Torrance, CA 90509	1	43
Analytic Decisions, Inc. Attn: Mr. Gary Glaser 1401 Wilson Blv. Arlington, VA 22209	1	44
Ford Aerospace & Communications Corp. Drs. I. P. Leliakov and P. Barba, MS/G80 3939 Fabian way Palo Alto, California 94304	1	45
Center for Analysis Mr. James Justice 13 Corporate Plaza Newport Beach, CA 92660	1	46

W. J. Schafer Associates Dr. R. Kappesser Suite 800 1901 Fort Meyer Drive Arlington, VA 22209	1	47
General Research Corp Attn: Mr. Thomas Zakrzewski 7655 Old Springhouse Road McLean, VA 22101	1	48
Air Force Weapons Laboratory Attn: Lt Col D. Washburn ARAA Kirtland AFB, NM 87117	2	49
Karman Sciences Corp. Attn: Dr. Walter E. Ware 1500 Garden of the Gods Road P. O. Box 7463 Colorado Springs, CO 80933	1	50
MRJ, Inc. 10400 Eaton Place Suite 300 Fairfax, VA 22030	1	51
Photon Research Associates Attn: mr. Jim Myer P. O. Box 1318 La Jolla, CA 92038	1	52
Rockwell International Attn: Russell Loftman (Space Systems Group) (Mail Code - SL56) 12214 Lakewood Blvd. Downey, CA 90241	1	53
Science Applications, Inc. Attn: Mr. Richard Ryan 3 Preston Court Bedford, MA 01730	1	54
U. S. Army Missile Command Attn: DRSMI-RAS/Mr. Fred Haak Redstone Arsenal, AL	1	55

Naval Electronic Systems Command Attn: Mr. Charles Good PME_106-4 National Center I Washington, DC 20360	1	56
Lockheed Palo Alto Research Laboratory Attn: Dr. J. N. Aubrun, O/52-56 3251 Hanover Street Palo Alto, California 94304-1187	2	57
U. S. Army/DARCOM Attn: Mr. Bernie Chasnov AMC Bldg 5001 Eisenhower Ave Alexandria, VA 22333	1	58
R. Carman RADC/OCSE	5	59
Honeywell Inc. Attn: Dr. Thomas B. Cunningham Attn: Dr. Michael F. Barrett 2600 Ridgway Parkway MN 17-2375 Minneapolis, MN 55413	2	60
NASA Marshal Space Flight Center Attn: Dr. J. C. Blair, EDO1 Henry B. Waites Marshal Space Flight Center, AL 35812 q	2	61
TRW Attn: Robert Benhabib Bldg 82/2024 One Space Park Redondo Beach, CA 90278	1	62
NASA Langley Research Center Attn: Dr. L. Pinson MS - 230 Hampton, VA 23665	1	63
H. R. Textron Attn: Mr. Richard Quartararo 2485 McCabe Way Irvine, CA 92714	1	64
Naval Research Lab Attn: W. Bennett Mail Code: 7926 Washington, DC 20375	1	65



MISSION
of
Rome Air Development Center

RADC plans and executes research, development, test and selected acquisition programs in support of Command, Control Communications and Intelligence (C³I) activities. Technical and engineering support within areas of technical competence is provided to ESD Program Offices (POs) and other ESD elements. The principal technical mission areas are communications, electromagnetic guidance and control, surveillance of ground and aerospace objects, intelligence data collection and handling, information system technology, ionospheric propagation, solid state sciences, microwave physics and electronic reliability, maintainability and compatibility.

END

FILMED

1-84

DTIC